ABSTRACT

Title of Document:	APPLICATION OF COMPOUND COMPRESSIBLE FLOW TO HYPERSONIC THREE-DIMENSIONAL INLETS
	Gillian Mary Harding Bussey, M.S., 2009
Directed By:	Professor Mark J. Lewis, Department of Aerospace Engineering

A method for correcting flow non-uniformities and incorporating multiple oblique shocks waves into compound compressible flow is presented. This method has several applications and is specifically presented for the problem of creating a streamline-traced hypersonic three-dimensional inlet. This method uses compound compressible flow theory to solve for the freestream flow entering a pre-defined duct with a desired downstream profile. This method allows for multiple iterations of the design space and is computational inexpensive. A method is also presented for modeling a laminar or turbulent boundary layer to compare inlet designs and to determine the viscous correction to the inlet. Two different Mach 6 designs were evaluated, with a rectangular capture area and circular combustor with a uniform temperature, pressure, and Mach number profile. Comparison with other three-dimensional inlets indicates those designed with this method demonstrate good

inviscid performance. These inlets also have the ability to correct incoming flow non-uniformities.

APPLICATION OF COMPOUND COMPRESSIBLE FLOW TO HYPERSONIC
THREE-DIMENSIONAL INLETS.

By

GILLIAN MARY HARDING BUSSEY.

Thesis submitted to the Faculty of the Graduate School of the
University of Maryland, College Park, in partial fulfillment
of the requirements for the degree of
Master of Science
2009

Advisory Committee:
Professor Mark J. Lewis, Chair
Associate Professor Kenneth Yu
Professor Ashwani Gupta

Dedication

I'd like to thank my parents for all of their support through my years at MIT and during my time in graduate school here at the University of Maryland – College Park. I'd also like to show my appreciation to my husband George for putting up with my long hours of working, taking classes, and doing research and the support he provided.

Acknowledgements

I would like to thank my advisor, Dr. Mark J. Lewis, for his guidance, wisdom, and advice during the past year and a half on this project, on graduate school, and the field of hypersonics. I would also like to thank the committee members Dr. Kenneth Yu and Dr. Ashwani Gupta for serving on my thesis committee.

I would also like to extend thanks to Charles Brink and Richard Mutzman from ARFL for providing information on the X-51 inlet. I appreciate the support my employer provided in allowing me to spend a year at Maryland attending classes and working on this research and putting up with my strange hours while I continue my education.

I'd also like to thank the fellow members of my research group for their advice, knowledge, laughs, and support. Finally, my husband George is owed much thanks for his putting up with my long hours

Table of Contents

List of Tables

List of Figures

List of Symbols

A = Area

A_c = Area of inlet at the cowl

A_i^* = Area of streamtube i at throat and sonic conditions

A_δ = Area of boundary layer

A_1 = Area of subsonic streamtube in 2-stream model

A_2 = Area of supersonic streamtube in 2-stream model

α = Ratio of streamtube areas in 2-stream model

B = Compound compressible flow parameter

β = Shock angle

$\beta_{F.S.}$ = Falkner-Skan parameter characterizing pressure gradient

b = Bottom of inlet height change

C = Constant

c = Chapman-Rubesin parameter

CR = Contraction ratio

C_D = Coefficent of drag

D = Hydraulic diameter

δ = Boundary layer height

δ_* = Boundary layer displacement thickness

δ_{99} = Boundary layer thickness based on where velocity is 99% of edge

δ_s = Shoulder angle

f = Streamfunction

f' = Velocity normalized by edge of boundary layer

γ = Ratio of specific heats

H = Channel height

h_i = Height of streamtube

h = Enthalpy

L = Length of inlet

L_{in}/d_h = Normalized isolator length

M = Mach number

M_{avg} = Mass-averaged Mach number

$\overline{M}$ = Uniform equivalent Mach number

M_N = Mach number normal to shock

m = Exponent of velocity distribution

m_c = Mass captured

μ = Coefficient of viscosity

n_y, n_z = Streamtube number

N = Number of streamtubes

η, ξ = Similarity coordinates

η_{KE} = Kinetic energy efficiency

η_c = Adiabatic compression effeciency

P = Pressure

$\overline{P}$ = Average pressure

ρ = Density
π_c = Total pressure recovery
r = Radius
R = Real gas constant
Re   = Reynolds number
Re_T = Reynolds number at transition to turbulent flow
S = Enthalpy function
σ_p = Standard deviation of pressure
ψ = Static temperature ratio
T = Temperature
T_r = Recovery temperature
τ = Shear stress
θ = Truncation angle
u,v,w = Velocity coordinates
w_i = Mass flow of streamtube
W = Mass flow constant
x,y,z = Physical coordinates
$y_{capture}$ = Height at capture plane
Δy = Increase in height of streamtube at sonic line

Subscript

i = Index specifying local conditions
w = Wall
∞ = Freestream
t = Throat
0 = Stagnation condition
c = Cowl
e = Edge

Chapter 1: Introduction

1.1 Motivation

Despite advances in computational methods for analyzing hypersonic flow problems, an analytic method to characterize hypersonic flows can provide additional insight into the performance and design of hypersonic vehicles and propulsion systems. In the present work, an analytical method is developed for generic hypersonic inviscid flow problems with multiple shock waves and a boundary layer and then applied to the problem of designing a scramjet inlet.

An efficient inlet is a crucial component in the operation of a scramjet-powered hypersonic vehicle. A scramjet is a supersonic combustion ramjet with supersonic flow entering the combustor that operates at Mach numbers typically above Mach 4.5 – when ramjets lose their ability to provide thrust. An effective scramjet inlet must provide efficient compression, enough mass flow, a high enough static temperature ratio, and generally uniform flow into the combustor with minimal total pressure losses. In a scramjet, the greatest losses occur in the combustor either from mixing or shock losses, requiring the inlet to be as efficient as possible in order to generate enough thrust to overcome drag. An effective inlet would also have good starting characteristics at ramjet/scramjet take-over speeds (Mach 4 to Mach 5) and operate over a large Mach number range and flight conditions for some applications.

Viscous drag and shock losses should also be minimal. For all applications, the inlet should also have a geometry that reduces structural weight, and for some configurations, a capture shape such that the inlets can be stacked with no mass flow loss or have a variable area for operation over a range of flight conditions. Numerous types of inlets have been researched for applications to hypersonic flow, with so-called "two-dimensional" inlets favored in most designs. Additional research has focused on three-dimensional inward turning inlets – specifically an inlet with a rectangular capture area and a circular or elliptical combustor shape.

Three-dimensional inlets that blend a rectangular capture area with a circular or elliptical combustor could provide several advantages over inward-turning inlets with a circular capture area and combustor or rectangular inlets with rectangular capture areas and combustors. A three-dimensional inlet is curved, not axi-symmetric, and usually consists of different cross-section shapes along the inlet. Rectangular or two-dimensional inlets have reduced boundary layer losses because of their shorter lengths. A given vehicle design may require that inlets be stackable or operate over a range of flight conditions. An inlet with a circular capture area will have flow leakage between inlets, while an inlet with a rectangular capture area can be stacked without mass flow loss. However, rectangular inlets have generally been designed to have a rectangular combustor, which has several disadvantages over a circular or elliptical combustor. Circular combustors require less structural weight for a given pressure. This combustor geometry has a lower wetted surface and hydraulic diameter, thus reducing drag and viscous effects in the combustor, and has fewer problems due to

hypersonic corner flow, resulting in higher performance. An elliptical combustor may also improve fuel injection over a circular combustor. An effective design of a rectangular-to-circular transition would provide the advantages of a rectangular capture area with those of a circular or elliptical combustor.

Compound compressible flow theory as presented in this work can provide the basis for an analytic tool to describe hypersonic flows with multiple shock waves like a scramjet inlet. As the governing equations are algebraic, propagating the flow solution is fairly simple and can be done relatively quickly compared to most computational methods. This allows for several quick design iterations while providing deep physical insight. The present work adds on to classical compound compressible flow theory by presenting an inverse method for handling several shock waves in the flow to solve for the upstream conditions given a desired downstream flow. While this analytic tool is applied in the present work as a method for specifically solving for the case of an arbitrary capture shape transitioning to a three-dimensional combustor, it can be used for a variety of hypersonic flow applications.

1.2 Inlet performance parameters

The parameters typically used to evaluate the performance of scramjet inlets are static temperature ratio ψ, total pressure recovery π_c, kinetic energy efficiency η_{KE}, and adiabatic compression efficiency η_c. These are defined below[1]:

$$\psi = \frac{T_{throat}}{T_\infty} = \left[\frac{1 + \frac{\gamma - 1}{2} M_\infty^2}{1 + \frac{\gamma - 1}{2} M_{throat}^2} \right] \tag{1.1}$$

Because the compression procession is adiabatic, total temperature is conserved.

$$\pi_c = \frac{P_{0,throat}}{P_{0,\infty}} = \frac{P_{throat}}{P_\infty} \left[\frac{1 + \frac{\gamma - 1}{2} M_{throat}^2}{1 + \frac{\gamma - 1}{2} M_\infty^2} \right]^{\frac{\gamma}{\gamma - 1}} \tag{1.2}$$

$$\eta_c = \frac{\psi - \left(\frac{1}{\pi_c} \right)^{\frac{\gamma - 1}{\gamma}}}{\psi - 1} \tag{1.3}$$

Adiabatic compression efficiency is the ratio of the actual change to the ideal, isentropic change in static enthalpy. The dependence of adiabatic compression efficiency on total pressure ratio is such that even a modest decrease in adiabatic compression results in a large decrease in total pressure. This is partially why the total pressure ratio is not always the best figure of merit for determining performance of scramjets. This can be determined knowing the total pressure recovery and static temperature ratio ψ,

4

$$\eta_{KE} = 1 - \frac{2}{(\gamma-1)M_\infty^2}\left[\left(\frac{1}{\pi_c}\right)^{\frac{\gamma-1}{\gamma}} - 1\right] \tag{1.4}$$

Kinetic energy efficiency is defined as the ratio of the square of the velocity that the exit flow would have if it were isentropically expanded to the freestream pressure to the square of the freestream velocity. Because of the high velocities in hypersonic flow, large changes in adiabatic compression efficiency result in only modest changes in kinetic energy efficiency. Kinetic energy efficiency needs to be calculated to three decimal places in order to be accurate.

1.3 Previous work – inlets

Much of scramjet inlet research since the late 1990's has focused on streamline traced axi-symmetric inward-turning Busemann inlets and inlets that transition from a rectangular capture area to a circular combustor. In the 1950s, inlet designs and research focused on inward-turning axi-symmetric inlets. These designs fell out of favor with a preference for rectangular two-dimensional inlets. The late 1990's saw a renewed interest in inlets with circular or elliptical combustors specially inward-turning or shape-changing inlets.[2]

1.3.1 Streamline-traced axi-symmetric inward-turning inlets

A much-studied candidate for a streamline traced axi-symmetric inlet is the Busemann inlet[3,4]. These inlets have several benefits including relatively high pressure recovery, the ability to easily blend with a circular combustor, and can be

5

designed based on an inviscid flow field that is completely known analytically.

Busemann first proposed an internal axi-symmetric flow that consisted of internal

isentropic compression followed by a conical shock.[3] Molder and Szpiro[4] proposed an

inlet based on using any stream surface of this flow field proposed by Busemann as

the inlet wall. This flow field obeys the Taylor-Maccoll equations for axi-symmetric

conical flow:

$$u_R'^2(u_R + u_R'') = \frac{(\gamma-1)}{2}(1 - u_R^2 - u_R'^2)(u_R'' + u_R' \cot\theta + 2u_R) \qquad (1.5)$$

where u_R is the radial velocity non-dimensionalized with respect to the freestream

speed[3]. The tangential velocity u_θ is found from the irrotationality condition

$$u_\theta = u_R' = \frac{du_R}{d\theta} \qquad (1.6)$$

where θ is the angle emanating from the conical shock from the center of the inlet to

the entrance of the inlet. The conical shock turns the flow such the flow is uniform

and parallel to the inlet wall coming into the combustor. The shock then cancels at the

shoulder during on-design conditions. Figure 1.1 shows the shock structure in a

Busemann inlet.
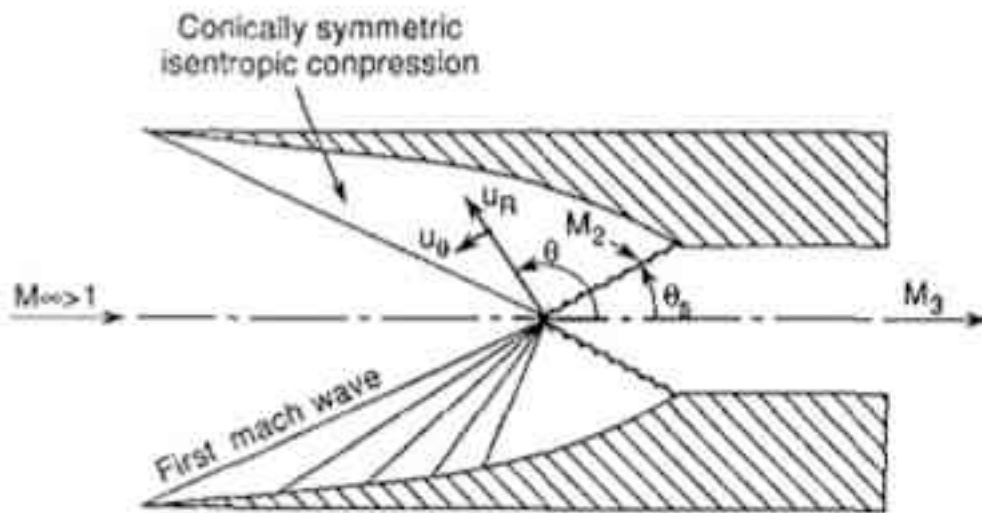
Figure 1.1 The Busemann inlet[5]

Van Wie and Molder developed a numerical method for designing these inlets.[5] The Taylor-Maccoll ordinary differential equation combined with the irrotationality condition can be numerically integrated as a system of first order equations to find the inviscid flow field. Because of the existence of a singularity at the freestream condition, the integration starts at $\theta = \theta_s$ with the Mach number behind the shock and total pressure ratio of the inlet chosen, and marches forward in θ until the freestream Mach angle is met. The freestream Mach number is determined as a part of the solution process.

Although these inlets have relatively high total pressure recovery, they have several drawbacks. Busemann inlets have such high contraction ratios that they will not start in steady flow. The contraction ratio determines the minimum Mach number the inlet can operate and how much the flow can be compressed before it chokes.

7

When the inlet unstarts, a normal shock adjusts the flow and the flow becomes

subsonic entering the combustor. A preliminary estimate of whether an inlet will

unstart can be obtained from the Kantrowitz limit[6]:

$$\left(\frac{A_c}{A_{throat}}\right)_{Kantrowitz} = \frac{1}{M_c}\left[\frac{(\gamma+1)M_c^2}{(\gamma-1)M_c^2+2}\right]^{\frac{\gamma}{\gamma-1}}\left[\frac{\gamma+1}{2\gamma M_c^2-(\gamma-1)}\right]^{\frac{1}{\gamma-1}}\left[\frac{1+\gamma-1/2M_c^2}{\gamma+1/2}\right]^{\frac{\gamma+1}{2(\gamma-1)}}$$

(1.7)

Van Wie and Molder have proposed a streamline tracing method within the basic

flow field to create a modular Busemann inlet that avoids contraction ratios that are

too high. They noted that the freestream streamtube can also be selected such that the

leading edges of a modular Busemann inlet are highly swept as shown in Figure 1.2.[5]
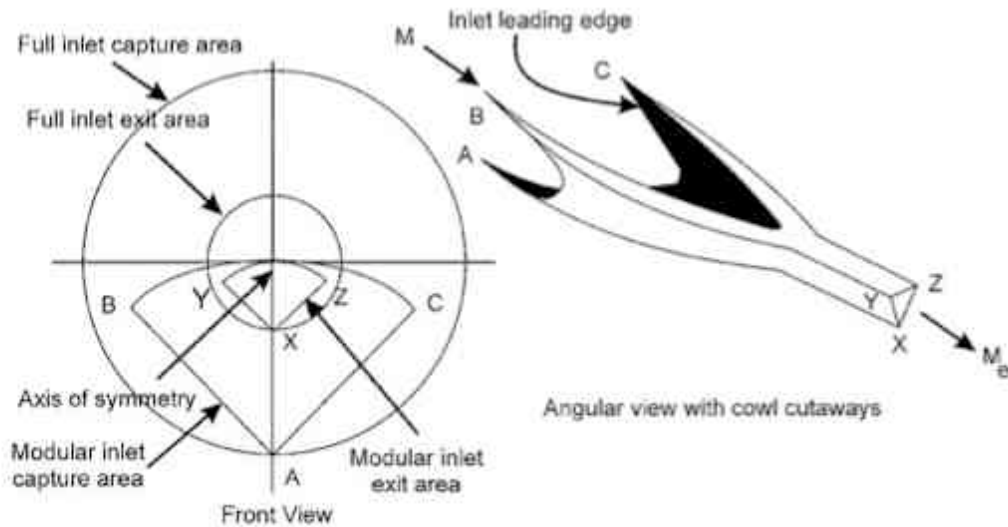
Figure 1.2. Streamline tracing technique for modular Busemann inlet with swept

leading edges. [5]

Kothari and Billig proposed circumventing this problem by introducing a radial-deviation parameter for axi-symmetric flows to specify internal contraction ratios.[7] The effect of this parameter was incorporated into the axi-symmetric method-of-characteristics solution with the introduction of a core conical inviscid flow.

These inlets also tend be very long, resulting in high viscous losses due to boundary layer growth and higher heating loads. This can be mitigated somewhat by truncating the inlet with an initial turning angle at the leading edge, although the oblique shock formed at the sharp leading edge leads to some total pressure losses. Drayna, Nompelis and Chandler[8] examined the effect of changing the truncation angle on inlet performance at angles of 0, 2, 4, and 5.5 degrees using computational fluid dynamics for inviscid and viscous flow. They held the freestream Mach number and capture height constant while varying the throat Mach number until a specified contraction ratio was obtained. They found that as the truncation angle increased, the length of the inlet decreased rapidly with significantly less drag and heating loads and better performance for a small truncation angle (between 2 and 4 degrees).
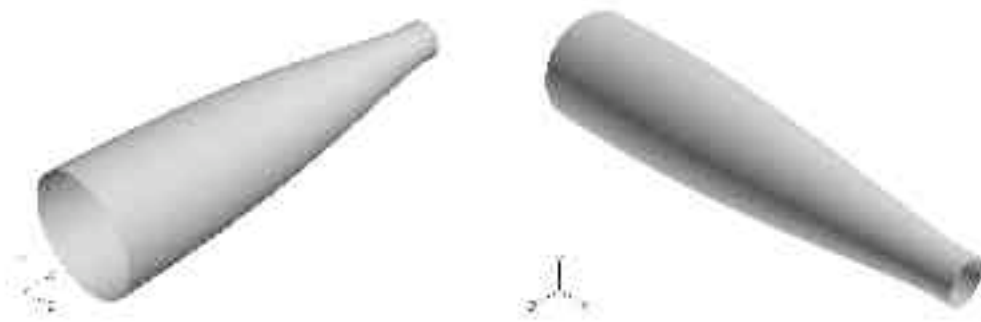
Figure 1.3. Representation of Busemann inlets[9]

Busemann inlets in particular have poor off –design performance because of their sensitivity to flow angularity particularly if the inlet has no truncation angle or a sharp leading edge. Ramasubramanian et al.[9,10] conducted two inviscid numerical studies varying the flight angle or Mach number for a Busemann and quasi-Busemann inlet, respectively. When the inlet was under- or over-sped or flown at an angle, shock cancellation at the shoulder no longer occurred – leading to viscous and inviscid losses. They found that designing for a higher Mach number would lead to fewer total pressure losses as these inlets had lower total pressure losses under-sped than over-sped. For off-design angles, performance degradation because of misplaced shocks was considerable even at 3 degrees. At 9 degrees the inlet failed completely
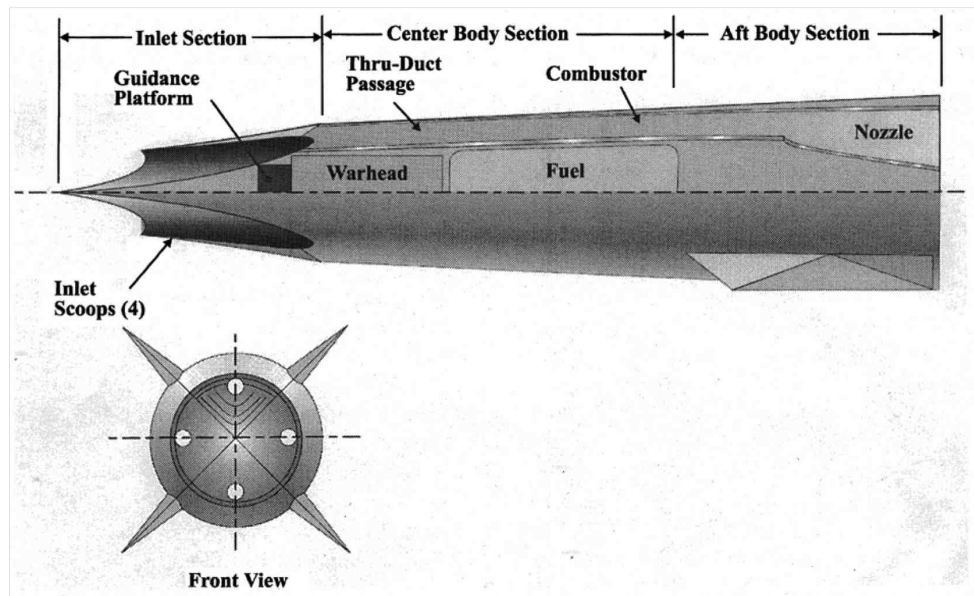
Figure 1.4. SCRAM missile concept employing four inward-turning streamline traced inlets[2]

with very low total pressure recovery of 0.655 and unphysical results for the adiabatic compressible efficiency. Figure 1.4 shows one of the first propulsion systems using a streamline-traced inward-turning inlet. The SCRAM missile concept was developed in the early 1960s and mid-1970s by the John Hopkins Applied Physics Laboratory and had successful operation during wind tunnel experiments at Mach 5 to 7.2[11].

1.3.2 Blended three-dimensional inlets

1.3.2.a REST inlets

The design of a transition duct from a rectangular capture area to an elliptical combustor has been the focus of several papers. Inlets with a rectangular capture area and circular combustor can combine many of the benefits of rectangular inlets and circular combustors. However, streamline tracing in a parent flow field with uniform inflow and outflow requires the same shape at freestream as at the throat. Streamline-traced inlets contain the features of the parent flow field. Most efforts to create this transition duct have involved elegantly blending together the two parent flow fields – rectangular and Busemann.

In particular, considerable work on these inlets has been done by Smart, who used a modified-streamline tracing method involving blending together multiple sets of streamlines to form the transition duct of rectangular-to-elliptical "REST" inlet.[12] The process involved calculating a pre-determined capture area and pressure ratio required for the inlet. First, an axi-symmetric compression flow field with the

required pressure ratio was calculated. Several capture shapes and inlets varying from

rectangular to elliptical were defined. The path of the streamlines from the inlet

entrance to the exit plane was calculated. Specifically, a streamline-traced inlet with

rectangular-like capture shape like in Figure 1.5.b. was determined. A second

streamline-traced inlet with a capture area like Figure 1.5.b. but with radiuses corners

as shown in Figure 1.6.a. was then calculated. A third inlet shape with an elliptical

throat with the same area as Figure 1.5.b. was calculated and similar to that shown in

Figure 1.6.b. All three shapes were smoothly blended together to form a REST inlet

with the rectangular capture shape of Figure 1.5.b., the cross-sectional shape of

Figure 1.6.a. at the cowl closure, and the throat shape of Figure 1.6.b.
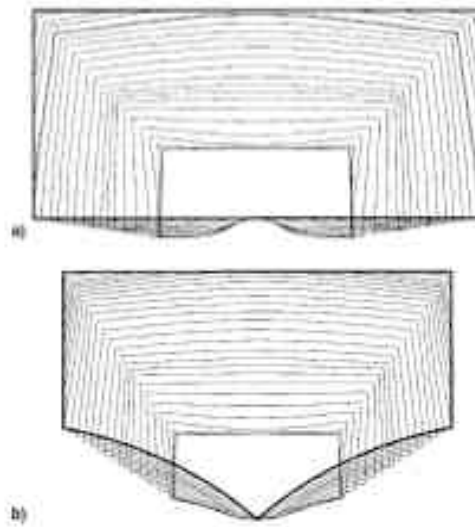
Figure 1.5. Inlet cross-sectional shape distributions for different rectangular capture

areas. *a.) Rectangular capture shape b.) Rectangular shape used for REST inlets.*[12]
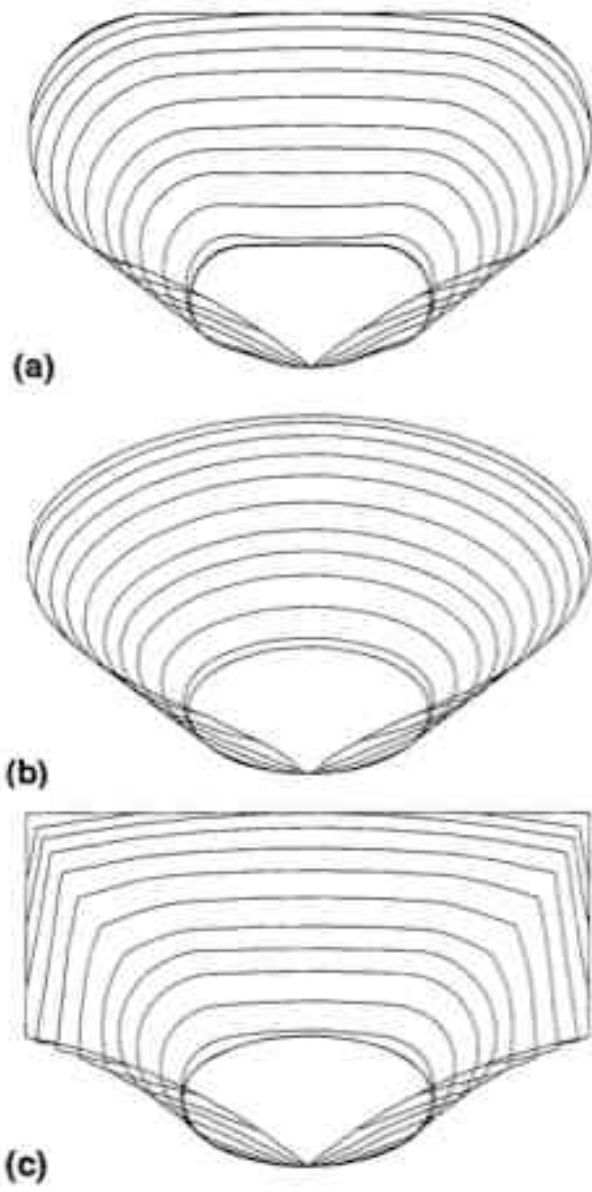
Figure 1.6. Cross-sectional shapes for the three blended inlets for constructing

a REST inlet.[13]

A mathematical lofting procedure smoothly blended the streamlines together to produce a smooth transition from rectangular capture area to elliptical combustor. Smart used the lofting procedure developed by Barger[14] with a free parameter that can be adjusted to optimize the inlet for maximum total pressure recovery or minimum exit flow non-uniformity. The blended inlet cross-section between inlet capture x_{ca} and cowl closure x_{cc} was calculated using the following formula with $f_1(y)$ and $f_2(y)$ represented by the cross sections of the shapes in Figures 1.5.b and 1.6.a. respectively:

$$f(y) = [f_1(y)]^{1-E(x)} [f_2(y)]^{E(x)} \tag{1.8}$$

where

$$E(x) = \left(\frac{x - x_{ca}}{x_{cc} - x_{ca}} \right)^{\alpha} \tag{1.9}$$

and α is a parameter always greater than zero that can be modified to optimize the performance of the transition duct. Smart used a similar calculation procedure to blend the shapes in Figures 1.6.b and 1.6.c. A resulting transition is shown in Figure 1.7.
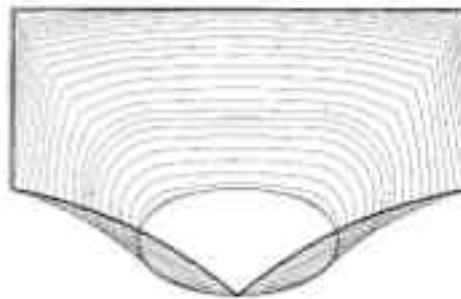
Figure 1.7. Cross-sections of a blended REST inlet.[12]

The above design procedure produced an inlet that performs better than similar two-dimensional inlets. The inlets Smart designed assumed a vehicle cruising at Mach 7 with Mach 6 flow entering the inlet with a required inlet compression ratio $\frac{P_{throat}}{P_\infty} = 13.50$. Because the flow is not necessarily uniform at the throat, Smart used mass-averaging to calculate these parameters. There are other methods of calculating the total performance of the inlet with flow non-uniformities such as area- or temperature-averaging, although mass-averaging is typically used for inlet performance analysis. All of these methods still have their flaws as they are averages. Tables 1.1-1.3 contain these performance values calculated with a three-dimensional CFD flow solver for a Mach 6.0 REST inlet under inviscid flow assumptions for on-design and off-design Mach numbers compared to a rectangular inlet. Even at off-design conditions, the REST inlet performed better than the rectangular inlet.

Property	Mach 3.6	Mach 4.8	Mach 6.0
m_c	84.40%	94.00%	99.50%
P_{throat}/P_∞	14.8 +/- 3.0%	13.7 +/- 19.1%	13.8 +/- 9.8%
ψ	2.19 +/- 2.2%	2.16 +/- 5.8%	2.16 +/- 6.4%
M_{throat}	1.77 +/- 2.7%	2.82 +/- 5/3%	3.74 +/- 4.2%

Table 1.1. Characteristics of inviscid Mach 6.0 REST inlet

Property	Mach 3.6	Mach 4.8	Mach 6.0
π_c	0.960	0.932	0.926
η_{KE}	0.995	0.996	0.997
η_{KD}	0.99	0.982	0.981
C_D	0.349	0.185	0.114
L_{in}/d_h	17.57	17.57	17.57

Table 1.2. Inviscid performance of Mach 6.0 REST inlet

Property	Mach 3.6	Mach 4.8	Mach 6.0
π_c	0.784	0.795	0.791
η_{KE}	0.972	0.985	0.99
η_{KD}	0.945	0.946	0.945
C_D	0.348	0.193	0.125
L_{in}/d_h	7.9	13.26	18.08

Table 1.3. Inviscid performance of 2D rectangular inlet for comparison[12]

The final stage of constructing REST inlets consisted of finding an inlet height correction to correct for the boundary layer growth in the inlet. To determine the viscous correction, Smart used a finite difference boundary layer code based on several assumptions that simplify the full three-dimensional turbulent boundary layer equations.

- $w \ll u$ where w is the cross flow velocity and u is the stream-wise velocity

- Cross flow derivatives $\partial/\partial z$ are small compared to other terms in the governing equations.

Corner flows are not examined as corners in REST inlets are quickly smoothed out. Smart calculated a Mach 6.0 REST inlet to have a total pressure ratio of 0.465, kinetic energy efficiency of 0.966, and adiabatic compression efficiency of 0.849 with the boundary layer comprising 36% of the inlet exit flow. A Mach 6.0 REST inlet was also tested experimentally and found to have slightly lower performance than predicted but higher performance than previously-tested three-dimensional inlets.[15]

Sabean and Lewis developed a method for designing the transition duct of a rectangular-to-circular inlet to transform non-uniform inflow into uniform flow into the combustor.[16,17] Sabean used two optimizations for developing the transition duct – a configuration with uniform flow entering the inlet and an inversely derived power law flow field inflow. The objective was to produce uniform flow to the combustor for a Hyper-X like cruiser at Mach 10. To achieve this objective, a numerical optimization was used to iteratively determine geometries that minimize the standard deviation in pressure across the combustor plane. To bound the design space and reduce runtime of the optimization, a Bezier-Bernstein curve was used with six coordinates as control points corresponding to portions of the inlet that are allowed to vary.

The shapes of the cross-sections were determined by averaging the combustor cross-section shape with the capture shape defined by a hyper ellipse of power $n = 20$. For intermediate planes, the cross-sectional shape were averaged using two fractional values - Δ_u and Δ_x - that were included as design variables for six intermediate planes that can change during the optimization. The radius for a given angle for the intermediate plane was determined by:

$$(1-\Delta_x)(R_{hyperellipse})+\Delta_x(R_{circle})= R_{final} \tag{1.10}$$
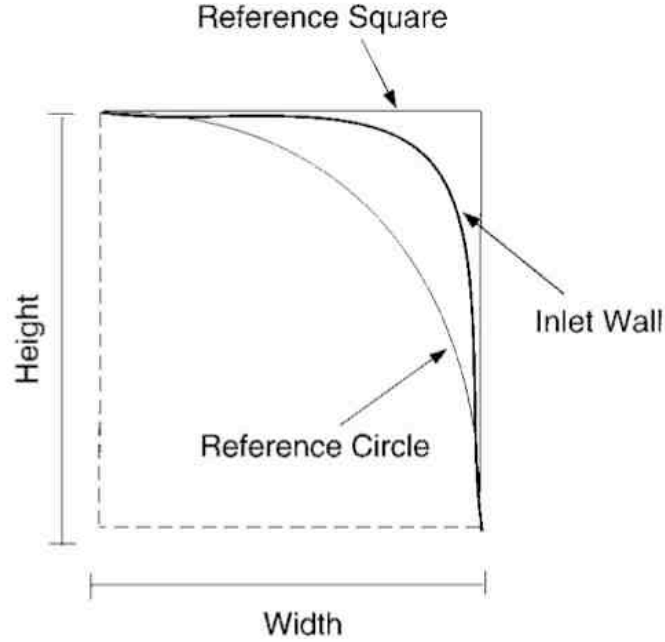
Figure 1.8. Geometric parameters used during construction of cross-sections

This shape was then scaled by the height of the plane determined by the Bezier-Bernstein curve and the width of the plane. An example of this process is shown in Figure 1.8.

An area-averaged standard deviation of the pressure was chosen as the objective function for optimization. Average pressure is calculated as follows:

$$\bar{P} = \frac{\sum P_i A_i}{\sum A_i} \tag{1.11}$$

and standard deviation of pressure calculated from the area-averaged pressure is as follows:

$$\sigma_p = \sqrt{\frac{\sum A_i (P_i - \bar{P})^2}{\sum A_i}} \tag{1.12}$$

18

This was calculated over three planes between the expansion corner and the exit, averaging each value to ensure that the optimizer does not converge to a local minimum at exactly where the shock wave reflects off of the wall. This was necessary as otherwise the optimizer would pick a flow that while produced the desired outflow at the exit, it would diverge and not follow the isolator wall. The calculation was also extended into the combustor to minimize expansion and compression waves going into the combustor. Figure 1.9 shows the pressure contours inside the optimized non-uniform inflow inlet.
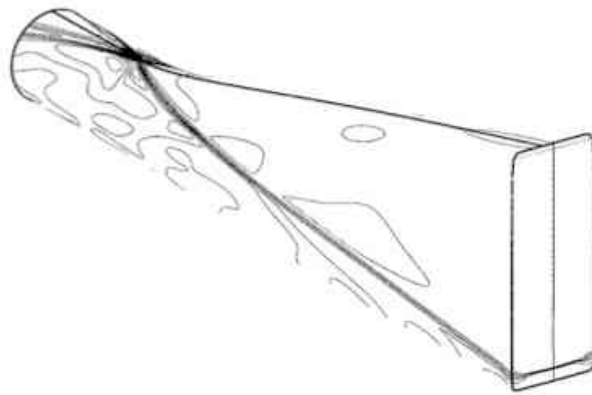
Figure 1.9. Pressure contours for optimized non-uniform inflow inlet

Sabean found that under inviscid flow assumptions the optimized inlet with uniform flow across the capture plane performed slightly better than comparable two-dimensional inlets at on-design and off-design Mach numbers. Calculated results for total pressure recovery π_c, adiabatic compression efficiency η_c, and kinetic energy efficiency η_{KE} compared to a comparable two-dimensional inlet are shown in

Tables 1.4-1.6. Sabean also found that some of the geometries that cancelled the shock waves were non-intuitive such as an inlet shape that transitioned multiple times between rectangular and a circular cross-sections. Inlets produced with this method could also correct non-uniformities inherent in the flow off the fore-body.

Efficiency	Mach 6.0	Mach 8.0	Mach 10.0
π_c	0.689	0.543	0.413
η_c	0.949	0.934	0.924
η_{KE}	0.984	0.985	0.924

Table 1.4. Efficiencies of inlet created with an optimized rectangular-to-circular transition with a power law compression.

Efficiency	Mach 6.0	Mach 8.0	Mach 10.0
π_c	0.736	0.614	0.489
η_c	0.958	0.946	0.937
η_{KE}	0.987	0.988	0.988

Table 1.5. Efficiencies of inlet with an optimized rectangular-to-circular transition with uniform inflow.

Efficiency	Mach 6.0	Mach 8.0	Mach 10.0
π_c	0.716	0.560	0.427
η_c	0.944	0.934	0.929
η_{KE}	0.986	0.986	0.986

Table 1.6. Efficiencies of 2D inlet for comparison.

Taylor and Van Wie studied another method for creating the transition duct that involved using several functions to blend together two separate flow fields corresponding to the desired capture and combustor shapes[18]. A Busemann inlet was selected as the parent flow field. Pairs of streamlines corresponding to the Busemann flow field and a rectangular inlet flow field were blended together with blending functions by using a weighted average of the coordinates on the streamlines. The location where the streamlines were blended was chosen such that each point was on the same conically symmetric ray on the parent Busemann flow field. Figure 1.10 illustrates this method and how morphing and tracing pairs were determined. Blending functions chosen are shown in Figures 1.11 and Figure 1.12. These blending functions were normalized to vary between 0 at the freestream and 1 at the inlet exit as a function of the angle swept from freestream to exit. The value on the y-axis was normalized such that it was multiplied by the coordinates of the second streamline (combustor shape). The first streamline (capture area shape) was multiplied by one minus the y-axis value.
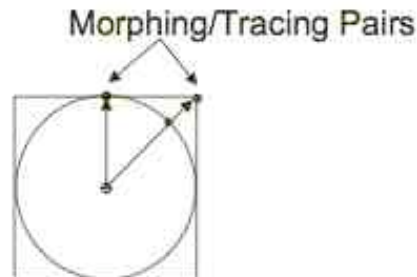
Figure 1.10. Morphing and tracing pairs for calculating inlet transition[18]

Taylor and Van Wie found that the inverse tangent blending function led to the best performance for an inlet designed for a freestream Mach number of 7. They used a CFD code VULCAN that is a full Navier-Stokes solver with finite-rate kinetics capabilities. The viscous solution was run with a k-omega turbulence model. Results for the inviscid and viscous cases are shown in Tables 1.7 and 1.8. The blending functions that performed the best had more gradual change in the middle of the angle sweep (middle of the inlet) and most of the transition near the entrance or throat of the inlet. Quickly changing streamlines near the center of the floor of the inlet caused additional losses that became significant when viscous effects were included. The ideal blending functions found might not necessarily be the better blending function at different Mach numbers.

$$\text{invtan\_f}(x) := \frac{1}{2} + \frac{1}{10} \cdot \tan(2 \cdot x \cdot \text{atan}(5) - \text{atan}(5))$$

$$\text{pp5\_f}(x) := x^{0.5}$$

$$\text{pow\_f}(x) := 1 - 1000^{-x}$$

$$\text{line\_f}(x) := x$$

$$\text{p2\_f}(x) := x^{2}$$

$$\text{tan\_f}(x) := \frac{\text{atan}(x \cdot 10 - 5) - \text{atan}(-5)}{-2 \cdot \text{atan}(-5)}$$

Figure 1.11. Blending functions[18]
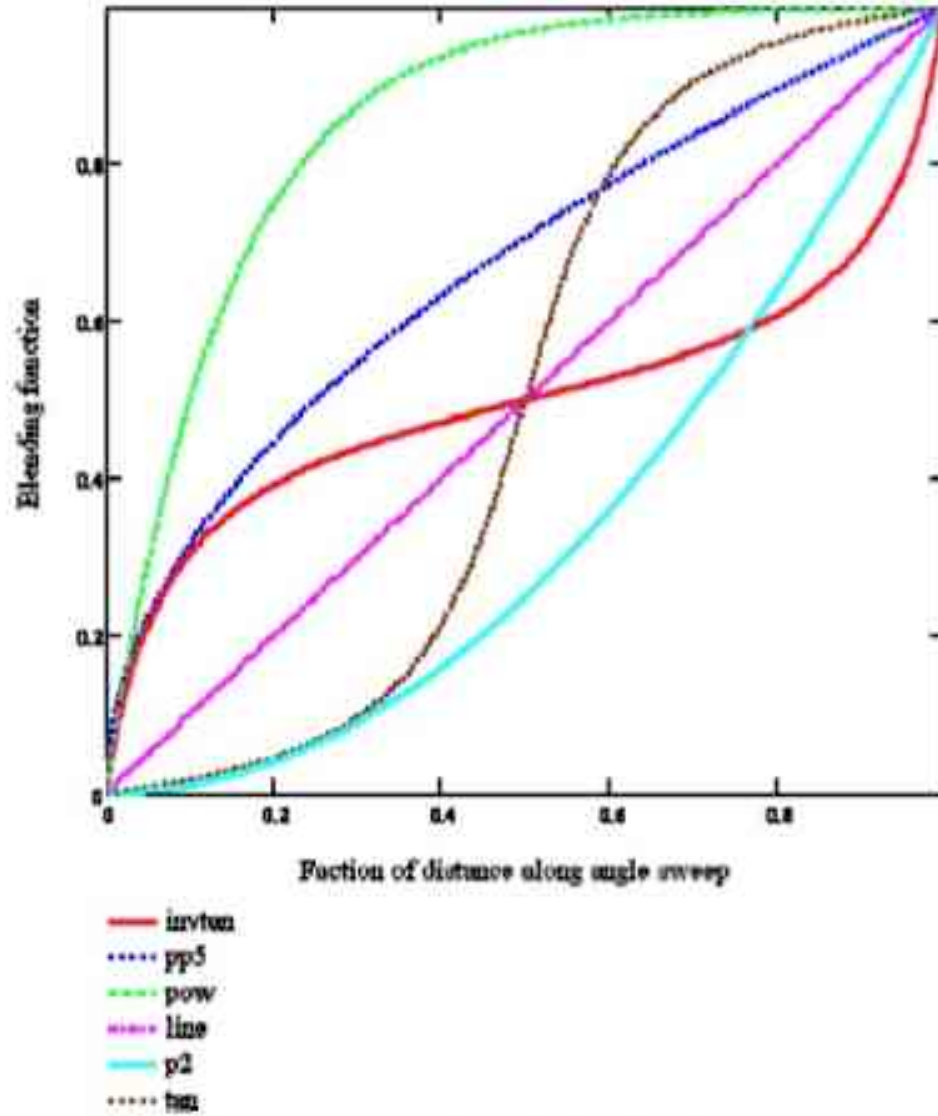
Figure 1.12. Weighting value for each blending function[18]

Function	Total Pressure Loss %	Drag Increase %
invtan	2.300	1.220
pp5	3.16	1.97
power law	3.34	2.27
line	3.92	3.14
p2	4.82	4.29
tan	14.66	17.01

Table 1.7. Inviscid performance results for each blending function

Function	Total Pressure Loss %
Baseline	28.842
invtan	34.875
pp5	34.977
power law	37.101
line	36.562
p2	37.418
tan	57.68

Table 1.8. Viscous performance results for each blending function

1.3.3. Summary and motivation

An analytical method based on the aerodynamics of the flow entering the inlet could provide additional insight into the design and performance of three-dimensional blended inlets. Current methods for designing these inlets are based on geometric, computational, or mathematical formulations rather than using aerodynamics to create the transition between the two shapes. A streamline traced inlet or an inlet designed based on aerodynamic analysis rather than computation or geometric methods could potentially have better performance. This study examines the feasibility of using compound compressible flow theory to construct and analyze an inlet with a rectangular capture shape and a circular or elliptical combustor.

1.4 Compound compressible flow

1.4.1 Compound compressible flow theory

Compound compressible flow theory as developed by Bernstein, Heiser, and Hevenor[19] is pursued in the present work to provide an analytical aerodynamic method for analyzing the flow in a three-dimensional inlet. Compound compressible flow theory uses Shapiro's classic influence coefficient method[20] for quasi-one-dimensional flow to model the behavior of non-uniform quasi-one-dimensional flows of discretized streamtubes. Shapiro's influence coefficient method writes the governing equations of fluid flow as a series of logarithmic differentials such as pressure dP/P, Mach number squared dM^2/M^2, and temperature dT/T as dependent variables and differentials such as area dA/A, the shear force $4f\,dx/D$, and heat added or subtracted dT_0/T_0 as independent variables to model a quasi-one-dimensional flow. The coefficients of the independent variables are termed *influence coefficients* as they indicate the influence of each independent variable on the dependent variables. These relations are derived from the equations for conservation of mass, momentum, and energy and relations between the variables. Classic solutions for propulsion analysis using these influence coefficients include flow in a duct with area change and flow in a duct with constant area and friction (Fanno) or heat added (Rayleigh). The relations for flow with area change, constant mass flow, no friction effects or heat added are the following:

25

$$\frac{dP}{P} = \frac{\gamma M^2}{1 - M^2} \frac{dA}{A} \qquad (1.13)$$

$$\frac{dM^2}{M^2} = \frac{-2\left(1 + \frac{\gamma - 1}{2} M^2\right)}{1 - M^2} \frac{dA}{A} \qquad (1.14)$$

$$\frac{dT}{T} = \frac{(\gamma - 1) M^2}{1 - M^2} \frac{dA}{A} \qquad (1.15)$$

Bernstein, Heiser, and Hevenor modified Shapiro's influence coefficient method by extending it to a number of quasi-one-dimensional streamtubes with different properties. They used compound compressible flow theory to analyze the behavior of one or more gas streams flowing through a single nozzle.[19] Comparison to experimental test results by Bernstein, Heiser, and Hevenor show excellent agreement with numerical predictions from this theory. In compound compressible flow theory, each streamtube is treated independently as a single-stream one-dimensional flow but compounded together with pressure chosen as the dependent matching variable for the whole flow. Pressure is chosen because it can only vary along the axial direction of the duct in a one-dimensional flow, while all other streamtube properties can change from streamtube to streamtube. This assumes that flow in each streamtube is adiabatic, isentropic, steady, and that each fluid is a perfect gas with constant thermodynamic properties. By matching the pressure across N streamtubes at each axial location, the evolution of streamtubes in an inlet can be traced based on the local area change A_i, area of the inlet A, pressure P, and local Mach number M_i

according to the relationships found by Bernstein, Heiser, and Hevenor. From Eqn. 1.13 for pressure and the following expressions for area change,

$$A = \sum_{i=1}^{n} A_i \qquad (1.16)$$

$$\frac{dA_i}{dx} = \frac{A_i}{\gamma}\left(\frac{1}{M_i^2} - 1\right)\frac{d \ln P}{dx} \qquad (1.17)$$

Eqns. 1.16 and 1.17 can be combined to form an expression for the compound flow parameter B

$$\frac{d \ln P}{dx} = \frac{dA/dx}{\displaystyle\sum_{i=1}^{n} \frac{A_i}{\gamma}\left(\frac{1}{M_i^2} - 1\right)} = \frac{1}{B}\frac{dA}{dx} \qquad (1.18)$$

where the compound compressible flow parameter is defined by,

$$B = \sum_{i=1}^{n} \frac{A_i}{\gamma}\left(\frac{1}{M_i^2} - 1\right) \qquad (1.19)$$

When B is positive, the channel is "compound subsonic" even if some streamtubes are supersonic, meaning that the overall flow is elliptical in nature and behaves as a subsonic flow. With a negative value of B, the entire flow is hyperbolic and behaves as a supersonic flow. A value of B equal to zero corresponds to choked flow and the flow will not accept further reductions in area. This method does not work so well for streamtubes with low Mach numbers such as streamtubes near the wall in a boundary layer as those streamtubes will dominate the flow because of the $\frac{1}{M^2}$ dependence. Methods for incorporating streamtubes near the wall is presented in the viscous methodology section later in this work.

For the case of hypersonic flow through an inlet, the flow is generally

compound supersonic and the flow properties become uncoupled when the initial and

final pressures are know. The pressure matching assumption holds if streamtube

curvature is sufficiently negligible that transverse pressure gradients can be neglected

or specified because the crossflow velocity gradients are negligible. Otherwise, if the

transverse pressure gradients are significant, the flow can no longer be considered a

quasi-one-dimensional flow and the streamtubes are no longer at the same pressure.

Once the pressure matching condition is satisfied, the streamtubes can be treated

independently. These flow properties can be determined by treating each streamtube

as a quasi-one dimensional flow governed by Shapiro's influence coefficient method

with Eqns. 1.14 and 1.15 for a simple area change without heat addition or frictional

effects.

1.4.2 Previous work using compound compressible flow

Although Bernstein, Heiser, and Hevenor developed compound compressible

flow theory for modeling compound choking in nozzle flow, this method can be used

for modeling hypersonic flow in any duct or on a vehicle fore-body as outlined in

Lewis and Hastings[21,22] and Barkmeyer[23]. Barkmeyer developed an analytic

methodology based on compound compressible flow theory for constructing a duct

for high-speed wind tunnels to correct flow non-uniformities upstream of a test model

or an inlet. When initial and final conditions are specified, an inverse design for the

correcting duct defined by the total area change of the flow can be created. Figure

1.13 shows the problem for which the methodology was developed.

28
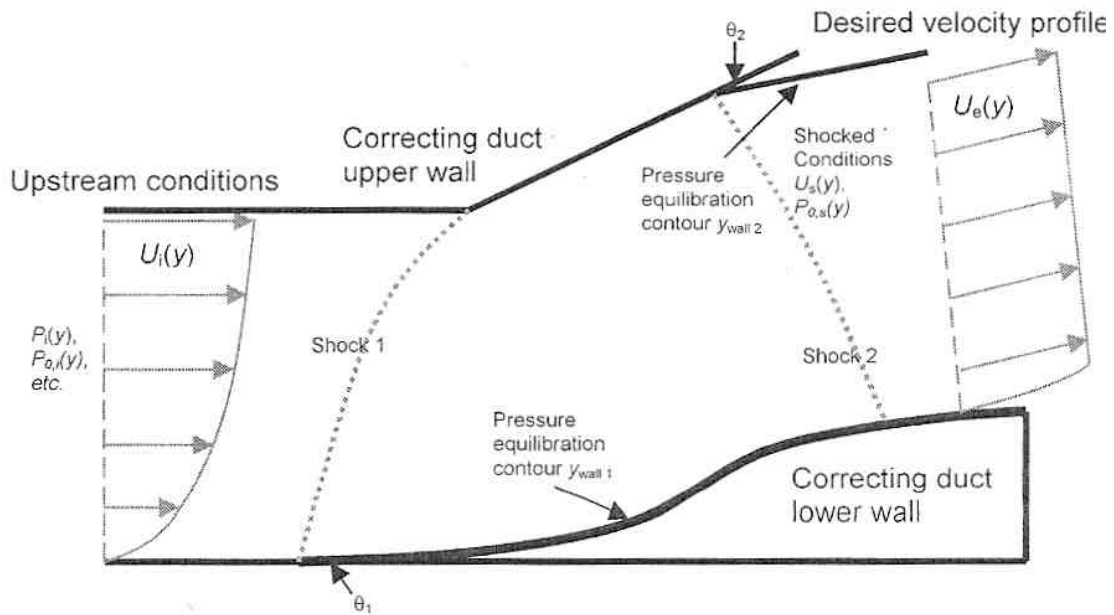
Figure 1.13. Development of correcting duct

Barkmayer used a power law variation in Mach number as the incoming profile. As the duct had shock waves inside, some modifications were required. A shock wave solution was determined that would distort the flow into a desired arbitrary flow profile. Using the pressure matching condition along with a single tube relation from Lewis[24] for the channel height based on the pressure of each streamtube immediately behind the shock for hypersonic flow,

$$H = \left(\frac{1}{H} \int_0^H P_i^{\frac{1}{\gamma}} \, dy \right)^{\gamma} \tag{1.20}$$

the equilibration pressure and profiles behind each shock were determined. The final static pressure was found by Newtonian iteration to match the exit flow to a total

29

pressure that matched the conditions for equilibrium. Compound compressible flow theory was then used to model pressure, temperature, and Mach number behind the shockwave as pressure was increased or decreased to the equilibrated pressure.

This method originally tried to match a final velocity profile but had to be altered to find a total pressure profile at the exit rather than a specified velocity profile, because many combinations of exit and entrance flow profiles required nearly sonic flow behind the last shockwave. Compound compressible flow tends to fail as the flow approaches sonic conditions. In addition, subsonic or nearly sonic solutions are not applicable to flow in a scramjet. An optimization scheme was used to find the optimal number of wedge shocks to produce the total pressure profile determined. This method was able to correct the flow into a uniform flow but produced shock shapes that demonstrated rippling – a non-physical solution.

1.4.2.a Viscous Analysis – Compound Compressible Flow in a Combustor

Lewis and Hastings[21,22] used a multi-stream compound compressible flow model to calculate flow in a combustor and model a boundary layer. They also defined parameters to match a non-uniform flow to a corresponding uniform flow. For a non-uniform flow, a uniform equivalent Mach number $\bar{M}$ determined by,

$$\left(\frac{1}{\bar{M}^2}-1\right)\sum_i \frac{A_i}{\gamma_i} \equiv \sum_i \frac{A_i}{\gamma_i}\left(\frac{1}{M_i^2}-1\right)$$

$$\bar{M} = \frac{1}{\sqrt{1+\dfrac{\gamma_{average}}{A_{total}}}} \tag{1.21}$$

A streamtube with a uniform equivalent Mach number $\bar{M}$ subjected to area change

will behave the same as the non-uniform flow consisting of multiple streamtubes over

the same area. However, this only applies at a given station in the channel. A new

uniform equivalent Mach number must be calculated for a different area change. The

entire non-uniform flow cannot be replaced by this Mach number.

A two-stream model was also analyzed to compare the effect of a low Mach

number streamtube – perhaps corresponding to a boundary layer – on a hypersonic

streamtube. If one of the streamtubes has a low Mach number M_1, the hypersonic

streamtube at M_2 will experience little area change. The hypersonic streamtube

experiences an area change equivalent to

$$\frac{dA_2}{A_2} = \left[\frac{1}{1+(M_2^2/M_1^2)\left[(1-M_1^2)/(1-M_2^2)\alpha\right]}\right]\frac{dA}{A_2} \tag{1.22}$$

and the low-velocity streamtube will experience an area change equal to

$$dA_1 = \left[\frac{-(1-M_1^2)\alpha}{M_1^2-(1-M_1^2)\alpha}\right]dA \tag{1.23}$$

where $\alpha = \dfrac{A_1}{A_2}$ and $A = A_1 + A_2$.

For values of $M_1^2 < \dfrac{\alpha}{\alpha-1}$, the hypersonic streamtube will experience an area

change in the opposite direction to that of the channel. If the low Mach number

streamtube takes up enough area, it could drive the behavior of the entire channel. As

the streamtubes are coupled because of pressure matching, the two streamtubes will

accelerate or decelerate together. Comparing the behavior of Mach number of a single

streamtube to that of double streamtube, demonstrates that the two-stream flow in a

converging channel will tend towards choking. This has ramifications for a scramjet,

which may have a thick boundary layer that could drive the flow towards choking

even if the Mach number of the hypersonic streamtube has decreased slightly. Lewis

and Hastings also evaluated methods for modeling a boundary layer and handling low

velocity streamtubes near the wall that incorrectly dominate the solution. This

analysis will serve as the basis for some of the viscous solutions presented later as a

part of this current research. This analysis was extended to the case of a constant area

combustor with heat addition with analytical closed form solutions analyzed and

boundary layer growth numerically calculated to study the effects of the boundary

layer on the flow in the combustor.

Chapter 2: Compound Compressible Flow Methodology

2.1 Objectives

This present work focuses on developing a methodology for designing a scramjet inlet with a different capture than combustor shape using compound compressible flow theory for both inviscid and viscous flow with a shock wave is presented. Compound compressible flow theory is used to provide a streamline-traced inlet for three-dimensional shape-changing inlets and an analytical method for analyzing the performance of these inlets. Other design methods for these inlets are computationally intensive, requiring computational fluid dynamics and often designing and calculating the flow through multiple inlets. The compound compressible flow method presented here for designing an inlet presented can provide a rapid first order solution and allow for many multiple design iterations to inform the design process. This method is based on first principles and the basic physics of hypersonic flow through an inlet.

Because the goal of a hypersonic scramjet inlet is to produce a particular inflow into the combustor, streamtube properties are traced inversely from the inlet throat to capture plane with the intention of solving for a flow entering the inlet that will produce the desired profile entering the combustor for a given rectangular-to-circular area transition. A profile can be specified at the throat with the intention of finding a shock structure and incoming flow that will produce that

specified profile at the throat. Although this research was motivated by finding an

analytic process for designing the transition in a three-dimensional rectangular-to-

circular inlet, it can apply to a variety of inlet types and design and flow problems

that incorporate a shock wave with a specified downstream flow profile. Specific

examples of this methodology developed are presented for two three-dimensional

inlet designs with a rectangular capture area and circular combustor.

2.2 Inviscid

Inverse streamtube tracing in an inlet adds several simplifications to compound

compressible flow theory. As mass is conserved in the inlet, an additional relationship

for constant mass flow described in Bernstein et al.[19] governs the evolution of each

streamtube under the assumptions of isentropic flow. The adjacent static pressure

between two adjacent streamtubes for constant γ and specific gas constant R can be

described by

$$\frac{w_2\sqrt{T_{0,2}}}{w_1\sqrt{T_{0,1}}} = \sqrt{\left[\frac{A}{A_1^*}\left(\frac{2}{\gamma-1}\right)\left(\frac{\gamma+1}{2}\right)^{\frac{\gamma+1}{\gamma-1}}\right] - \left(\frac{P_{0,1}}{P}\right)^{\frac{1}{\gamma}}}\sqrt{\left[1-\left(\frac{P}{P_{0,1}}\right)^{\frac{\gamma-1}{\gamma}}\right]} \times \sqrt{\left[1-\left(\frac{P}{P_{0,2}}\right)^{\frac{\gamma-1}{\gamma}}\right]\left(\frac{P_{0,2}}{P_{0,1}}\right)\left(\frac{P}{P_{0,2}}\right)^{\frac{1}{\gamma}}}$$

(2.1)

where A_i^* and w_i - assuming constant and known total pressure $P_{0,i}$, total

temperature $T_{0,i}$, and gas properties - are described by

34

$$A_1^* = \frac{w_i \sqrt{T_{0,i}}}{p_{0,i}} \sqrt{\frac{R}{\gamma}\left(\frac{\gamma+1}{2}\right)^{\frac{\gamma+1}{\gamma-1}}} \tag{2.2}$$

$$w_i = \frac{A_i P_{0,i}}{\sqrt{T_{0,i}}}\left(\frac{P}{P_{0,i}}\right)^{\frac{1}{\gamma}} \sqrt{\frac{2}{R}\left(\frac{\gamma}{\gamma-1}\right)\left(1-\left(\frac{P}{P_{0,i}}\right)^{\frac{\gamma-1}{\gamma}}\right)} \tag{2.3}$$

Because flow through the inlet is adiabatic, isentropic between the shock waves, and is uniform at the start of the inverse streamtube process, this equation can be reduced to a constant W for all streamtubes based on γ, M_i, $P_{0,i}$, and P_i that can be used to determine A_i

$$W = A_i P_{0,i}\left(\frac{P}{P_{0,i}}\right)^{\frac{1}{\gamma}} \sqrt{1-\left(\frac{P}{P_{0,i}}\right)^{\frac{\gamma-1}{\gamma}}} \tag{2.4}$$

Solving for A_i at each step in each streamtube combined with Eqns. 1.14, 1.15, 1.18 and 1.19 for temperature, Mach number, pressure, the compound compressible flow parameter, and the pressure matching criteria will fully specify the flow as the solution is propagated in an isentropically and adiabatically in a duct with an arbitrary profile.

Although most applications of compound compressible quasi-one dimensional flow theory have involved axi-symmetric or two-dimensional shapes, the methodology works with three-dimensional shapes as well. For the two-dimensional case consisting of a discrete series of streamtubes the compound compressible flow parameter is,

$$B = \sum_{0}^{N_H} \frac{h_i}{\gamma} \left(\frac{1}{M(y)^2} - 1 \right) \tag{2.5}$$

where H is the height of the channel. Because the compound compressible flow parameters add linearly, they can be calculated at each channel along the cross-wise direction (z-axis) and summed accordingly,

$$B = \sum_{0}^{N_A} \frac{A_i}{\gamma} \left(\frac{1}{M(y,z)^2} - 1 \right) \tag{2.6}$$

where conceptually the change in area has the same effect as a change in height.

However, in the case of significant three-dimensional effects like large surface curvature, the pressure matching criteria no longer holds because of the existence of a pressure gradient created by centrifugal effects and the assumption that the flow is essentially one-dimensional no longer holds. In addition, the presence of a curved shock caused by non-uniform flow also creates a pressure gradient that requires modification to this theory.

2.3 Inviscid with shock wave

The presence of a shock wave in the inlet does present some complications requiring slight modifications to this method. The current work includes a method for incorporating an oblique shock into compound compressible flow theory. A previous attempt was made to incorporate a shock wave into compound compressible flow theory by Barkmeyer.[23] However, this method presented by Barkmeyer took a known non-uniform upstream flow and tried to solve for a shock wave that would produce a to-be-determined uniform flow at the exit. Calculations using this method often produced unphysical solutions such as rippling shocks or non-applicable solutions or singularities, such subsonic or nearly sonic flow behind the final shock, which made the method not applicable for a scramjet. The method developed for the research presented here avoids these problems by using a known uniform flow downstream and solving for the flow upstream ahead of the shock based on propagating the solution from the exit to the shock boundary. This flow will not be subsonic or transonic behind any shock wave and the greater flexibility in choosing the shock wave avoids shock ringing and unphysical shocks. This method that follows is also conceptually easier to understand, analyze, and implement.

As this is an inverse method, the exact shock wave shape is not known because the Mach number in front of each shock boundary is not uniform, and is thus determined based on the flow properties behind the shock wave resulting from tracing

the streamtubes. An initial constant shock angle β and location is assumed based on the chosen length of the inlet L, contraction ratio CR, and cowl location x_c. The pressure in front of the shock is determined based on reverse solution of the Rankine-Hugoniot equations. The Mach number, total pressure and the actual shock angle are determined by the oblique shock relations with the constraint that the Mach number normal to and in front of the shock $M^2 \sin^2 \beta$ produces a pressure ratio determined by the pressure matching criteria.
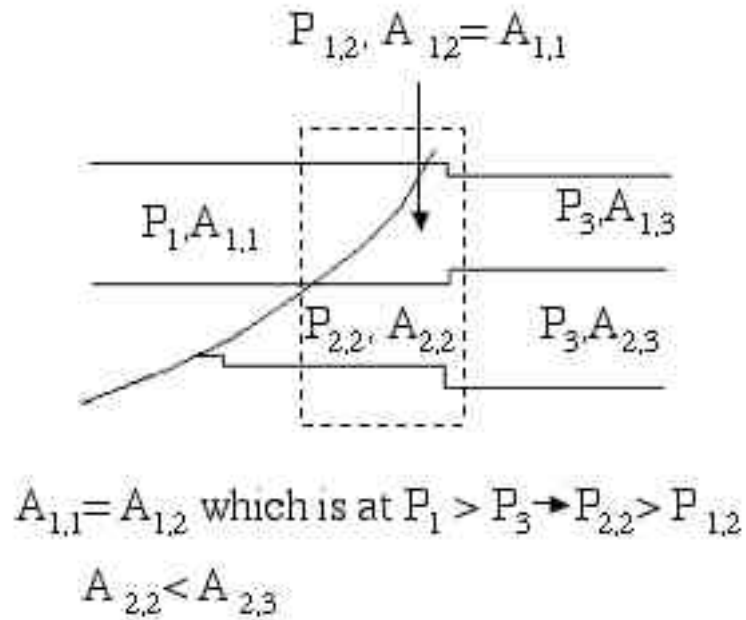

Figure 2.1. Pressure gradient established behind curved shock

Because of mass conservation in each streamtube and the non-uniformity of the flow and the curved shock, a pressure, temperature and Mach number gradient results behind the shock. Because of mass conservation requiring the streamtubes to have the same area on both sides of the shock, streamtubes crossing the shock wave from a lower pressure will have a higher area relative to the other streamtubes at a higher pressure behind the shock wave. The streamtube crossing the shock boundary will take up a larger area, causing the higher-pressure streamtubes to experience a reduction in area and decrease their areas and Mach numbers and increase their pressure and temperatures. The other streamtubes behind the shock wave respond to an area change equivalent to the change in the channel plus the change in area of the individual streamtube about to cross the shock boundary as shown in Figure 2.1. The pressure gradient allows the streamtubes to adjust their areas and smoothes out velocity, total pressure, and temperature gradients. Although the curved shock introduces a pressure gradient, the streamtubes re-equilibrate quickly.

For the inviscid solution, a pressure gradient behind the shock wave can be chosen to produce the desired shock strength with pressure in front of the shock wave determined by pressure matching between streamtubes. In previous research, because the conditions behind the shock were not known, the pressure gradient and pressure equilibration process was determined by Eqn 1.20. By knowing the conditions behind the shock and gradient, the pressure of the streamtube crossing the shock boundary can be arbitrarily chosen to maximize total pressure recovery for example or optimized along with the shock angle for some required attribute. The pressure

gradient is also constrained such as the solution is matched forward the shock angle either remains constant or decreases and towards the inlet sides that the shock angle either remains constant or increases. The temperature and area of the streamtube crossing the shock boundary corresponding to the gradient directly behind the shock wave is determined based on conserving mass, energy, and momentum. Because this is an inviscid solution and the equilibrated pressure is already known, this can be accomplished in one computational step as long as the pressure gradients are reasonable.

The location of the shock in the next streamtube is determining by propagating the shock through the inlet and solving at each streamtube for the shock angle, total pressure, and Mach number that satisfies the pressure matching criteria. In the calculated inlets, the shock is calculated at the top of each streamtube so the first shock calculation occurs for the first streamtube at the corner rather than a few steps into the inlet. Similarly, for the bottom streamtube, the shock is calculated one streamtube height above the floor for the initial and reflected shock. The shock angle at the cowl is specified based on a shock angle slightly higher than required to intersect the leading edge. For successful transition area functions, as the flow will have some non-uniformity, the shock angle is expected to vary only by a fraction across the streamtubes thus centrifugal effects resulting from highly curved shock waves that would invalidate using compressible flow theory will not be an issue. For a two-dimensional or axi-symmetric inlet, the shock wave is calculated when the

height of the shock minus the height of the streamtube next to cross the shock is less than zero.

For the three-dimensional case because area not height changes are tracked, the height of the shock is calculated based on the shock angle for the center streamtubes. To find the next shock calculation point, the distance between the current shock location and the intersection point with the top or bottom of the inlet is divided by the number of tubes that still need to cross the shock. Given that with a discrete profile the location of where the streamtube is calculated as crossing the shock boundary is somewhat arbitrary, for the sake of simplifying calculations, each streamtube channel crosses the shock boundary at the same location.

During streamtube propagation, the pressure on each side of the shock wave is determined using a compound compressible flow parameter B for only the streamtubes on the same side of the shock boundary. The streamtubes will experience an area change weighted by the number of tubes on the same side of the shock boundary. After calculating a new constant that governs mass flow based on inlet conditions W, a streamtube crossing the shock boundary can be propagated forward using the influence coefficient method and compound compressible flow parameter with the other streamtubes in front of the shock as presented in the previous section until a streamtube from that side of the shock boundary approaches a shock boundary and a gradient is formed. All streamtubes in front of a shock boundary are unaffected by the pressure gradient formed because information cannot be propagated forward in

supersonic flow and can be propagated all the way until either streamtubes meet another shock upstream or the capture plane.

2.4 Viscous

A modified version of compound compressible flow theory can also model a profile due to viscosity such as a boundary layer coming off a fore-body of a hypersonic vehicle into and through a scramjet inlet. At hypersonic speeds, boundary layer growth inside an inlet can have significant effects on engine performance. A large boundary layer can cause a blockage in the inlet, reducing the inlet contraction ratio and causing overcompression. If the blockage is too large, there is significant loss of mass flow to the engine and the inlet could unstart. There is also a reduction in static pressure recovery caused by shock and Mach waves no longer coalescing to a single shock. An analytic and computationally inexpensive method of calculating boundary layer growth in the transition duct of a three-dimensional inlet could provide a valuable design tool for increasing performance. However, this method is not intended to be a new method of calculating a boundary layer profile but rather to describe how the flow near the wall of the inlet responds to pressure changes and for the purposes of comparing the boundary layer growth in different inlet designs.

The model presented above for the inviscid case breaks down as Mach number goes to zero, causing the compound compressible flow parameter B to diverge and the lower Mach number streamtubes near the wall to dominate the flow despite their smaller areas. This implies that no matter how small the streamtubes

near the wall, the flow will be dominated by the wall. This results from the solution to the no-slip condition without viscosity of the one-dimensional conservation of momentum equation

$$\frac{du}{dx} = -\frac{1}{\rho u}\left(\frac{dP}{dx} - \frac{\partial \tau}{\partial y}\right)$$ (2.7)

and corresponds to the inviscid solution when $\partial \tau/\partial y = 0$. By adding a shear gradient term equivalent to the pressure gradient along the inlet, the flow near the wall can be correctly incorporated.

2.4.1 Viscous inlet shape correction

For designing a three-dimensional transition duct for a rectangular to elliptical or circular inlet, a viscous correction can be added to the base inviscid flow conceptually similar to the viscous correction described in Walsh et. al.[25] A correction to the inlet shape can be applied equivalent to the amount of mass displaced δ_* by the boundary layer, which is expressed by

$$\delta_* = \int_0^{\delta_{99}}\left(1 - \frac{\rho u}{\rho_e u_e}\right)dy$$ (2.8)
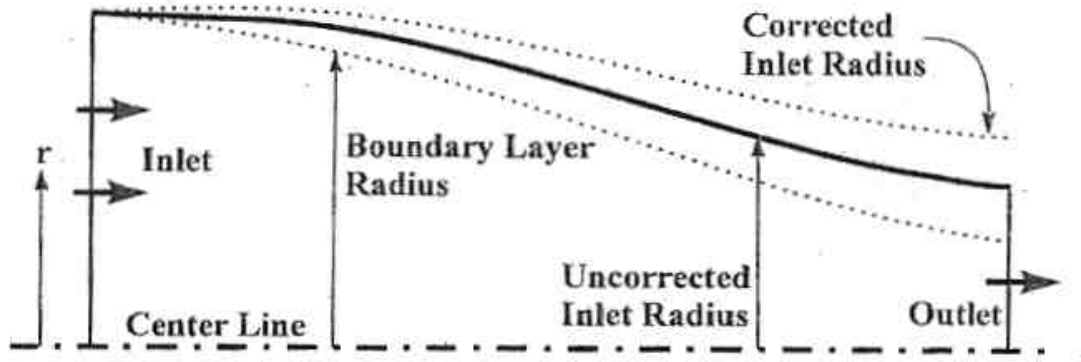
Figure 2.2. Corrected versus uncorrected inlet radius. [25]

It is assumed that this additional mass is added to the inviscid flow to produce a streamline displacement seen in the viscous solution. At hypersonic speeds, it is a well-known result that the displacement thickness and the height of the boundary layer where the velocity is 99% of the inviscid velocity are about the same thickness. An illustration of this is shown in Figure 2.2 for an axi-symmetric inlet. Walsh et al found that redesigning the inlet with this correction can decrease the overcompression from 24% to 3% and total pressure losses by 17%.[25] However, this method is often an iterative process that sometimes does not reach a converged solution. Previous research using compound compressible flow in a combustor by Lewis analyzed the effect of the boundary layer as a low-speed streamtube in a two-stream flow on the inviscid flow as the viscous and inviscid streamtubes were compounded together.[21] In this research, using a known underlying inviscid flow field, compound compressible flow theory can be used to find the height or area of the viscous correction, which is equal to the height or area of the boundary layer. From Shapiro's influence coefficient method[20] for pressure for flow with friction, using the explicit form for the shear gradient:

$$\frac{dP}{P} = \frac{\gamma M^2}{1-M^2}\frac{dA}{A} - \frac{1+(\gamma-1)M^2}{M^2-1}\frac{\partial\tau}{\partial y}\frac{dx}{P} \qquad (2.9)$$

The goal is to find the required area of the boundary layer to produce a pressure that matches the underlying inviscid flow. The pressure change dP/P is known already from the solution to the inviscid case. At $M_i = 0$, dP/dx exactly cancels $\partial\tau/\partial y$. The area used to determine the change in Mach number and temperature is the area of the total channel flow – the underlying inviscid flow area plus the area of the boundary layer. Unlike the inviscid solution, the solution is propagated from the capture area to the throat. Because pressure is matched to the inviscid flow and $\boldsymbol{B}$ can be added linearly, the compound viscous flow can be treated independently from the compound compressible inviscid flow. Because the compound compressible flow parameters add linearly and pressure is uniform and specified, for a three-dimensional inlet with non-uniform inviscid flow in a duct with different heights at each cross-stream station, constructing the three-dimensional boundary layer can be condensed to a two-dimensional compound compressible flow problem. The height of inviscid channel replaces the area of the channel in Eqns. 2.12 and 2.13 and the boundary layer height replaces the area and area change of the boundary layer in Eqns. 2.9 to 2.14. By re-arranging to solve for area change and knowing the pressure gradient, the area of the boundary layer can be found from

$$\frac{dA}{A} = \frac{-(M^2-1)}{\gamma M^2}\frac{dP}{P} + \frac{1+(\gamma-1)M^2}{\gamma M^2}\frac{\partial\tau}{\partial y}\frac{dx}{P} \qquad (2.10)$$

45

$$\frac{dA}{dx} = \sum_{-z}^{+z} \sum_{y=0}^{\delta_{99}} \frac{A_i}{\gamma} \left(\frac{1}{M^2} - 1 \right) \left(1 - \frac{\partial \tau / \partial y}{dP/dx} \right) \frac{d \ln P}{dx} - A_i \frac{\partial \tau / \partial y}{P} \tag{2.11}$$

where A is the area of the boundary layer A_δ. The first term represents the inviscid

solution for the effect of the logarithmic pressure gradient on the area change with a

viscous correction. The second term is new to the viscous solution and represents the

total shear at the wall. The compound compressible flow parameter for viscous flow

is thus,

$$B = \sum_0^A \frac{A_i}{\gamma} \left[\frac{1}{M^2 - 1} \right] \left(1 - \frac{\partial \tau / \partial y}{dP / dx} \right) \tag{2.12}$$

Without viscous effects, the compound compressible flow parameter and area change

relationship reduce to the inviscid limit and the form used by Bernstein et. al. Mach

number and temperature can also be propagated with an additional shear term:

$$\frac{dT}{T} = \frac{(\gamma - 1)M^2}{1 - M^2} \frac{dA}{A} + \frac{(\gamma - 1)M^2}{1 - M^2} \frac{\partial \tau}{\partial y} \frac{dx}{P} \tag{2.13}$$

$$\frac{dM^2}{M^2} = -\frac{2(1 + \frac{(\gamma - 1)}{2} M^2)}{1 - M^2} \frac{dA}{A} - \frac{2(1 + \frac{\gamma - 1}{2} M^2)}{1 - M^2} \frac{\partial \tau}{\partial y} \frac{dx}{P} \tag{2.14}$$

2.4.2 Corrections at the wall

Although the $1/M^2$ singularity cancels when $M = 0$ at the wall, low Mach number streamtubes will still dominate the flow. As discussed in Lewis and Hastings[21,22], it is insufficient to just cancel $1/M^2$ by setting $(1 - \frac{\partial\tau/\partial y}{dP/dx}) = 0$, rather $(1 - \frac{\partial\tau/\partial y}{dP/dx})$ must go as $1/M^2$ as M^2 approaches zero. In this model, $(1 - \frac{\partial\tau/\partial y}{dP/dx})$ will be assumed to be quadratic such that $(1 - \frac{\partial\tau/\partial y}{dP/dx}) = 1$ at the sonic line. This can be set to 1 above the sonic line because pressure changes are transmitted upstream only in the subsonic streamtubes. Because the sonic line is close to the wall in a hypersonic boundary layer, the exact power used is not important as long as the singularity at the wall is canceled. Subsonic streamtubes in this model will use this correction.

2.4.3 Fore-body assumptions

For the purpose of determining a boundary layer ingested into the inlet and the transition point to turbulent flow, some assumptions will be made about the nature of the flow coming off the fore-body. For the inlets constructed in this study, assuming an X-51 like configuration traveling at $M_\infty = 7$ at 80,000 feet, the inlet will be placed 1.5 meters along the fore-body. The X-51 is a missile with a scramjet designed to go between Mach 6 and 7 with a rectangular inlet placed about 1.5 meters along the fore-

body. These calculations assume a cold wall at 300 K. Any transition criteria can be used, but for the purposes of this research the transition point will be calculated based on a relation found by Lewis[22] from experimental results by Sheetz[26]

$$\mathrm{Re}_T = 6400(M_\infty)^{3.66} \qquad (2.15)$$

Other more recently developed methods can be used, such as an exponential e^N formulation developed by Malik[27] based on a correlating experimental results for transition with linear stability theory[28] of the growth of small disturbances in a laminar boundary layer. Using Eqn. 2.15 results in transition to a turbulent boundary layer at 1.69 meters or 0.19 meters in the inlet along the top and 1.69 meters along the sides. This method allows for a quick estimate of where transition occurs. The inviscid inlet height and area is scaled such that the shock off a fore-body with a 5-degree wedge angle will intersect the cowl.

2.4.4 Constructing the shear gradient

In addition, an initial boundary layer profile entering the inlet will need to be constructed. Once a profile is constructed – for either the laminar or turbulent case – it will be propagated down the channel with the intention of finding the boundary layer area or height according to Shapiro's influence coefficients with friction as outlined in Eqns 2.09 to 2.14. A shear gradient from friction effects solely at the wall will be calculated to determine how the profile propagates down the inlet.

Both a laminar and turbulent boundary layer will be evaluated for a three-dimensional inlet. Although the boundary layer is mostly turbulent along the top and a turbulent boundary layer is preferable for mixing in the combustor and decreased boundary layer separation, a laminar boundary layer will also be studied as this also represents the worst-case scenario. In addition, the flow along much of the bottom and sides of the inlet is laminar. The turbulent boundary layer velocity, temperature, and shear gradient profiles can be modeled using the velocity profile found by Perry and East[29] and temperature profile from Bertram and Cary[30] from experimental data.

$$\frac{u}{u_e} = \left(\frac{y}{\delta_{99}}\right)^{\frac{1}{7}} \tag{2.16}$$

$$\left(\frac{u}{u_e}\right)^2 = \frac{T_o - T_w}{T_{o,e} - T_w} \tag{2.17}$$

$$\frac{\partial \tau}{\partial y} = \mu(T)\frac{d^2 u}{dy^2} = -\frac{6}{49}\frac{\mu(T)}{\delta_{99}^2}\left(\frac{y}{\delta_{99}}\right)^{-\frac{13}{7}} + \frac{1}{7}\frac{d\mu(T)}{dy}\frac{1}{\delta_{99}}\left(\frac{y}{\delta_{99}}\right)^{-\frac{6}{7}} \tag{2.18}$$

where $\mu(T)$ for both the laminar and turbulent cases can be calculated based a power law relation because the temperature of each streamtube is known,

$$\mu(T) = \mu_e \left(\frac{T}{T_e} \right)^{.76}$$

(2.19)

Properties of the laminar boundary layer and the shear layer can be determined using analytical similarity solutions for a compressible boundary layer with a variable pressure gradient. Cohen and Reshotko[31] calculated similarity solutions for Falkner-Skan type compressible flows using a coordinate transformation to transform the problem into an incompressible flow problem with the coordinates ξ and η equal to

$$\eta = \sqrt{\frac{m+1}{2} \frac{u_e \rho_e}{\mu_e \xi} \frac{T_e}{T_0} \int_0^y \frac{T}{T_0} dy}$$

(2.20)

$$\xi = \int_0^x \rho_e(x) u_e(x) \mu_e(x) dx$$

(2.21)

Using a simplifying assumption that Prandtl number is equal to one to determine similarity solutions found by Cohen and Reshotko[32] to the momentum, enthalpy, and stagnation enthalpy equations for a laminar boundary layer will be used to determine the Mach number and temperature of the profile,

$$f''' + ff'' + \beta_{F.S.}(g - f'^2) = 0$$
$$g'' + fg' = -(\gamma-1)M^2 f''^2$$
$$S'' + fS' = 0$$

(2.22)

50

where $f'(\eta) = u/u_e$, the enthalpy function $S = h_s/h_0 - 1$ for a given $\beta_{F.S.}$, and

$S_w = T_w/T_0 - 1$. The exponent of velocity distribution based on the Falkner-Skan

parameter $\beta_{F.S.}$ that characterizes the underlying pressure gradient

$$m = \frac{\beta_{F.S.}}{2 - \beta_{F.S.}} \tag{2.23}$$

$$\beta_{F.S.} = \frac{2\xi}{u_e} \frac{du_e}{d\xi} \tag{2.24}$$

Using solutions to these relations, the Mach number and temperature can be

calculated as follows

$$T = T_0 \left[(1+S) - \frac{\left(\dfrac{\gamma-1}{2} M_e^2\right)}{\left(1 - \dfrac{\gamma-1}{2} M_e^2\right)} f'^2 \right] \tag{2.25}$$

$$M = \frac{u_e f'(\eta)}{\sqrt{\gamma R T}} = \frac{u_e f'(\eta)}{\sqrt{\gamma R T_o \left[(1+S) - \dfrac{\left(\dfrac{\gamma-1}{2} M_e^2\right)}{\left(1 - \dfrac{\gamma-1}{2} M_e^2\right)} f'^2 \right]}} \tag{2.26}$$

This creates a starting profile and shear layer that can be propagated using

Eqns. 2.13 and 2.14 for temperature and Mach number to then find the velocity ratio

f' to calculate η. Then, the height of the streamtube y and its area A_i can be

determined from mass conservation and summed over all the streamtubes to find the change in the boundary layer height. The shear stress

$$\tau = \mu_e \left(\frac{T}{T_e}\right)^{.76} u_e f''(\eta) \frac{d\eta}{dy} = \mu_e \left(\frac{T}{T_e}\right)^{.76} u_e f''(\eta) \frac{\int_0^{\eta_\delta} \frac{T}{T_o} d\eta}{\delta \frac{T}{T_0}}$$

$$\frac{\partial \tau}{\partial y} = \mu_e \left(\frac{T}{T_e}\right)^{.76} u_e f'''(\eta) \left[\frac{\int_0^{\eta_\delta} \frac{T}{T_o} d\eta}{\delta \frac{T}{T_0}}\right]^2 + \frac{\mu_e}{T_e}\left(\frac{T}{T_e}\right)^{-.24} \frac{dT}{dy} u_e f''(\eta) \frac{\int_0^{\eta_\delta} \frac{T}{T_o} d\eta}{\delta \frac{T}{T_0}}$$

(2.27)

and shear gradient can be calculated based on η in order to find the change in boundary layer height using Eqn. 2.4 and to march the solution for Mach number and temperature down the inlet. The starting boundary layer height δ based on the stated assumptions about the vehicle is 0.00272 meters (power law inlet) and .00149 (angle-defined inlet) calculated from

$$\delta_{99} = \sqrt{\frac{2}{(m+1)} \frac{\xi \mu_e}{u_e \rho_e} \frac{T_e}{T_o} \int_0^{\eta_\delta} \frac{T}{T_o} d\eta}$$

(2.28)

2.4.5 Modifications for flow near the sonic line

As the transonic streamtubes approach $M_i = 1$, a numerical instability results in the equations for propagating temperature and Mach number. As $M \rightarrow 1$, $\frac{1}{1 - M^2} \rightarrow \infty$ causing temperature and Mach number to blow up. For a boundary layer in an inlet and a reasonably constructed profile, at least one streamtube will approach Mach 1. This instability can be by-passed by changing the height of a streamtube too close to the sonic line by an infinitesimal amount - raising for a supersonic streamtube and lowering for the subsonic case. This is analogous to choosing to track another streamtube slightly higher or lower in a continuous profile. This modification occurred when Mach number was less than 1.08 for supersonic streamtubes and greater than 0.92 for subsonic streamtubes. Mass is still conserved as the model is tracking another streamtube and mass is conserved in a global sense by decreasing the mass of an adjacent streamtube. When the height of the streamtube is adjusted, the Mach number for that streamtube is calculated based on Eqn 2.26 as was used to set-up the original profile. The temperature and shear gradient are held constant. The similarity coordinate is calculated based on the adjusted height and the change in the similiarity coordinate with height. Streamtubes adjusted accordingly remain at about $M = 1$ with no instabilities in Mach number or temperature.

Chapter 3: Inlet Design

Although the above methodology can be used for a variety of hypersonic flow calculations with a shock wave or that require adding a correction due to a boundary layer, it will be tested specifically on two three-dimensional rectangular-to-circular inlet designs.

3.1 Design parameters

The feasibility of using this method is being studied using pre-designed area changes and geometries and approximate design performance parameters. The inlet will be designed for a X-51-like configuration traveling at Mach 7 with initial compression done by the fore-body to produce Mach 6 flow entering the inlet. The X-51 and the intended location on the fore-body is shown in Figures 3.1 and 3.2. The inlet geometries were chosen based on X-51 inlet and fore-body lines provided by AFRL[33]. The inlets were designed with the physical and performance parameters outlined in Table 3.1.
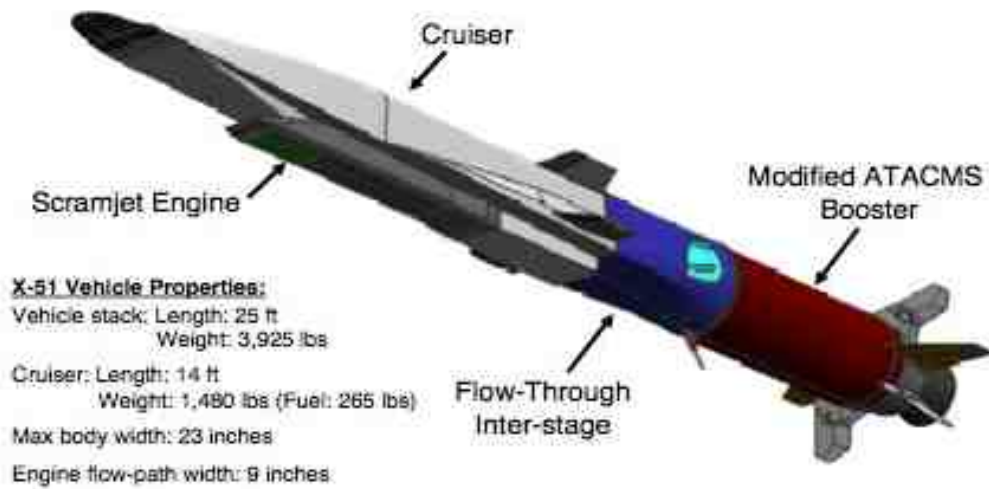
Figure 3.1. X-51A SED Vehicle Configuration with Rectangular inlet[34]
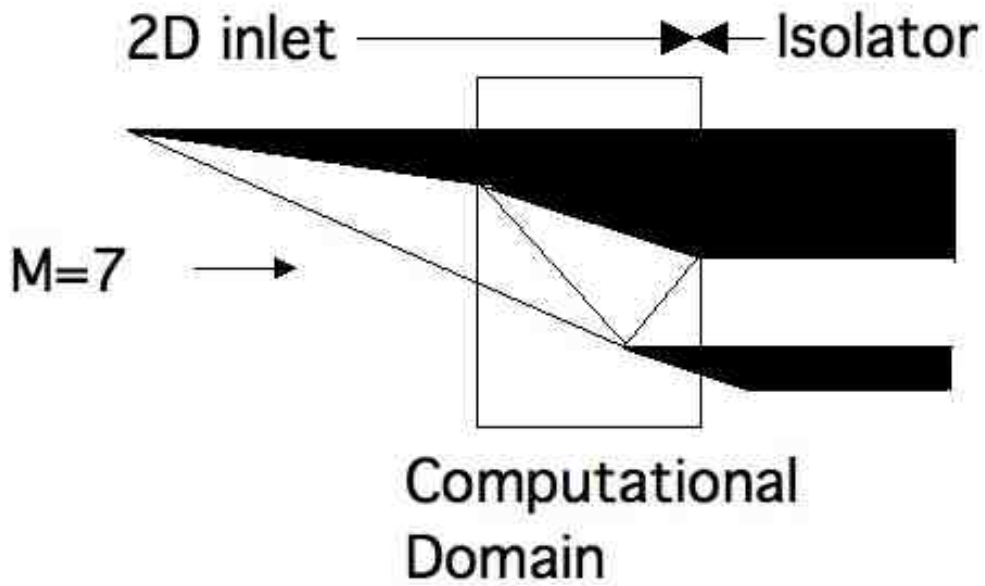
Figure 3.2. Fore-body with shocks and 2D inlet. *Computational domain shown for*

placement of three-dimensional inlet.

Parameter	Symbol	Power law design	Angle-specified design
Designed freestream Mach number	M_∞	6.0	6.0
Throat Mach number	M_t	3.58	3.58
Truncation angle	θ	4.23 degrees	4 degrees
Shoulder angle	δ_s	4.16 degrees	5 degrees
Inlet length	L	13.46 ft	13.86 ft
Cowl length	x_c	4.60 ft	4.60 ft
Capture height	$y_{capture}$	2.34 ft	2.41 ft
Contraction ratio	CR	2.98	3.07
Throat radius	r_t	.5 ft	.5 ft
Throat temperature	T_t	1000 K	1000 K
Throat total pressure	$P_{0,t}$	18.473 atm	18.473 atm
Throat pressure	P_t	.5 atm	.5 atm
Number of streamtubes	N	15 x 15	15 x 15

Table 3.1 Physical and design performance parameters for studied three-dimensional inlets

3.2 Inlets analyzed

Two area functions were chosen to create the three-dimensional inlets to study. For the first design, an area change function using a blend of power law functions that produced the desired capture and combustor height and wedge angles between 4 and 7 degrees along the centerline was initially chosen. The following function for the top of the inlet was chosen:

$$y(z,x) = (y_{capture} - y_t(z))\left[\frac{1}{2}(y_{capture} - y_t(z))\left(\left(\frac{\left(x-\frac{L}{2}\right)}{L}\right)^2 - \left(\frac{x}{L}\right)^{1.4}\right) + C_1(z)\right] \quad (3.1)$$

where y-coordinate of the top of the inlet, y_t is the height at the throat at z, and $C_1(z)$ is a constant. This design has a higher area change and higher wedge angles in the middle of the inlet. The top of the inlet was adjusted smoothly so that each streamtube would have the same flow angle at the capture and shoulder. The highest inlet angle along the center-line and the sides was 6.47 and 8.03 degrees respectively. The bottom profile $b(x,z)$ was determined by

$$b(z,x) = (-b_t(z))\left[\frac{1}{2}(-b_t(z))\left(\left(\frac{\left(x-\frac{L}{2}\right)}{L}\right)^2 - \left(\frac{x}{L}\right)^{1.4}\right] + C_2(z) \tag{3.2}$$

A second transition area was designed based on the results of propagating streamtubes in the first inlet by specifying the wedge angle at each location to produce more area change near the corner and inlet entrance and more gradual change in the middle of the inlet. The height of the inlet is the same as the height of the X-51 inlet and the same height to length scaling and cowl location as the first inlet.[34] An inlet with more gradual change in the center of the inlet and more transition near the corners will likely have fewer shock losses. The maximum flow angles of 9.15 and 9.95 along the center-line were 0.20 and 0.15 feet from the capture and shoulder, respectively. The minimum flow angle of 4.7 degrees occurred at 12.24 feet along the inlet. An angle-change profile was chosen along the center-line that produced a smooth transition from the specified capture height to combustor height with a four

degree initial wedge angle and five degree shoulder angle. The sides of the inlet were

calculated by increasing the angle by a constant and small amount such that the

required height change was smoothly produced. The bottom was scaled to match the

top as follows:

$$b(x,z) = \frac{y(L)\big(y(x-1)-y(x)\big)}{y(0)-y(L)} + b(x-1) \tag{3.3}$$

Each design is symmetric about the y-axis. The capture plane and combustor

were given a width or diameter of 1 ft. In many three-dimensional inlets, there is also

compression along the sides, but the same width along the center was used to simplify

calculations. To determine the total area of the three-dimensional inlet at each

location, the inlet was cut up into 65 strips with a bottom and top calculated every

1/64 feet and at $x = \pm\dfrac{31}{64}$ feet near the wall. The area for each strip was determined

by:

$$A(z,x) = \frac{1}{63}h(z) - \frac{1}{63}\left[\left(y(z)-y\left(z+\frac{1}{32}\right)\right)\frac{1}{2} + \left(b(z)-b\left(z+\frac{1}{32}\right)\right)\frac{1}{2}\right]$$

$$A(0,x) = \frac{A(z)}{2} \tag{3.4}$$

$$A(x) = \sum_{z=-.5}^{.5} A(z,x)$$

The total area change functions for each inlet are shown in Figure 3.3. The two three-dimensional inlets designed are shown in Figures 3.4 and 3.5 with each horizontal line representing the top and bottom streamlines.
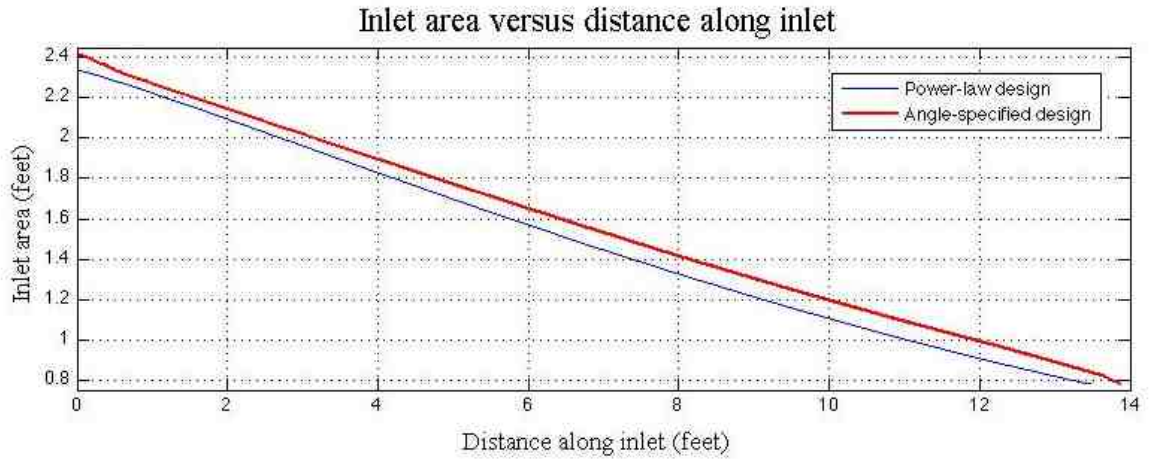
Figure 3.3. Inlet area change as a function of distance for each inlet studied.
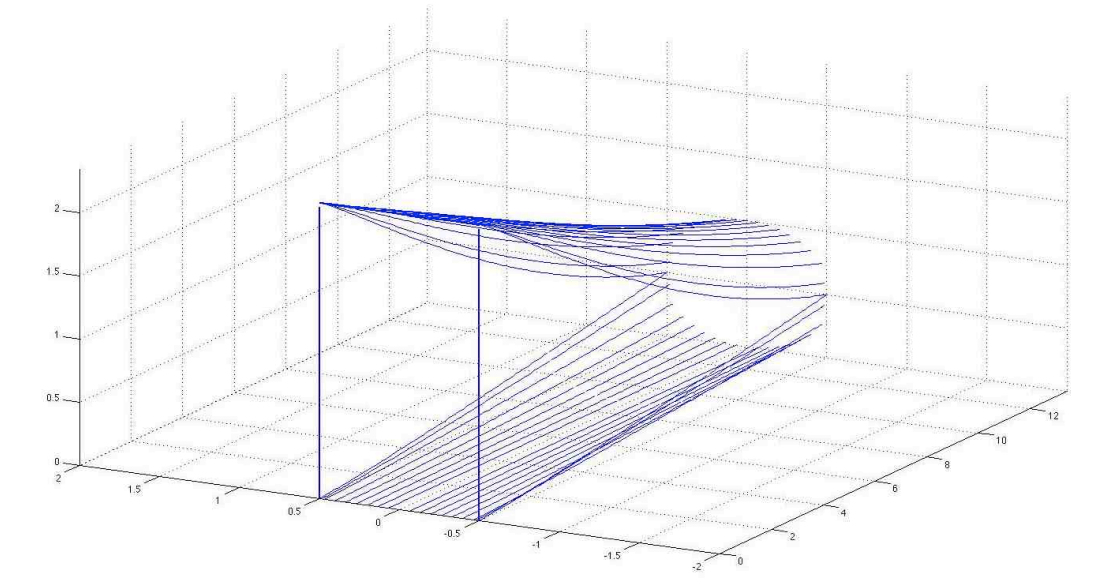
Figure 3.4. Streamlines in three-dimensional inlet with rectangular capture area and circular combustor (power law).
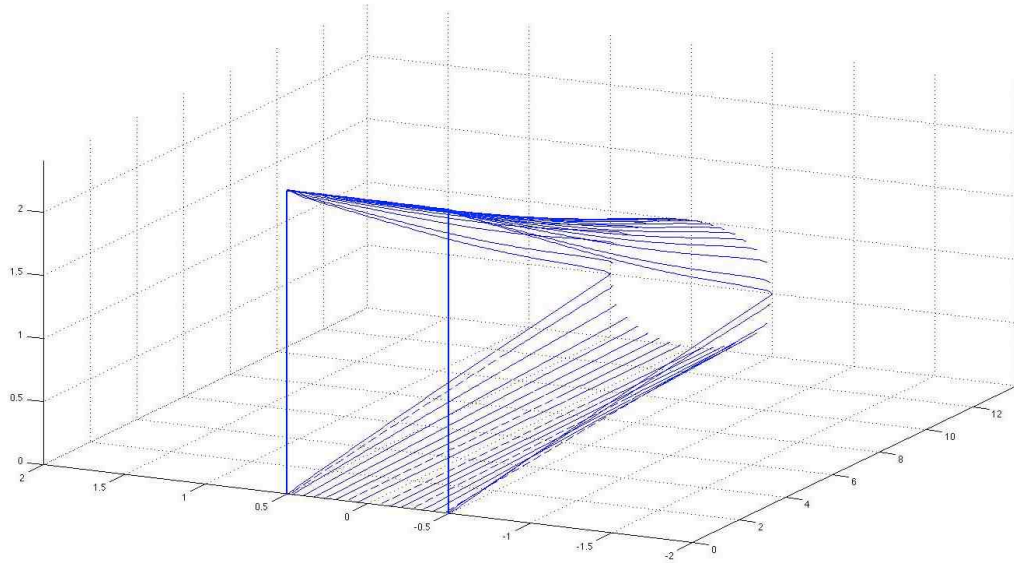
Figure 3.5. Streamlines in three-dimensional inlet with rectangular capture area and

circular combustor (angle-defined).

3.3 Streamtube grid

The grid constructed for streamtube propagation of the inviscid solution

consisted of 15-by-15 discrete streamtubes. For the viscous boundary layer, a grid of

8-by-8 streamtubes was used. The total number of streamtubes needs to exceed 100 to

ensure model fidelity. The inviscid solution should have at the very least 5

streamtubes to accurately characterize the non-uniformity and propagate the flow

across the shock wave. The viscous solution needs also at least 5 streamtubes – a

nearly zero velocity, an incompressible, a transonic, a supersonic, and a hypersonic

streamtube with the hypersonic streamtube for the inlets studied corresponding to the top of the boundary layer.

Each streamtube had an area determined by dividing the circular throat into a center channel denoted by $n_y = 0$ and $n_z = 0$ and seven symmetric channels on each side such that each channel contains 15 streamtubes. Rather than creating a grid that divided the circular throat into 225 equal areas, this grid was used for computational and conceptual reasons. Because the flow can be thought of and calculated as a series of independent streamtubes in a channel, it makes sense to create a grid that places an equal number of streamtubes in each channel. With this grid, each streamtube at a given height will cross the shock at the same time and each channel will have the same number of shock calculations. The grid used is shown in Figure 3.6. The starting areas of each streamtube are shown in Figure 3.7 and Table 3.2.
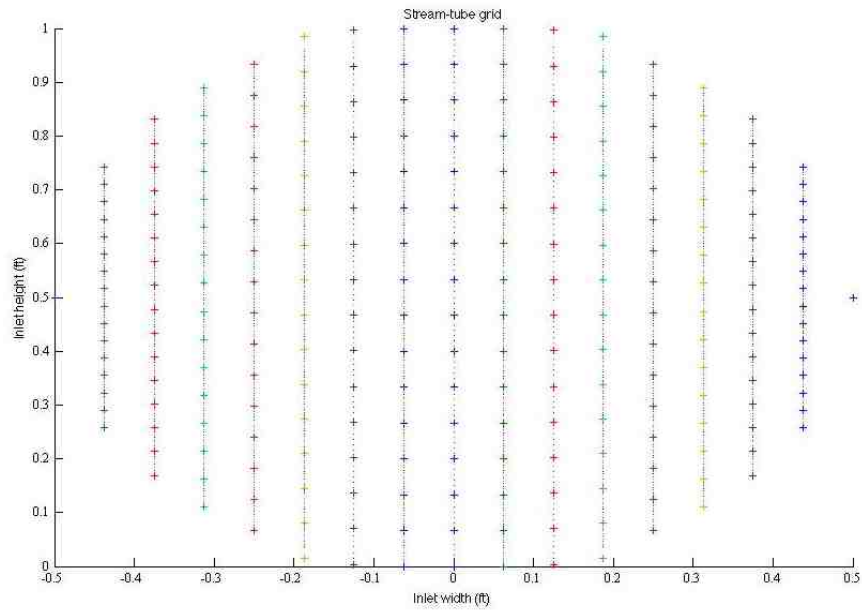
Figure 3.6. Streamtube grid. *Each cross represents location of streamtube*
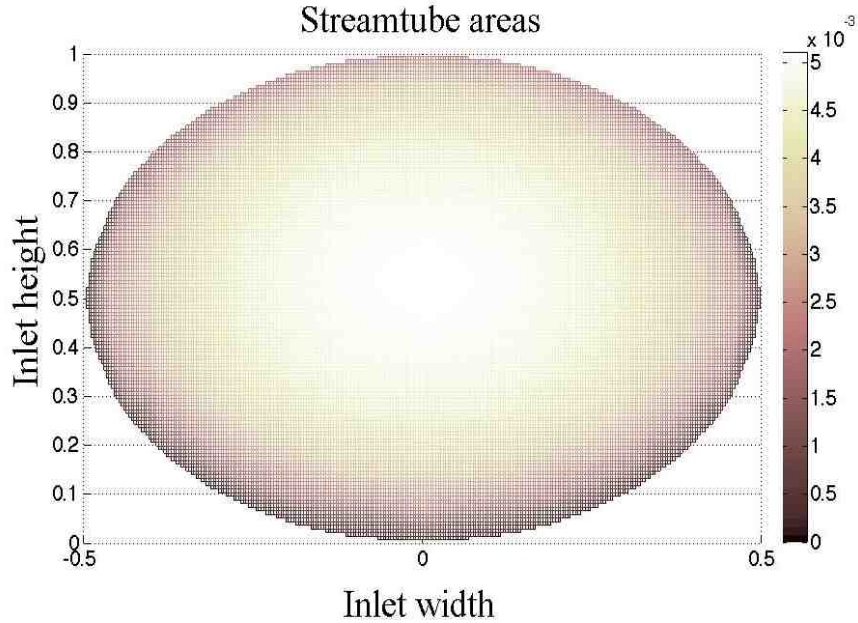
Figure 3.7. Streamtube areas at the throat.

Streamtube n_y along y-axis	Streamtube number n_z along z-axis							
	0	1	2	3	4	5	6	7
7	0.00266	0.00229	0.00225	0.00219	0.00210	0.00192	0.00166	0.00130
6	0.00356	0.00351	0.00344	0.00313	0.00300	0.00271	0.00237	0.00185
5	0.00414	0.00408	0.00400	0.00382	0.00366	0.00329	0.00285	0.00218
4	0.00463	0.00458	0.00448	0.00427	0.00409	0.00366	0.00316	0.00238
3	0.00484	0.00479	0.00475	0.00458	0.00433	0.00387	0.00333	0.00250
2	0.00508	0.00503	0.00492	0.00469	0.00448	0.00400	0.00344	0.00258
1	0.00519	0.00513	0.00503	0.00479	0.00458	0.00408	0.00351	0.00262
0	0.00523	0.00517	0.00506	0.00482	0.00461	0.00411	0.00353	0.00264
1	0.00517	0.00513	0.00503	0.00479	0.00458	0.00408	0.00351	0.00262
2	0.00506	0.00503	0.00492	0.00469	0.00448	0.00400	0.00344	0.00258
3	0.00482	0.00479	0.00475	0.00458	0.00433	0.00387	0.00333	0.00250
4	0.00461	0.00458	0.00448	0.00427	0.00409	0.00366	0.00316	0.00238
5	0.00411	0.00408	0.00400	0.00382	0.00366	0.00329	0.00285	0.00218
6	0.00353	0.00351	0.00344	0.00313	0.00300	0.00271	0.00237	0.00185
7	0.00264	0.00229	0.00225	0.00219	0.00210	0.00192	0.00166	0.00130

Table 3.2. Streamtube starting areas for 15x15 inviscid grid.

Although this grid does bias the streamtubes in the middle that have more area as streamtubes at a lower pressure and with more area will crowd out smaller area and higher-pressure streamtubes, the middle streamtubes have better total pressure recovery, adiabatic and kinematic efficiency. A profile entering the inlet calculated from a combustor streamtube grid weighted in this manner in favor of the streamtubes in the middle should produce a better performing inlet.

3.4 Computational details

A particular advantage of the method developed is that it allows for quick iteration of designs and does not require extensive computational resources. For example, these flow field solutions were propagated using an Excel spreadsheet. This method lends itself easily to using a few simple spreadsheets. Each n_y streamtube's properties was calculated in the same series of columns and each n_z streamtube's properties in the same rows with a step size of 0.01 feet. This approach makes sense from an analytical standpoint. First, because the method is algebraic, the solution can be easily marched upstream (inviscid) or downstream (viscous). Second, at each x-location, streamtube properties could be compared from the floor to the top of the inlet. Third, aside from pressure for each streamtube, its properties can be treated independently from the rest of the flow – except at locations where there is a pressure gradient. Separate worksheets were used for shock and results calculations. For the inviscid solutions, once the pressure ratio across the initial shock wave, shock angle, and streamtube area at and across the shock are determined, the properties of that streamtube are determined at the capture area within seconds independently of the

other streamtubes. Although an Excel spreadsheet was used for this analysis, a variety of programming languages and software could be used. Unlike with some of the other methods used to create transition ducts and model the flow inside a hypersonic three-dimensional inlet, this does not require computational fluid dynamics, extensive computing power, long run-times, or specialized software or codes.

For the inviscid solutions, temperature, Mach number, pressure, individual area, and the constant mass flow parameter were tracked and propagated for each streamtube. In addition, to aid in debugging and ensure the solution was physical, continuity, momentum conservation, and energy conservation were calculated for each streamtube at each step. For propagating the streamtubes between shocks, conservation of mass, momentum, and energy was required to be satisfied to within 10^{-5}. For the streamtube area behind the shockwave, this was relaxed to require the area to satisfy the conservation equations to within 1%. The total area of all the streamtubes also was compared to the area of the inlet to track error build-up and to check that the individual areas of the streamtubes was calculated correctly. The shock angle and required pressure ratio were iterated until the wedge angle from the solution to theta-beta-Mach number relation was to within 10^{-3}.

The viscous solutions required more time, several modifications and more calculations than the flow under inviscid assumptions. The pressure, areas, heights, and lengths were converted to Pascals and meters. The height and area of the inlet was scaled such that the bow shock reflected off the cowl. The ratio of the boundary

layer to required height of the inlet was 0.00362. With an initial boundary layer height of 0.00272 m, the inlet height is scaled down by 0.7514 times .3048 m/ft.

Similarity solutions were calculated and used for $\beta_{F.S.}$ in steps of 0.01 instead of for every $\beta_{F.S.}$. Similarity solutions for f, f', f'', f''', S, and S' were constructed for η to three decimal places using a numerical integrator. Because each profile with that resolution in η contained thousands of points, it was impractical to re-calculate the similarity solutions for every $\beta_{F.S.}$ The solutions, however, did not change enough to affect the results. Because the program needed to look up the tabulated similarity solutions for every streamtube at each step, this made the boundary layer calculation take several minutes. For the overall flow, the height of each channel, pressure gradient, pressure, Falker-Skan parameter, area of the inviscid inlet, wall shear, and inviscid solution for Mach number, temperature, density, velocity, and total temperature for the top streamtube was tracked. For each streamtube, the Mach number, temperature, density, individual area, total temperature, similarity coordinates, $d\eta/dy$, similarity solutions, $\mu(T)$, shear gradient, shear stress, y-coordinate, height from last streamtube, and a curve-fit term for the subsonic streamtubes was calculated.

Each channel was calculated separately to find the change in boundary layer height. The height of the last streamtube was set to the height of the boundary layer as it was chosen as the 99% velocity streamtube. The profiles – velocity versus height

and velocity versus similarity coordinate – were plotted to ensure that the boundary

layer maintained its profile as the solution was propagated down the inlet.

Chapter 4: Performance Analysis – Inviscid

Both inlets were evaluated to determine their performance and the effectiveness of using this method under both inviscid and viscous flow assumptions. Lessons learned on using this method and sources of errors are presented. The performance, incoming flow profile, non-uniformity at the capture plane, and propagated shock wave is compared for both inlets under inviscid flow assumptions.

4.1. Inviscid Performance Parameters

To assess the performance of these inlets propagated with compound compressible flow theory, several performance parameters are used. The ratio of total pressure between the free-stream and throat flow π_c for the inviscid case is better than that of rectangular inlets and comparable to other three-dimensional inlets with a rectangular capture area and circular combustor. The kinetic energy efficiencies η_{KE} and adiabatic compression efficiencies η_c also compare with other studied rectangular-to-circular inlets and are better than those calculated for rectangular inlets. Kinetic energy efficiency and adiabatic compression efficiency are defined as[1]:

$$\eta_c = \frac{\psi - \left(\dfrac{1}{\pi_c}\right)^{\frac{\gamma-1}{\gamma}}}{\psi - 1} \tag{4.1}$$

67

$$\eta_{KE} = 1 - \frac{2}{(\gamma-1)M^2_{\infty,avg}} \left[\left(\frac{1}{\pi_c}\right)^{\frac{\gamma-1}{\gamma}} - 1 \right]$$

(4.2)

Static temperature ratio ψ, total pressure recovery π_c, average free-stream Mach number $M_{\infty,avg}$, and the efficiency parameters are all mass-averaged quantities because of the non-uniformity at the rectangular entrance. Because the profile at the throat is uniform in Mach number and temperature, mass-averaging is the same as weighting each streamtube by its area A_i. Both inlets had the same performance results although the second inlet unsurprisingly because of its larger contraction ratio also had a higher static temperature and pressure ratio. The second inlet had a 3% higher contraction ratio, but a 14.6% higher static pressure ratio. The second inlet had 0.014% less total pressure recovery and 0.0002% less adiabatic compression efficiency, reflecting that small changes in adiabatic compression efficiency result in relatively large changes in total pressure recovery. The kinetic energy for both inlets was the same to four significant digits, which is not surprising as large differences in adiabatic compression equate to small changes in kinetic energy efficiency and at high Mach numbers must be quoted to at least three significant digits. That the two inlets had almost identical total pressure ratios, adiabatic compression efficiencies, and kinetic energy efficiencies is not surprising as neither inlet is required to have uniform flow entering the inlet and using compound compressible flow theory forces stream-line traced isentropic flow, minimizing shock loses. Each inlet studied had an average free-stream Mach number $M_{\infty,avg} = 6.15$ and the flow at the top of the inlet at $M_\infty = 6$. The second inlet had a higher Mach number at the shoulder because it had a

higher shoulder angle. Performance results under inviscid flow assumptions are

shown in Table 4.1. These are comparable to those for the REST inlet with similar

physical characteristics at Mach 6.0 in Table 1.2 and exceed those of a comparable

rectangular inlet with the performance characteristics outlined in Table 1.3. Figures

4.21 and 4.22 show total pressure recovery in the inlet for both designs.

Parameter	Symbol	Power law design	Angle-specified design
Static pressure ratio	$\dfrac{p_\infty}{p_{throat}}$	18.9411	22.1719
Static temperature ratio - mass-avg	ψ	2.3881	2.3992
Capture pressure	P_∞	0.0264	0.0226
Shoulder shock entrance Mach number	M_δ	3.8836	3.9389
Average capture Mach number - mass-avg	$M_{\infty,avg}$	6.1521	6.1544
Total pressure recovery - mass-avg	π_c	0.9301	0.9285
Kinetic energy efficiency – mass-avg	η_{KE}	0.9972	0.9972
Adiabatic compression efficiency – mass-avg	η_c	0.9849	0.9847

Table 4.1. Performance results and capture plane properties of simulated inlets

4.2 Inviscid Performance Analysis

4.2.1 Methodology and error analysis

Some difficulties resulted from using this method based on where most of the

compression occurred and due to too high turning angles on the sides. However, these

difficulties provided insight into good design procedures using this method. With the

69

first inlet studied, most of the area change occurred in the middle of the inlet. As more streamtubes passed forward across the reflected shock boundary towards the front of the inlet, the overall area change did not produce a pressure high enough for a physical solution for the streamtubes near the sides that had higher wedge angles. At that given wedge angle, a pressure gradient could not be specified that satisfied the pressure matching condition and matched the flow angle and resulted in a lower pressure and higher Mach number directly behind the shock compared to the other streamtubes on the same side of the shock boundary. The area change near these locations needed to be modified slightly to produce a physical solution. However, with a continuous profile or a profile with more streamtubes, this is not a realistic solution. A real inlet would have a continuous smooth area change and would have streamtubes crossing the shock at each location. A possible solution if this problem occurs is to modify the area of the inlet by producing more compression for the streamtubes near the bottom of the inlet. For future designs, more compression could be added to the inlet at the shoulder.

With this in mind, a second inlet was created by choosing a wedge angle at each location with higher angles near the corner and the capture plane. Specifically larger wedge angles nearer the throat established higher-pressure gradients directly behind the shock, allowing for more flexibility in choosing the shock strength and shock angle. However, this gradient ended up getting too large as more streamtubes passed forward through the shock boundary with large areas. The larger streamtubes at lower pressures crowded out the higher-pressure tubes, forcing them to decrease

their size and increase their pressure even more. The last two streamtubes to pass

through the shock wave produced larger errors in the total area of the streamtubes and

could not satisfy mass, momentum, and energy conservation to within 2%. A longer

inlet than the ones studied with more modest turning angles but slightly higher area

change near the throat would likely avoid these issues. An inlet design with higher

transition spread out more along the inlet but focused near the capture plane and the

corners than the second design might also avoid these issues. Figures 4.4, and 4.15-

4.20 particularly show the high pressure, temperature, and Mach number gradients for

the last streamtubes on the second inlet. As shown in Figures 4.1 and 4.2, the angle-

specified inlet design had larger streamtube areas at the entrance that crowded out the

streamtubes behind the shock wave, causing the large pressure gradients near the

cowl and the entrance.
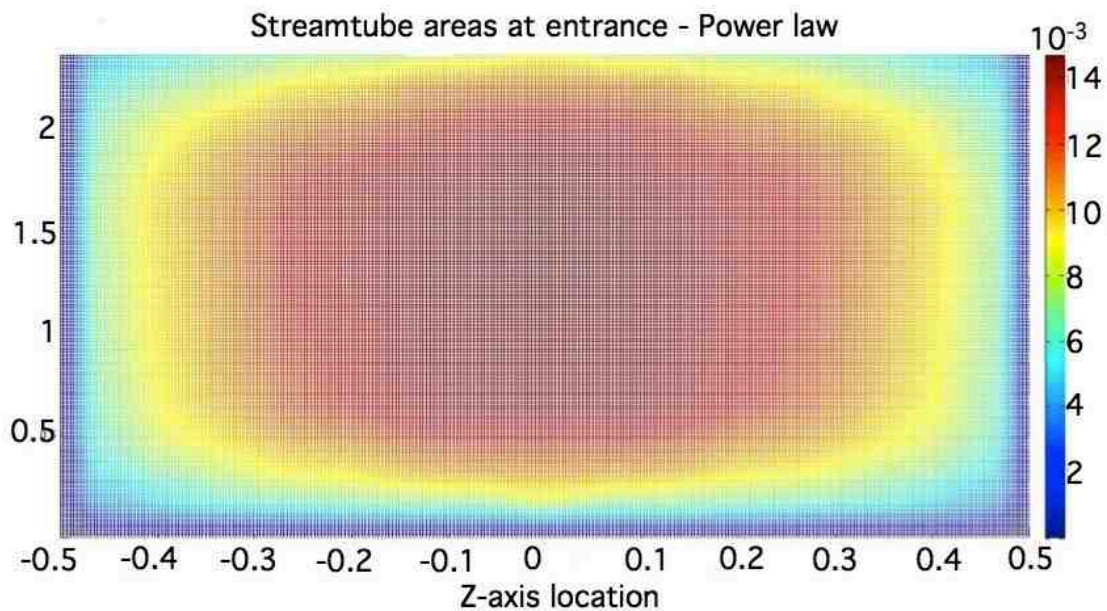
Figure 4.1 Streamtube areas at entrance – Power law design
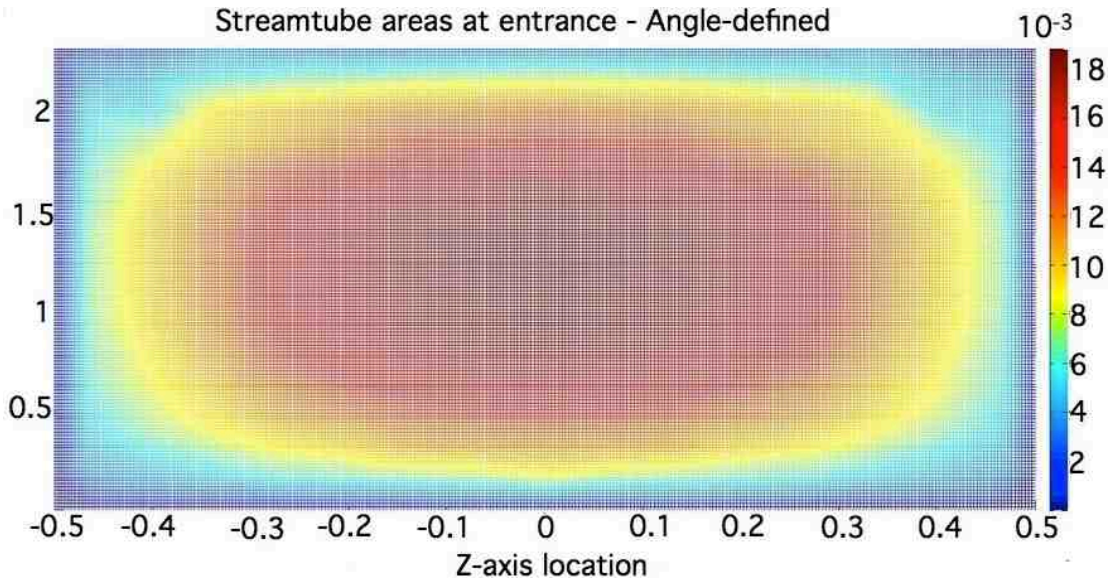
Figure 4.2. Streamtube areas at entrance – Angle-specified design
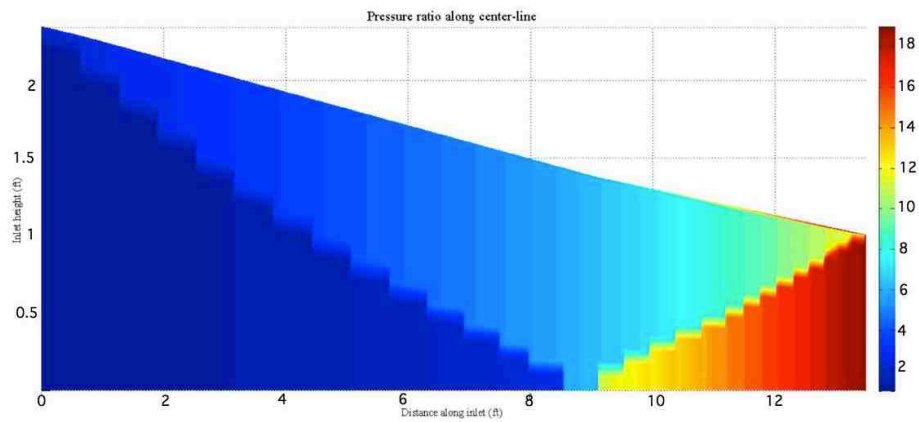
Figure 4.3. Pressure ratio along centerline for power law inlet
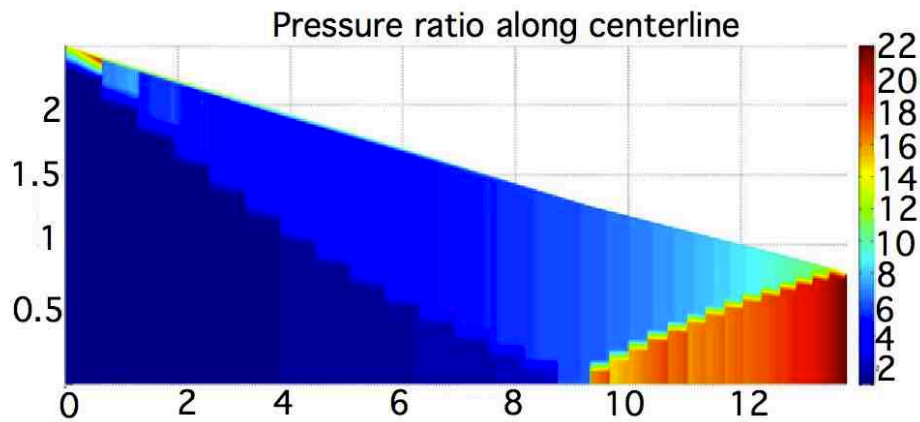
Figure 4.4. Pressure ratio for angle specified inlet along center

In addition to tracking conservation of mass, momentum, and energy, the total area of the streamtubes was compared to the designed area to check the fidelity of the solution. For the first inlet studied, the error in the total area prior to the initial shock wave was 0.6% and 0.06% at the capture plane. The error build-up for the second inlet was higher due to the higher pressure gradients near the cowl and capture plane – 0.99% prior to the initial shock and 1.5% at the capture plane. The areas of the streamtubes at the capture plane are shown in Figures 4.1 and 4.2.

4.2.2 Inlet performance analysis

The two designs studied produce qualitatively different profiles at the entrance because of where most of the compression occurs in each inlet. For the first design studied, because the middle of the inlet had higher wedge and lower shock angles, the center of the inlet had higher Mach numbers and lower temperatures at the entrance and the lowest Mach numbers and highest temperatures along the top and bottom. This is shown in Figures 4.5 and 4.6 for the first inlet. In the second design, Mach number was higher and temperature lower along the sides where compression is expected to be greater as shown in Figures 4.7 and 4.8. The second inlet had more uniform Mach number profile in the center around Mach 6, the intended Mach number and is probably a more realistic profile coming into the inlet.

73
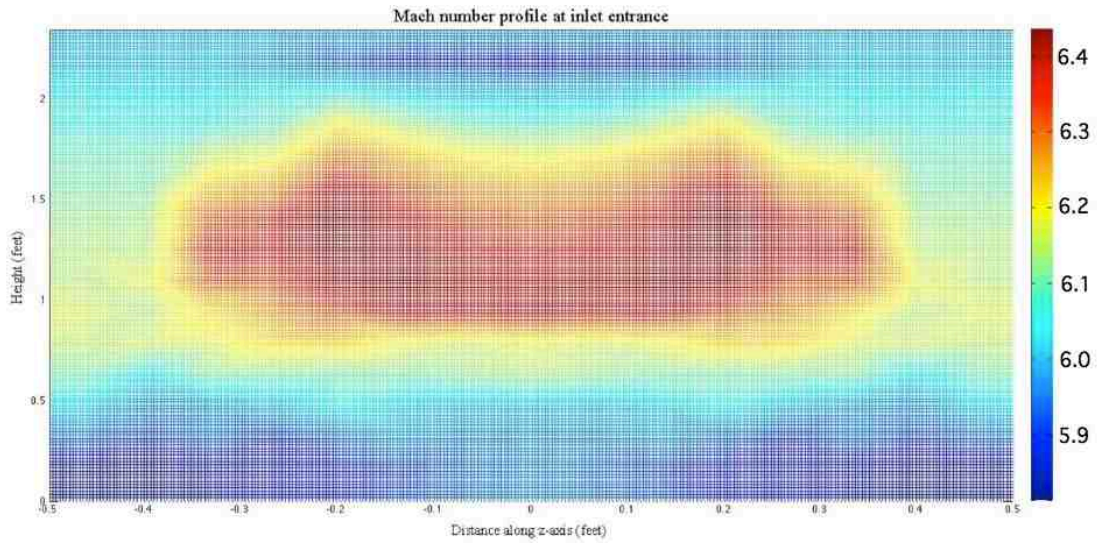
Figure 4.5. Mach number profile at inlet entrance – Power law inlet
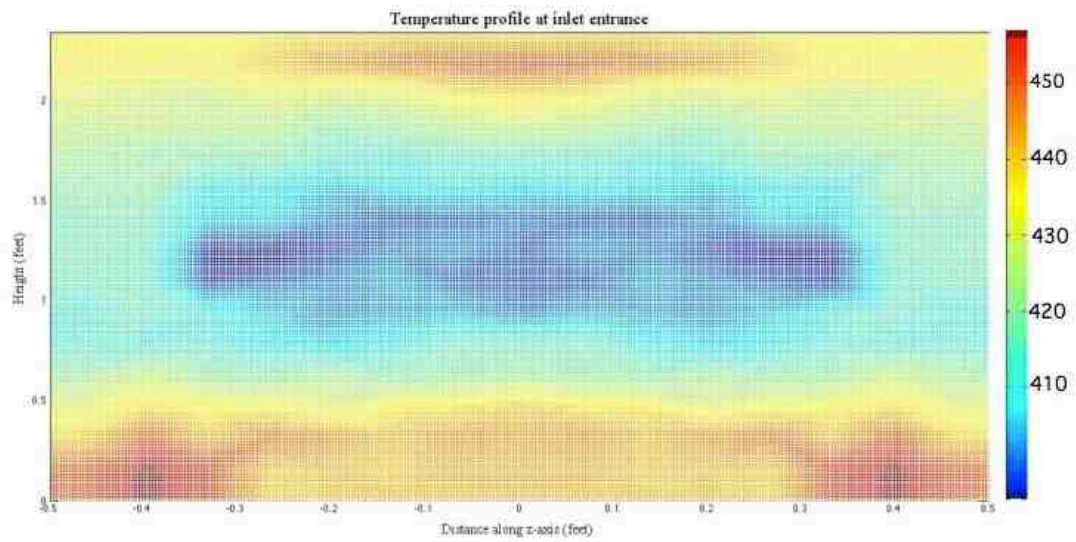
Figure 4.6. Temperature profile at inlet entrance – Power law inlet
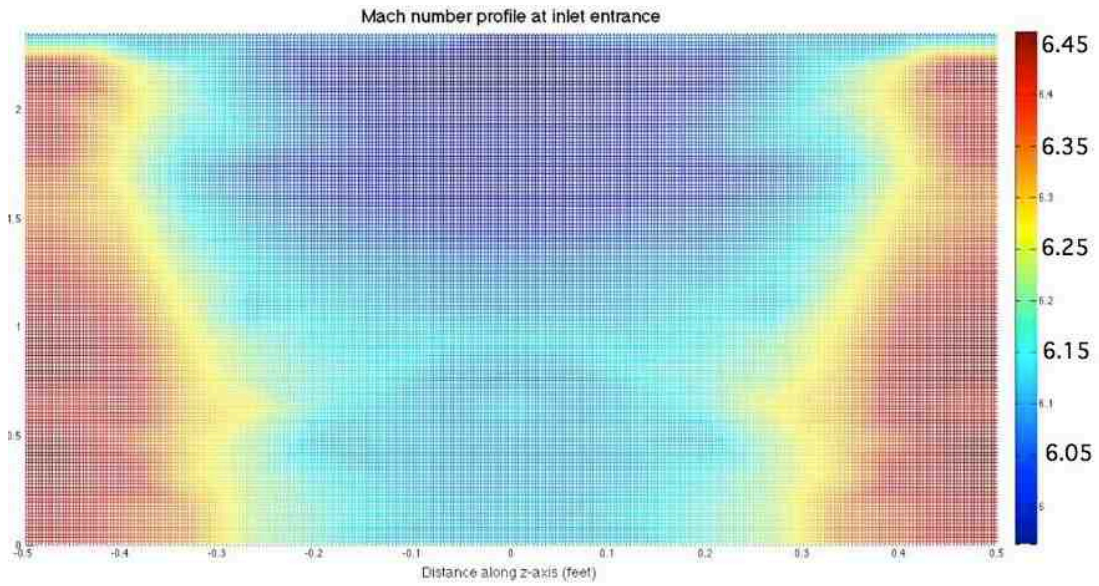
Figure 4.7. Mach number profile at inlet entrance – Angle specified design
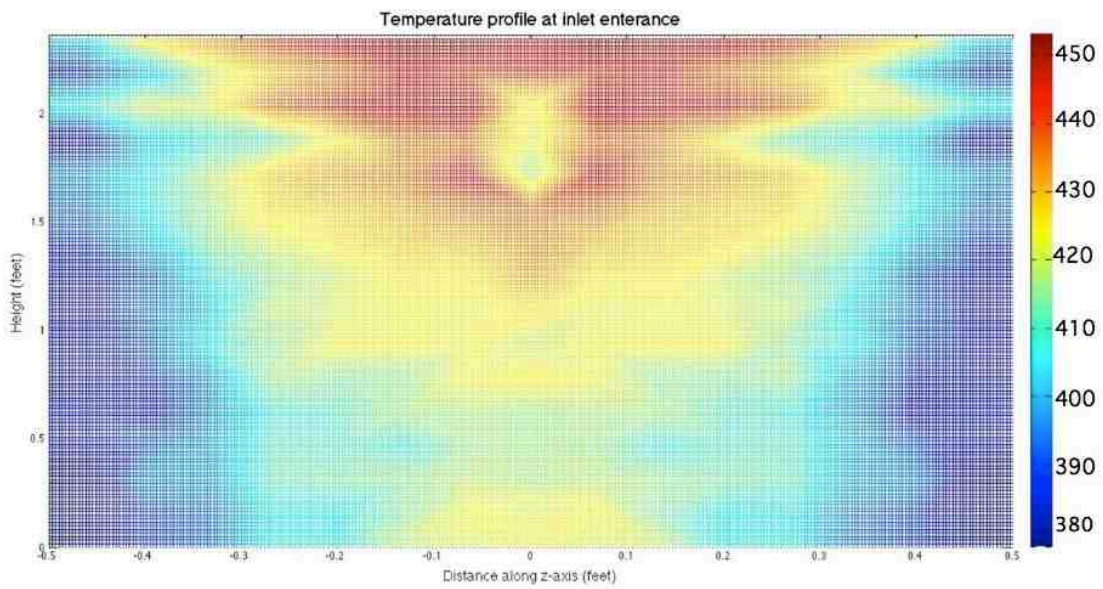
Figure 4.8. Temperature profile at inlet entrance – Angle specified design
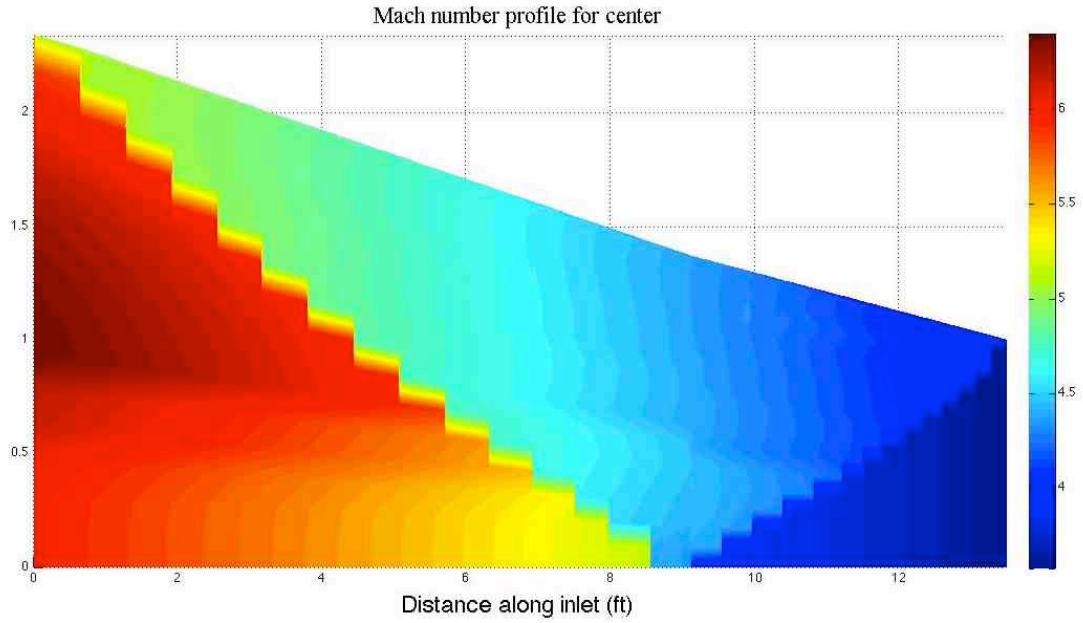
Figure 4.9. Mach number profile along center – power law inlet
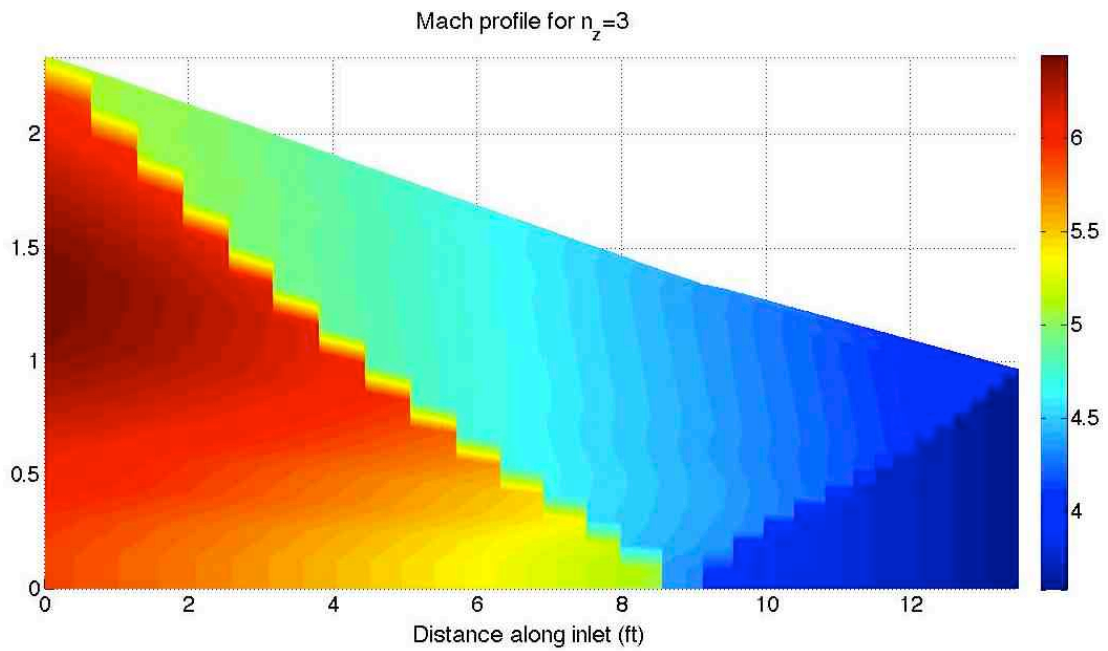
Figure 4.10. Mach number profile for $n_z = 3$ streamtube – power law inlet
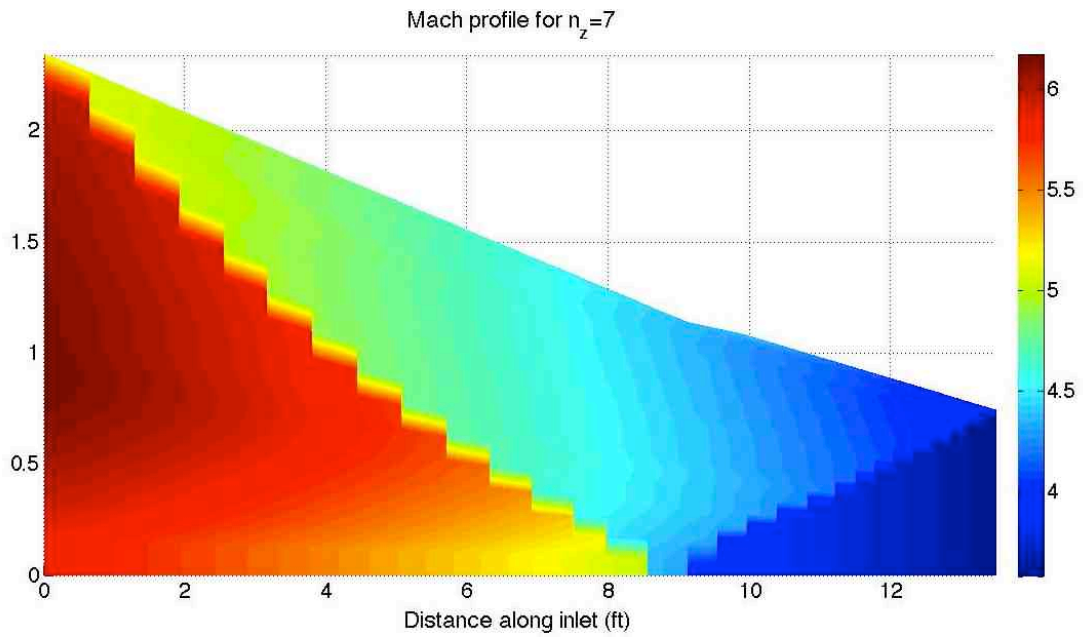
Figure 4.11. Mach number profile for $n_z = 7$ – power law inlet
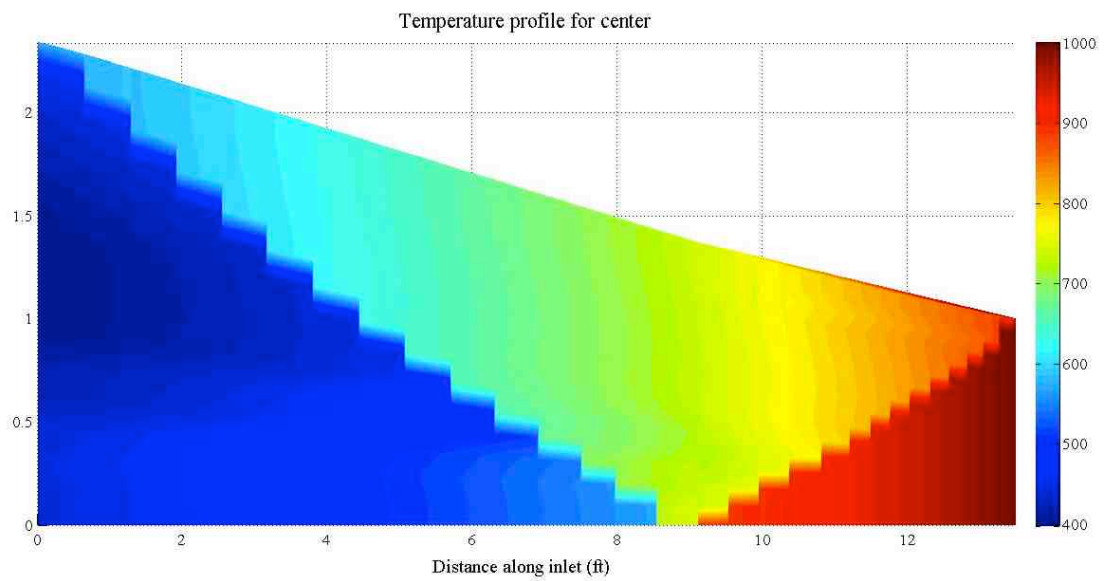
Figure 4.12. Temperature profile for center – power law inlet
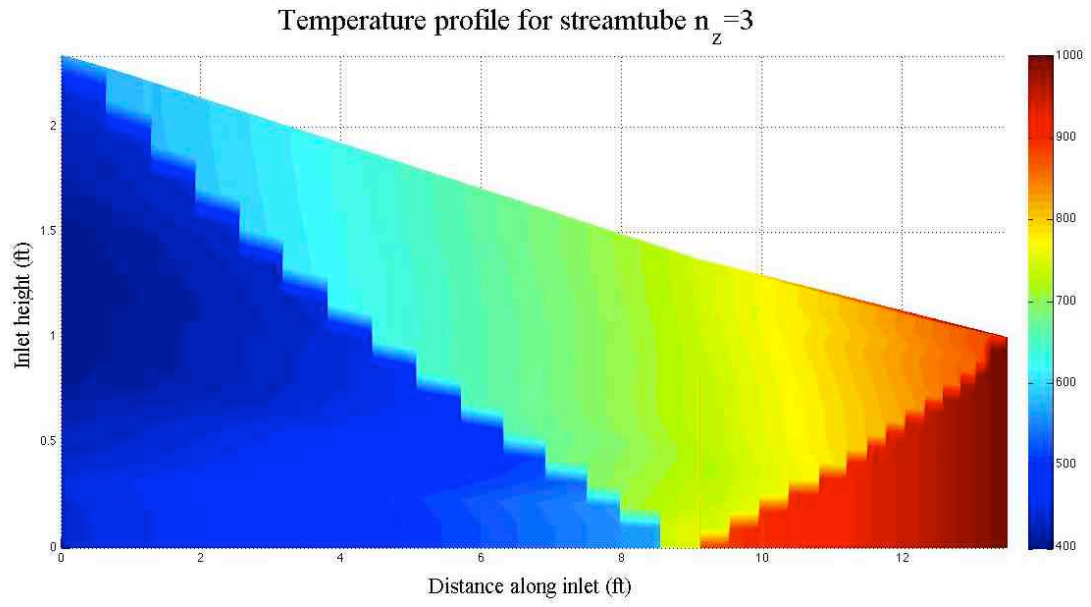
Figure 4.13. Temperature profile for streamtube $n_z = 3$ – power law inlet
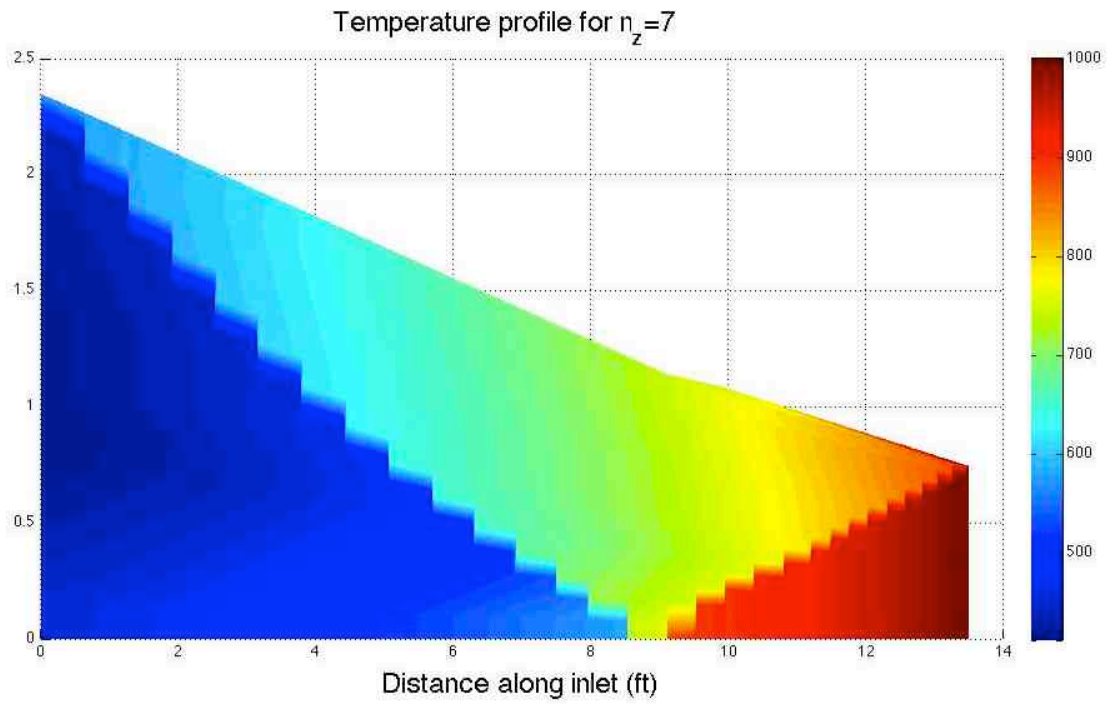
Figure 4.14. Temperature profile for streamtube $n_z = 7$ – power law inlet
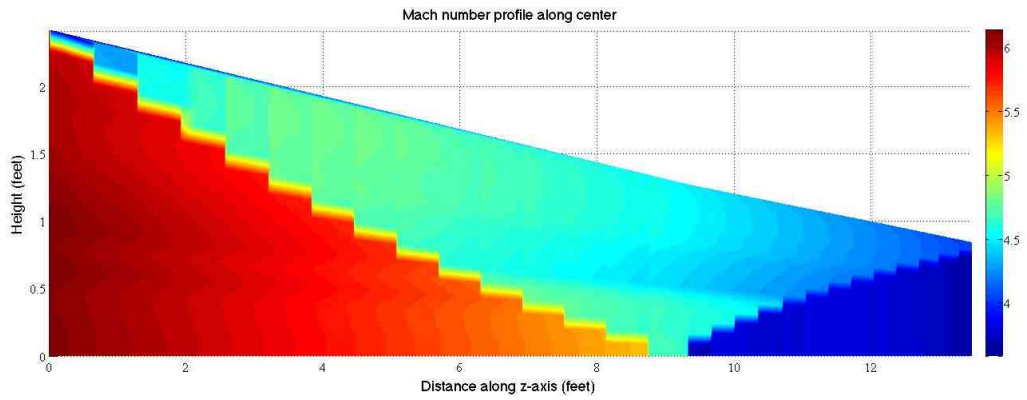
Figure 4.15. Mach number profile along center – angle specified inlet
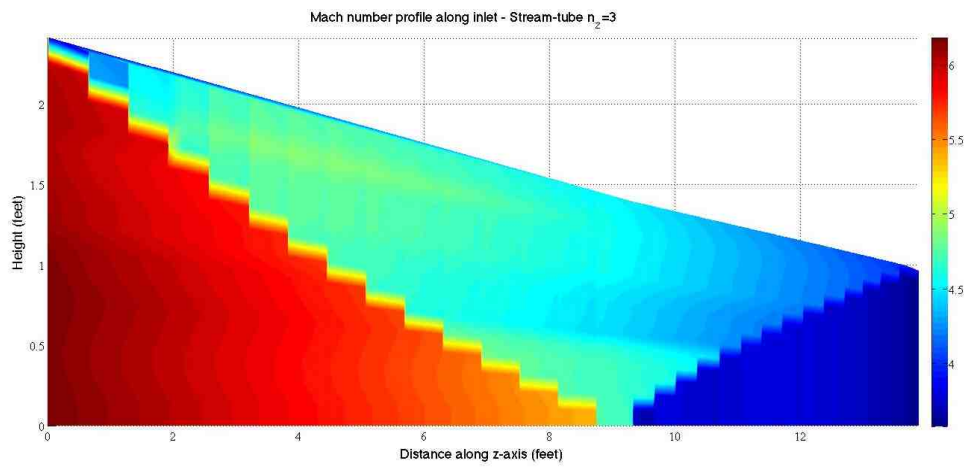
Figure 4.16. Mach number profile for $n_z = 3$ - angle specified inlet
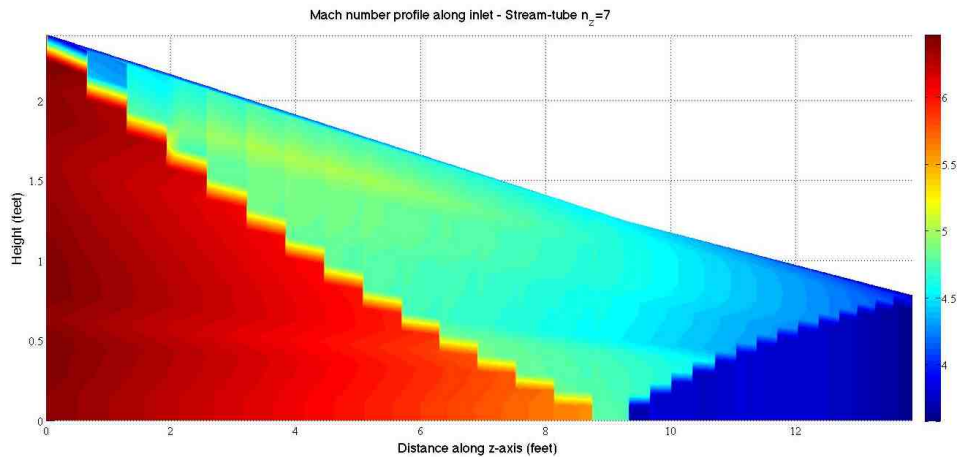
Figure 4.17. Mach number profile for $n_z = 7$ - angle specified inlet
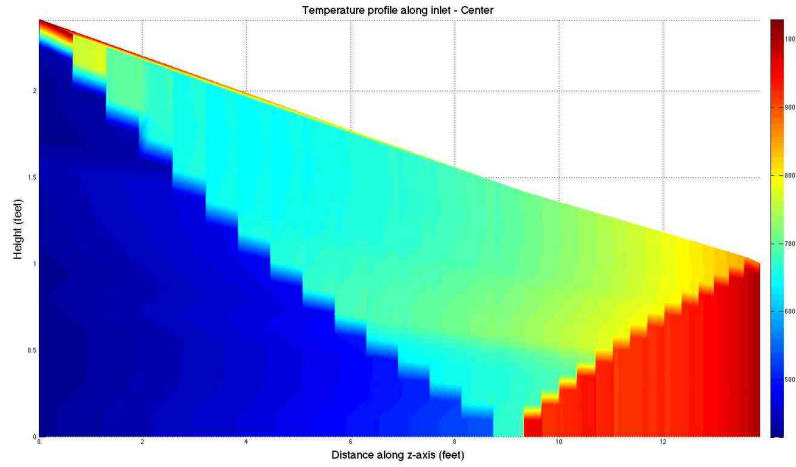
Figure 4.18. Temperature profile along center – angle specified inlet
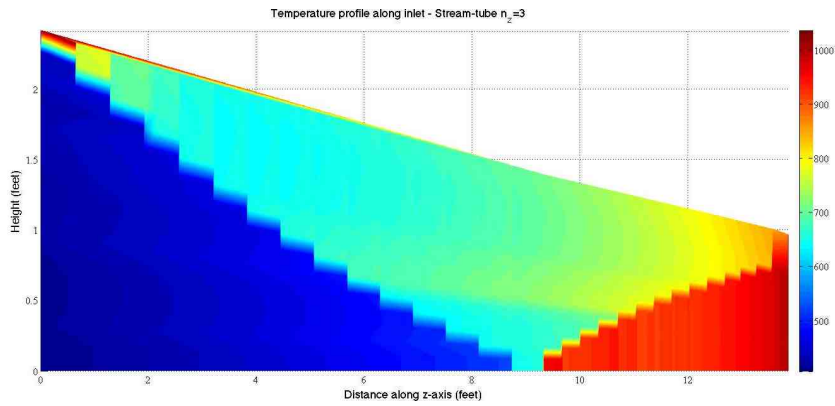
Figure 4.19. Temperature profile for streamtube $n_z = 3$ - angle specified inlet
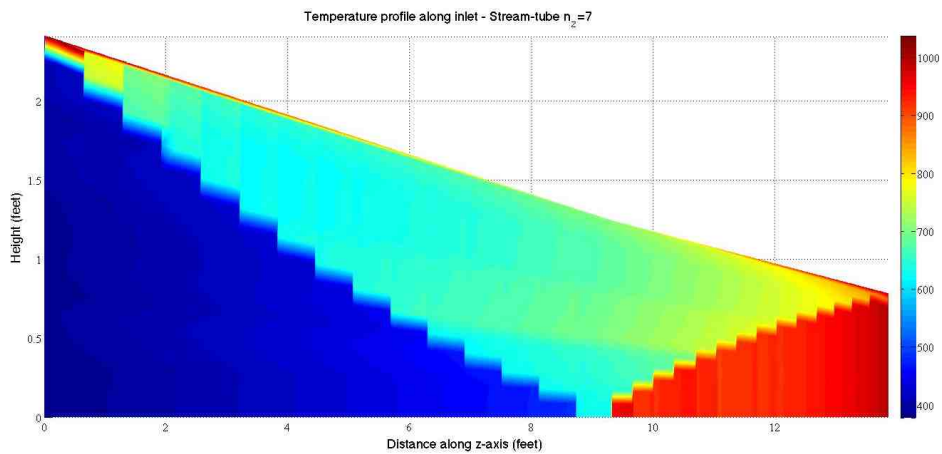
Figure 4.20. Temperature profile for streamtube $n_z = 7$ - angle specified inlet

80

Both inlets had relatively uniform total pressure recovery, with the second design having a larger area of uniform total pressure recovery in the center as shown in Figures 4.21 and 4.22. In the power law design, the highest pressure recovery was on the top and bottom with the lowest pressure recovery along the sides. Figure 4.22 shows several pockets of higher total pressure recovery in the second inlet. It may be preferable to have these pockets to increase mixing and combustion in a scramjet combustor. With this method, it is fairly straightforward to map locations of higher total pressure or temperature at the throat with where on the inlet to decrease or
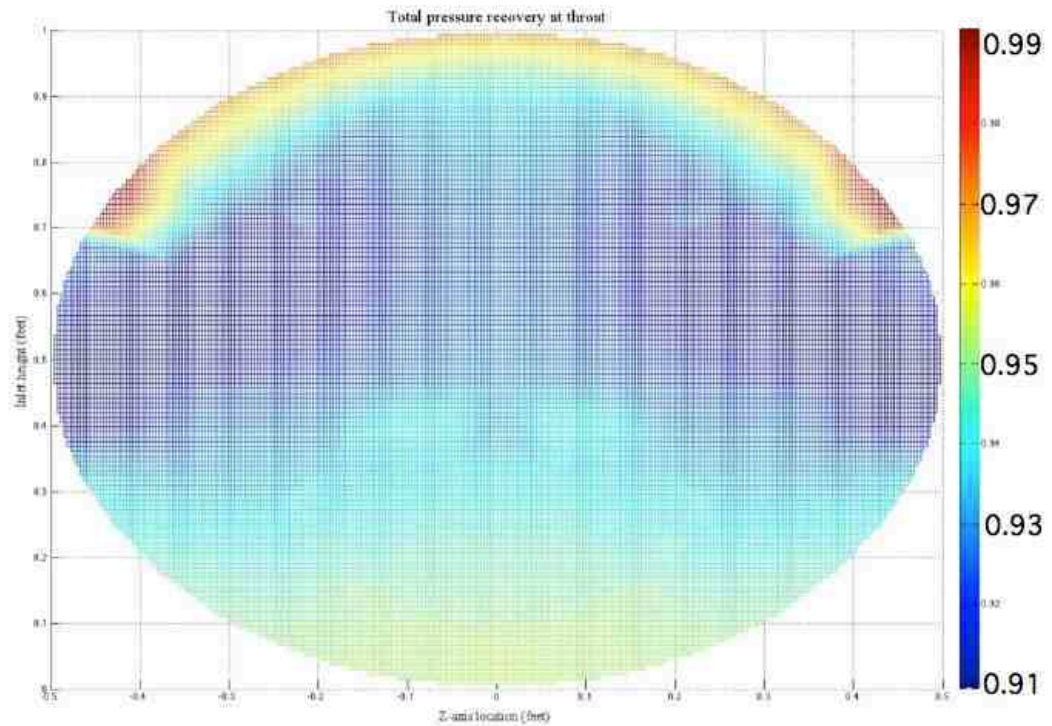
Figure 4.21. Total pressure recovery at throat – Power law design
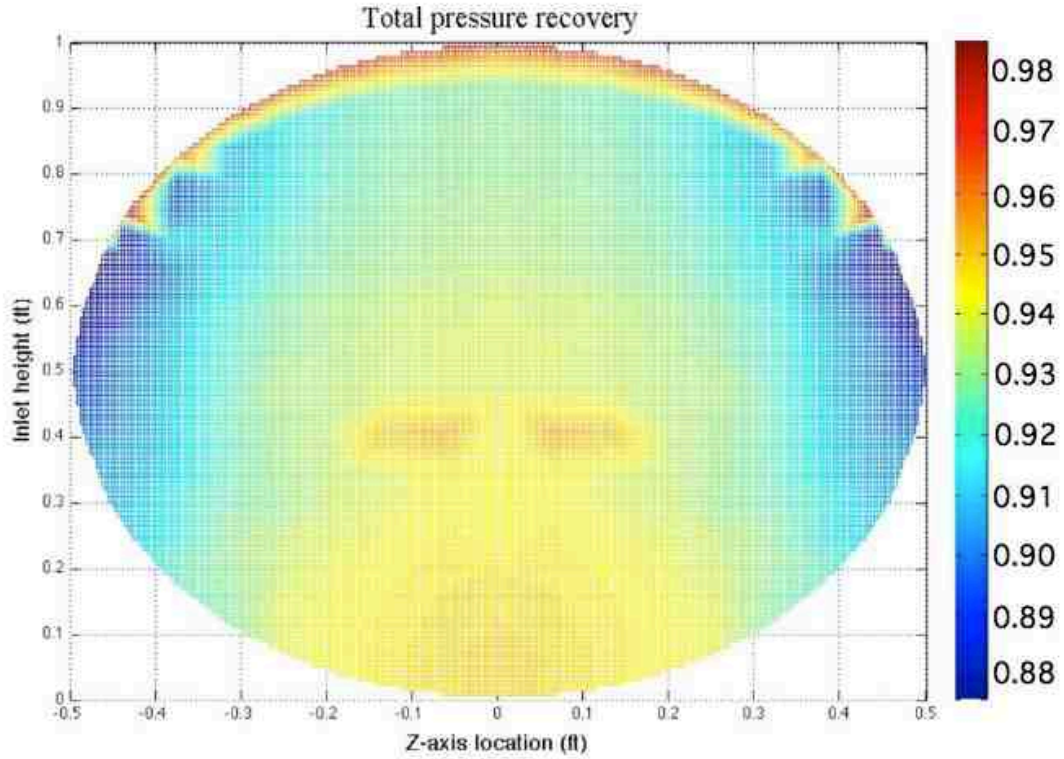
Figure 4.22. Total pressure recovery at throat – Angle-specified design
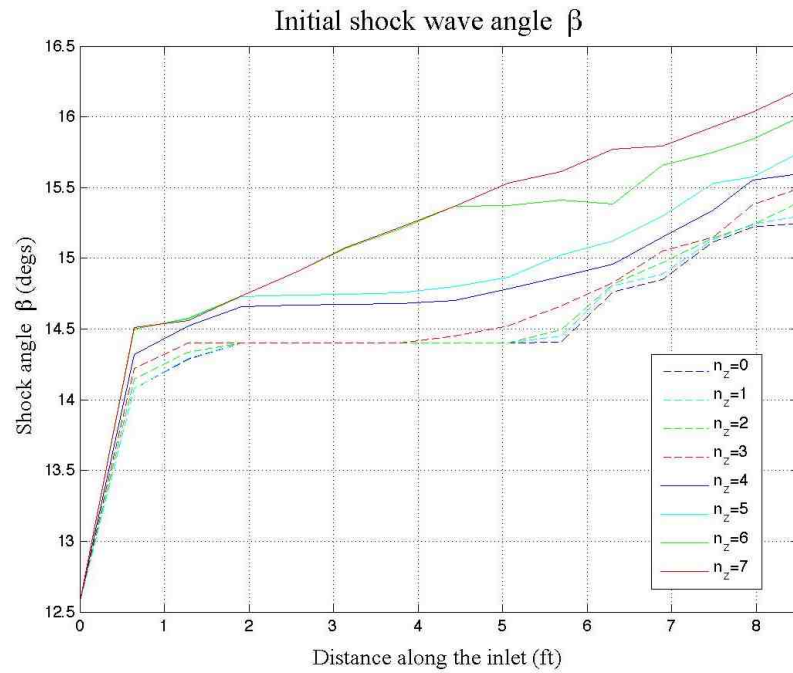
Figure 4.23. Initial shock wave from inlet capture for power law inlet

82
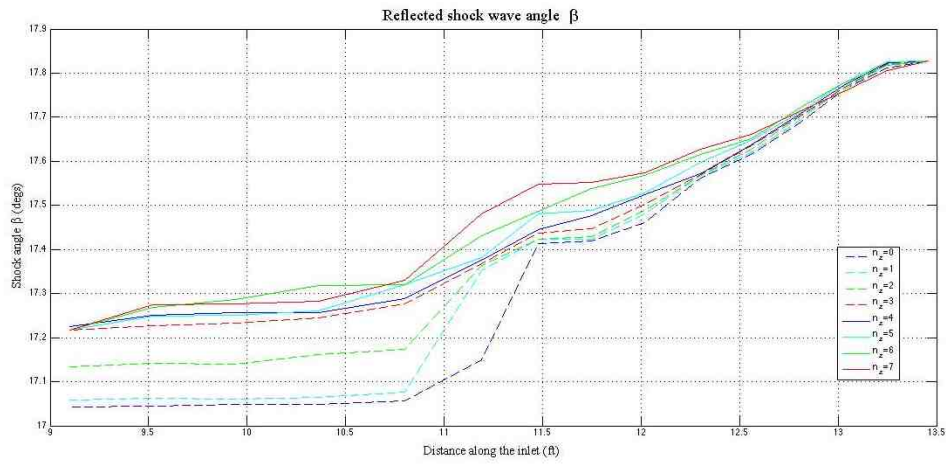
Figure 4.24. Reflected shock wave in studied power law design.
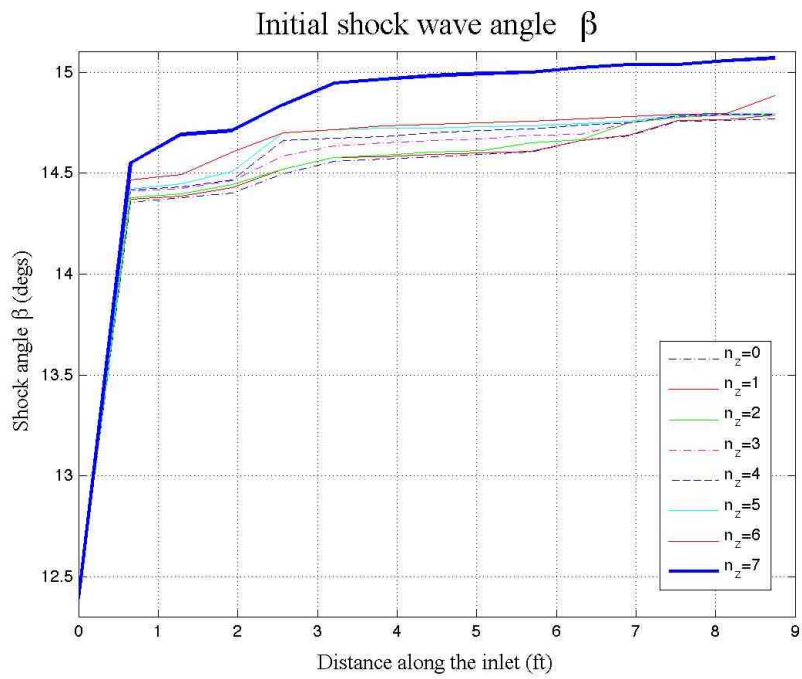
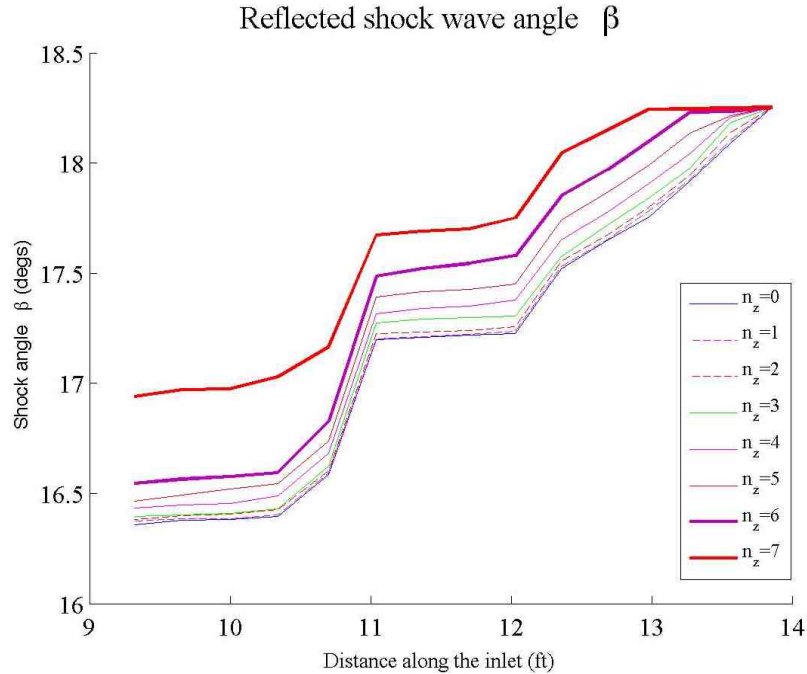Figure 4.25. Initial shock wave for angle-specified inlet

Figure 4.26. Reflected shock wave in angle-specified design

increase the wedge angle to create these structures. Although a throat profile can be created that produces these pockets, for a uniform inflow, this method can be used to determine where to change the wedge angle such that the total pressure recovery is higher or lower where needed.

This method allowed for some flexibility in designing the shock wave. Figures 4.23 and 4.26 show the evolution of the shock angle as the shock wave is propagated forward towards the capture plane. For the second inlet, the initial shock wave from the top of the inlet is relatively constant. The reflected shock wave has a similar shape for each streamtube but with the higher streamtubes having higher shock angles. The second inlet used smaller reflected and initial shock waves because of the larger wedge angle at the corner. The steps in the reflected shock angle graphed

in Figure 4.26 at 12 and 11 feet occur because the wedge angle decreased or increased by half a degree. The higher total pressure recovery pockets occurred due to the decrease in wedge angle in this portion. Because there is the most flexibility in characterizing the shock at the entrance and the corner – the same streamtubes – the top of the inlet had nearly complete total pressure recovery and was created to have $M_\infty = 6$ at the top of the inlet. Figures 4.3 and 4.4 also show the shock structure in the inlet.

Both inlets exhibited about the same amount of non-uniformity, although the first inlet had a slightly higher range of Mach numbers and temperatures at the entrance. Total pressures recoveries at the throat were slightly higher and were more uniform in the middle of the inlet from the bottom to the top in the second inlet. Mach number at the entrance ranged from 5.963 to 6.4637 with the mass-average Mach number at 6.154 for the second inlet. Mach number of the inflow to the first inlet varied from 5.812 to 6.437 with a mass-averaged Mach number of 6.152. The first inlet had a more uniform temperature profile at the entrance and a higher temperature range (from 390 to 460 K). Temperatures at the capture plane for the second inlet varied from 380 K to 450 K.

Chapter 5: Performance Analysis - Viscous

For each inlet, the growth of the boundary layer was calculated according to the viscous compound compressible flow based method presented previously. This method presents a qualitative method for comparing inlet designs under viscous flow assumptions with few computational resources and time. Although the boundary layer will likely transition to turbulent flow near the beginning of the inlet, only the laminar flow case was calculated in the present work, as propagating the laminar profile is more difficult. A laminar boundary layer also represents the worst-case scenario. However, this method should be able to work with any profile – laminar or turbulent. Only the ingested boundary layer from the fore-body that propagates along the top of the inlet was calculated. The boundary layer was propagated after the initial shock from the inlet entrance wedge angle. The starting boundary layer height was not the same for each inlet as calculated from Eqn. 2.28. This was necessary to ensure that the viscous propagation started at the right boundary layer height for the underlying inviscid flow properties and pressure gradient.

5.1 Boundary layer height

Inlet	Total Area	Center boundary layer height	Percentage of inlet	Flat plate[35]	Flat Plate[32]
Powerlaw	0.00169	0.00551	3.01488	0.00842	0.00575
Angle-defined	0.00368	0.00969	6.33823	0.0085	0.00669

Table 5.1. Comparison of centerline boundary layer versus flat plate solution

	Streamtube							
Inlet	Center	1	2	3	4	5	6	7
Power law	0.00551	0.00539	0.00555	0.00552	0.00548	0.00554	0.00572	0.00572
Angle-defined	0.00969	0.01114	0.01109	0.01020	0.00964	0.01128	0.01045	0.01180

Table 5.2. Final boundary layer heights for both inlets

The boundary layer growth was calculated for each inlet and found to be on the same order as the flat plate solution with the angle-defined inlet having twice the boundary layer growth. The boundary layer at the exit plane comprised 3 percent of the power law inlet. For the angle-defined inlet, the boundary layer comprised 6.33 percent of the exit plane. The flat plate solution was calculated to provide a sense of whether the boundary layer calculated using compound compressible flow methods is a representation of a realistic boundary layer. As shown in Table 5.1, the boundary layer calculated for the first inlet was under (65%) compared to the flat plate solution found using the relation found by Bertram and Blackstock[35]

$$\delta = .85x\left(\frac{T_w}{T_r} + .35\right)\sqrt{c}\,(\gamma - 1)M_\infty^2 \frac{1}{\sqrt{\mathrm{Re}_x}} \qquad (5.1)$$

where

$$\frac{T_r}{T\infty} = 1.816 = .5 + .5\frac{T_w}{T\infty} + .03M_\infty^2$$

$$c = \left(\frac{T_r}{T\infty}\right)^{.66-1} = .8196 \qquad (5.2)$$

and c is the Chapman-Rubesin parameter and T_r is the reference temperature

characterizing the temperature of the boundary layer. However, using the following

relation from White[28],

$$\delta = x\sqrt{\frac{2}{\text{Re}_x}}\int_0^{\eta(\delta)}\frac{T}{T_e}d\eta \tag{5.3}$$

for a laminar compressible boundary layer there is good agreement (within 1% to 7%)

between the calculated boundary layer and the flat plate solution. As shown in Figure

5.1, the streamtubes with the exception of the $n=1$ and $n=2$ streamtubes had the

same boundary layer growth until about 2.5 meters along the inlet, which is near the

inlet cowl. The $n=1$ and $n=2$ had the same growth but started off slightly larger.

After 2.5 meters along the inlet, the streamtubes had different rates of boundary layer

growth with the $n=7$ and $n=6$ boundary layers growing the most. The slight

increase in the boundary layer thickness for the $n=7$ streamtube at 3.5 meters is

caused by a slight instability in Mach number as the sixth of eight streamtubes in

profile reached the sonic line (Figure 5.12). Instead of oscillating around $M=1.08$,

the streamtube crossed the sonic line and oscillated around $M=0.9$ and crossed back

above the sonic line, settling around $M=1.1$. The other streamtubes did not have this

problem. The final boundary layer height for each streamtube is shown in Table 5.2.

Boundary layer height - Laminar
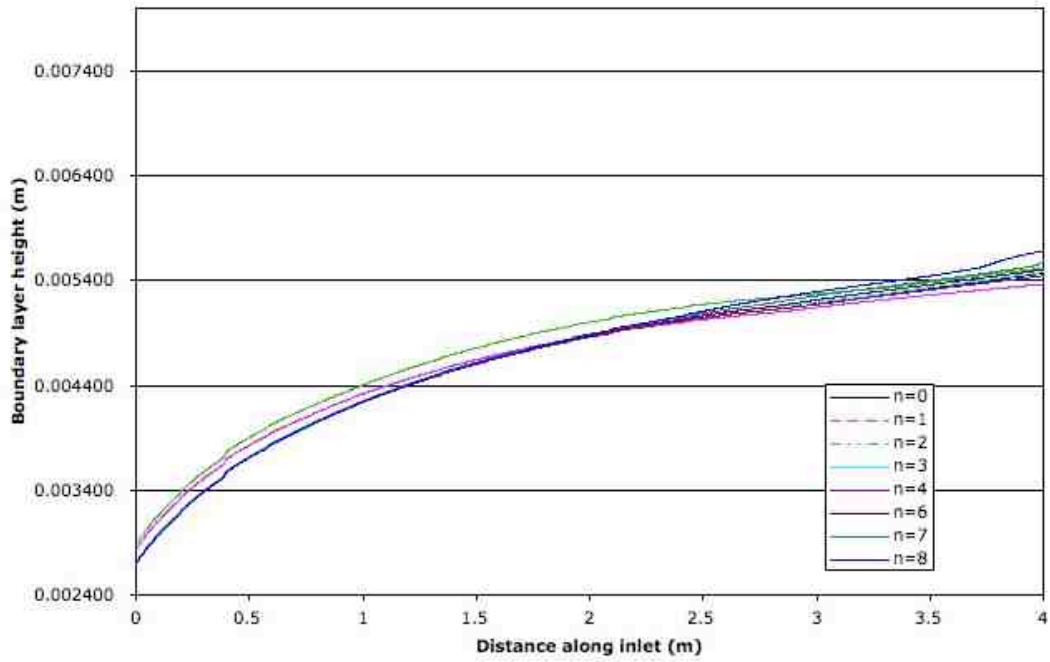
Figure 5.1 Boundary layer height for power law inlet assuming laminar flow

Boundary layer height - Laminar
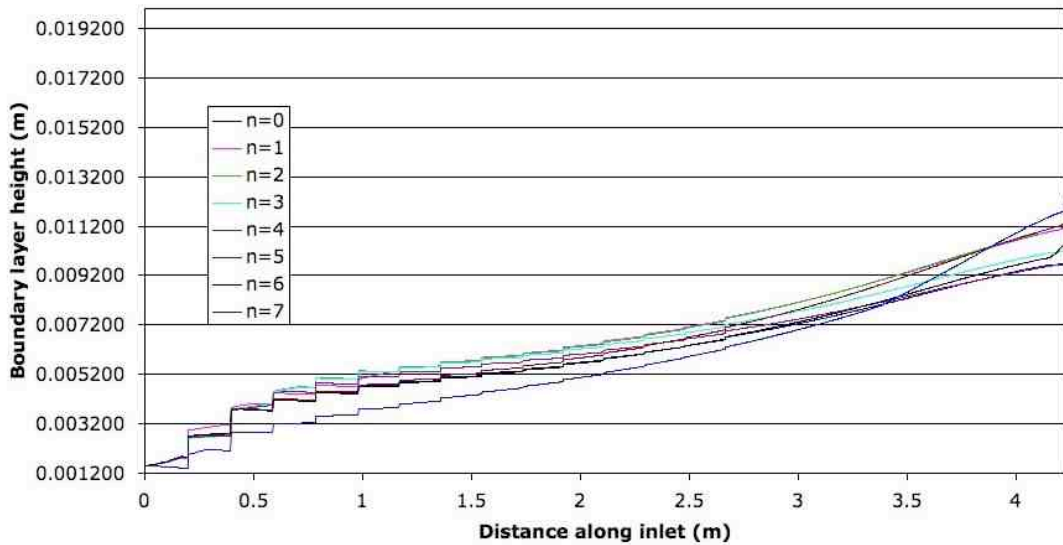
Figure 5.2. Boundary layer height for angle-defined inlet assuming laminar flow

89

The boundary layer for the angle-defined inlet was about twice as large as the boundary layer for the power law inlet at the exit plane because of the larger pressure gradients behind the shock near the entrance. After the first shock is calculated at 0.2 meters into the inlet, the large pressure gradient caused by the curved shock causes the boundary layer to increase about 0.0015 meters, which is about a quarter of the total boundary layer growth of the power law inlet. This effect can be seen clearly in Figure 5.2. As the pressure gradient decreases, the jaggedness of the boundary layer decreases. After the cowl, at 2.84 meters, the boundary layer growth is smooth and no longer subjected to jumps. This is likely because of the pressure gradient behind the shock and because after 2.84 meters, the top streamtube is in front of the shock off the cowl.

Despite these jumps, the overall trend in boundary layer growth remained relatively constant for the angle-defined inlet, while it gradually slowed down for the power law inlet until the cowl. After the cowl, the boundary layer growth was about 0.004 meters for the angle-defined inlet (35% to 40% of the total growth), while the growth after the cowl for the power law inlet was much smaller (8 to 10 percent of the total growth). An inlet with smaller pressure gradients behind the curved shocks will likely have a smaller boundary layer and with this method, produce a more accurate representation of the boundary layer growth.

The boundary layer streamtubes closer to the walls had less downstream growth than those in the center of the inlet. The streamtube closest to the side wall

90

($n = 7$) had accelerated growth about 3.5 meters along the inlet because the seventh

streamtube in the profile reached the sonic line (Figure 5.20), and instead of

oscillating around a Mach number close to the sonic line, it crossed the sonic line.

The increase in the $n = 6$ streamtube near the shoulder also occurred because the

seventh streamtube in the vertical profile passed the sonic line (Figure 5.19).

5.2 Effect on self-starting and inlet shape

New inlets were constructed that corrected for the boundary layer growth by

adding a correction equal to the boundary layer growth as developed by Walsh[25].

These new inlets had lower contraction ratios than the inviscid inlets, but did not

change much because the boundary layer ingested into the isolator was less than ten

percent of the total airflow. The corrected internal contraction ratio is still greater than

the Kantrowitz limit; however, experimental results indicate that a rectangular-to-

elliptical inlet with an internal contraction ratio well above the Kantrowitz limit at

Mach 6 will still self-start.[15] Because an unstarted hypersonic inlet has a higher

pressure recovery compared to a normal shock, internal contraction ratios higher than

the Kantrowitz limit can allow for inlet self-start. For some geometries such as

three-dimensional geometries, internal contraction ratios as high as two to three can

still allow for self-start.[36] Figure 5.3 shows the corrected inlet area compared to the

uncorrected inlet area for each inlet. Figure 5.4 shows the corrected and uncorrected

centerline height for each inlet.
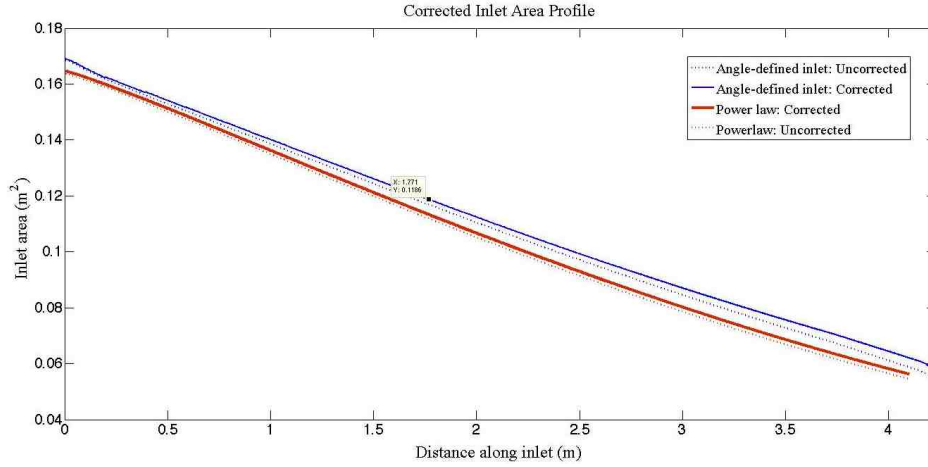
Figure 5.3. Comparison of corrected and uncorrected inlet areas
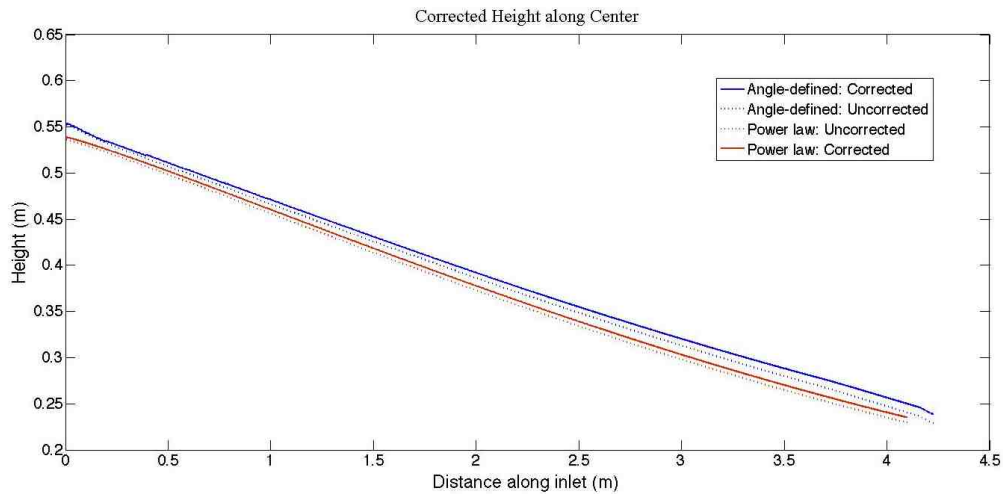
Figure 5.4. Comparison of corrected and uncorrected center heights

Inlet	Inviscid Internal CR	Viscous Internal CR	Kantrowitz Limit	Average Mach Number at Cowl	Boundary Layer Area at Cowl	Corrected Area at Cowl
Power law	1.54	1.52	1.25	4.374	0.00157	0.0841
Angle-defined	1.61	1.56	1.44	4.576	0.00237	0.0907

Table 5.3. Internal geometric contraction ratios

Inlet	New Capture Area	Viscous Exit Area	Inviscid CR	Viscous CR
Power law	0.1635	0.055	2.98	2.95
Angle-defined	0.1690	0.058	3.07	2.91

Table 5.4. Corrected inlet areas and external geometric contraction ratios

5.3 Mach number in boundary layer

In each inlet, the boundary layer streamtubes each trended towards the sonic line depending on the strength of the shear gradient. When a streamtube's Mach number approached too close to the sonic line, where the Mach number decreased or increased too rapidly towards $M = 1$ where the solution would blow up, the streamtube's height was adjusted and the Mach number re-adjusted based on the initial equation for determining Mach number in the profile. The Mach number at which this adjustment occurred – a re-adjustment trigger value – depends on the value of the shear gradient and how quickly a streamtube approached the sonic line. For the first supersonic streamtube to reach the sonic line and the streamtubes higher in profile ($n = 6$ or $n = 7$), higher Mach numbers ($1.09 < M < 1.12$) that this adjustment occurred were needed to keep the solution stable. The results when this number is not high enough can be shown for the streamtube channels closer to the wall for the $n = 6$ or $n = 7$ streamtube in the profile in Figures 5.13, 5.19, and 5.20. In these cases, the streamtubes oscillated above and below the sonic line or crossed the sonic line as shown in Figures 5.19 and 5.20 and stayed at a much lower subsonic

value. This resulted in a larger increase in the boundary layer than if the streamtubes had stayed above and near the sonic line. Generally, resetting the profile resulted in the Mach number oscillating around the trigger value and did not alter the boundary layer growth – provided the temperature and the shear gradient were handled correctly.

There are some slight anomalies in the Mach number profiles for the angle-defined inlet because of the large pressure gradient at the inlet entrance. For the second streamtube in the profile, the Mach number drops slightly from M=0.3 to M=0.16. This is due to the large positive pressure gradient from the curved shock at that location, because the shear gradient for the first two streamtubes in the profile was calculated based on curve fitting for $1 - \dfrac{\partial \tau / \partial y}{dP / dy} \sim M^2$. Because the streamtube at the wall always has a velocity near zero and increases its Mach number very little because the shear gradient ~ the pressure gradient, only the second streamtube in the profile is affected. In addition, the streamtube modeling the top of the boundary layer ($n = 8$) has a Mach number slightly higher than the underlying flow because of the large decrease in Mach number behind the shock at the entrance. This method cannot adjust the Mach number in the boundary layer to this instantaneous drop.

Most streamtubes reach the sonic line by the end of the inlet. On the angle-defined inlet especially, even the seventh streamtube in the profile reached the sonic line, leaving only the initially hypersonic streamtube representing the top of the boundary layer and the wall streamtube not at the sonic line. However, the angle-

defined inlet is also 0.12 meters longer. A more continuous profile with more tubes $0.8 < \eta < 0.99$ might be more accurate and representative of the boundary layer and fill some of the gaps in the profile towards the end of the inlet. In the power law inlet, the $n = 6$ streamtube barely reached the sonic line by the end of the inlet.
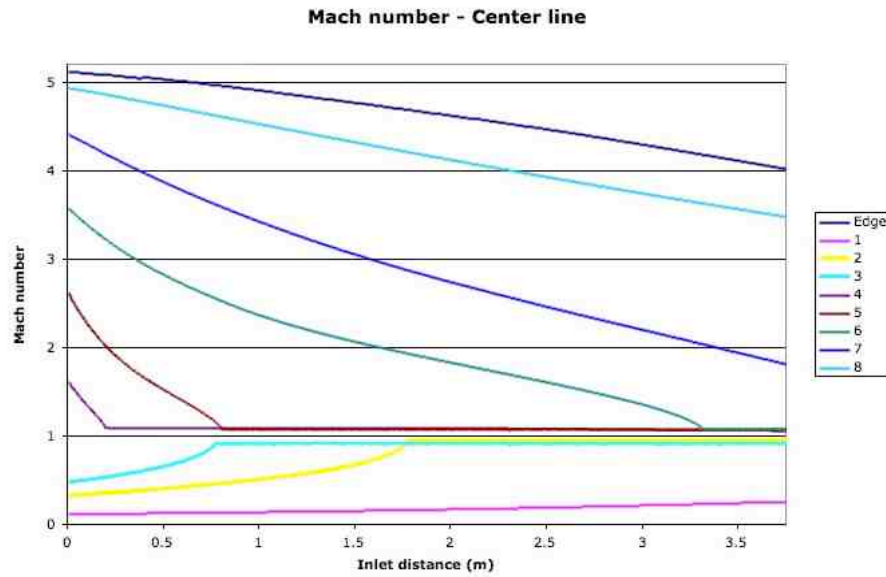
Figure 5.5. Mach number power law inlet – Center line
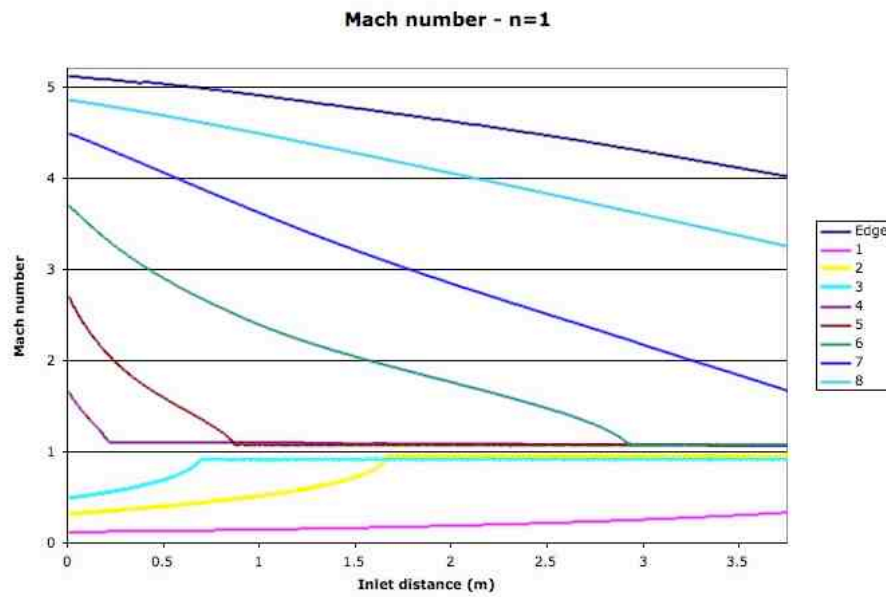
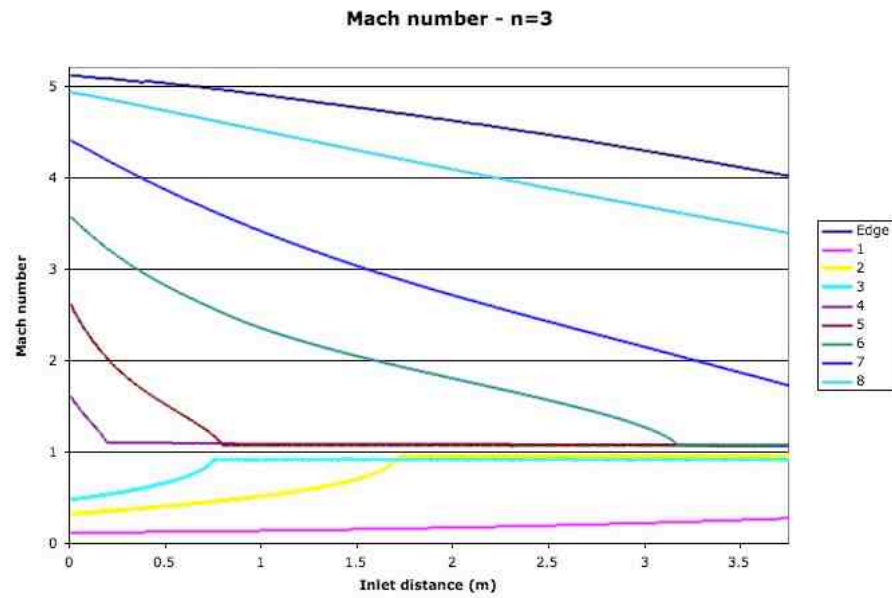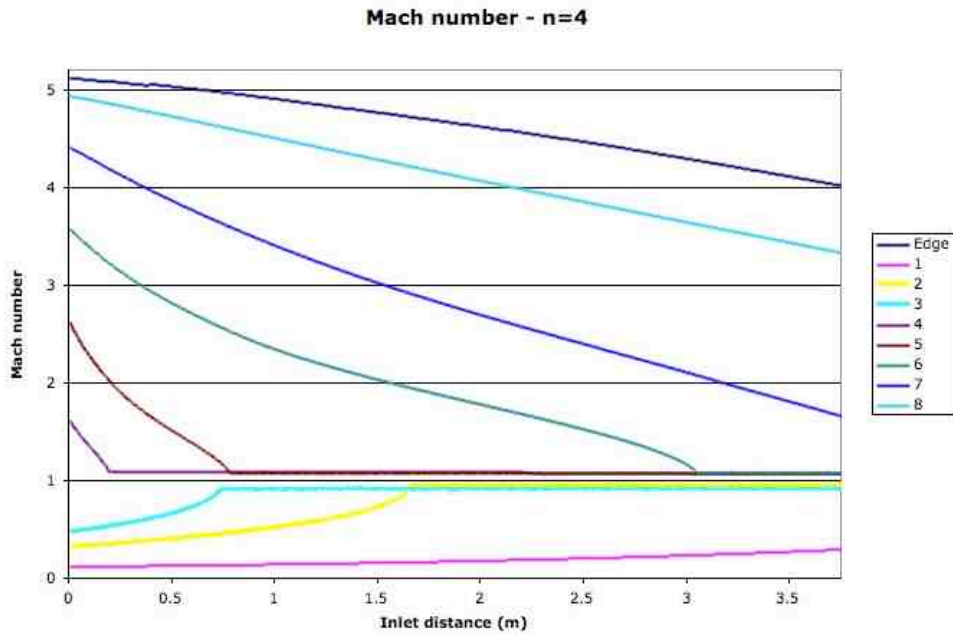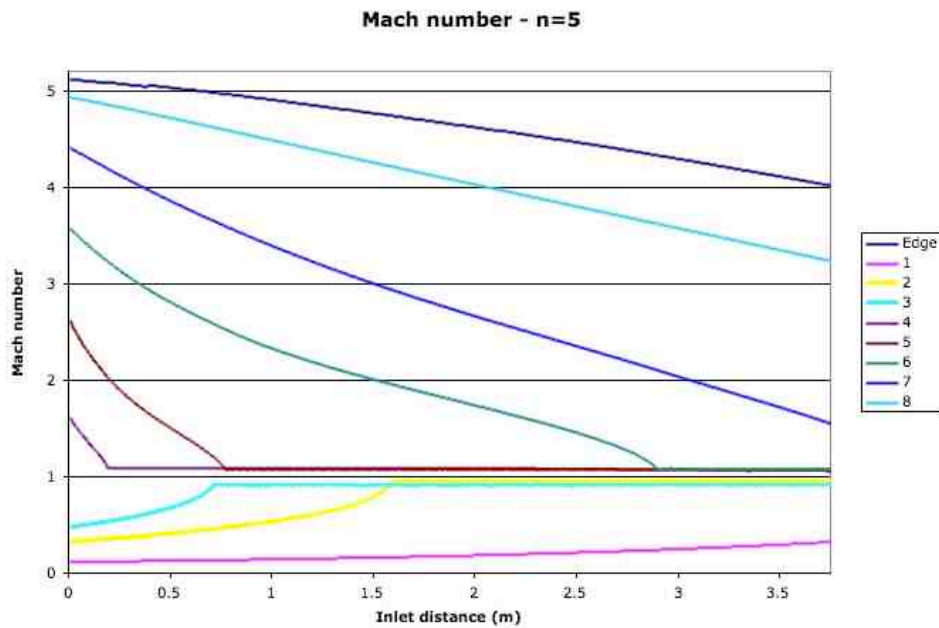Figure 5.6. Mach number power law inlet – n=1

95
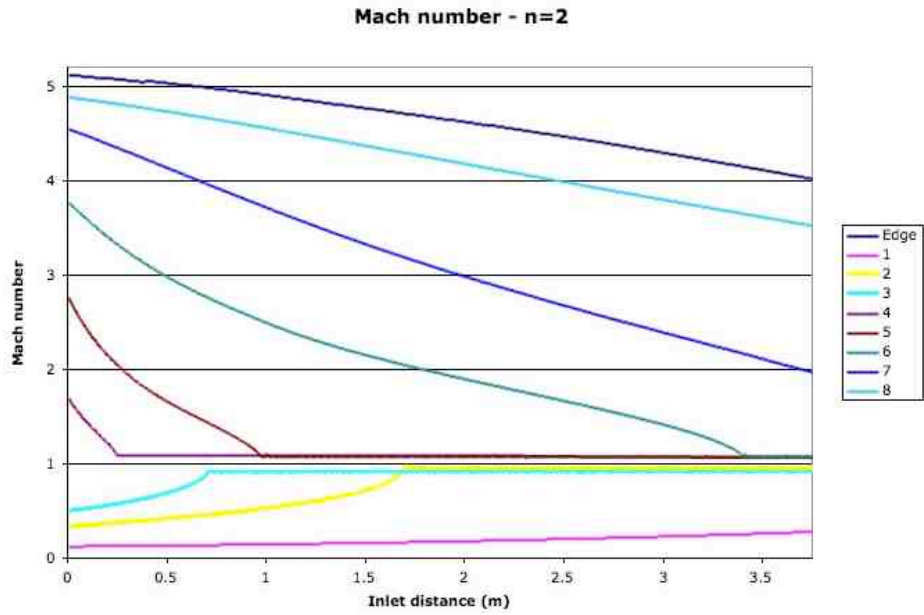
Figure 5.7. Mach number power law inlet – n=2

Figure 5.8. Mach number power law inlet – n=3

96

Figure 5.9. Mach number power law inlet – n=4

Figure 5.10. Mach number power law inlet – n=5
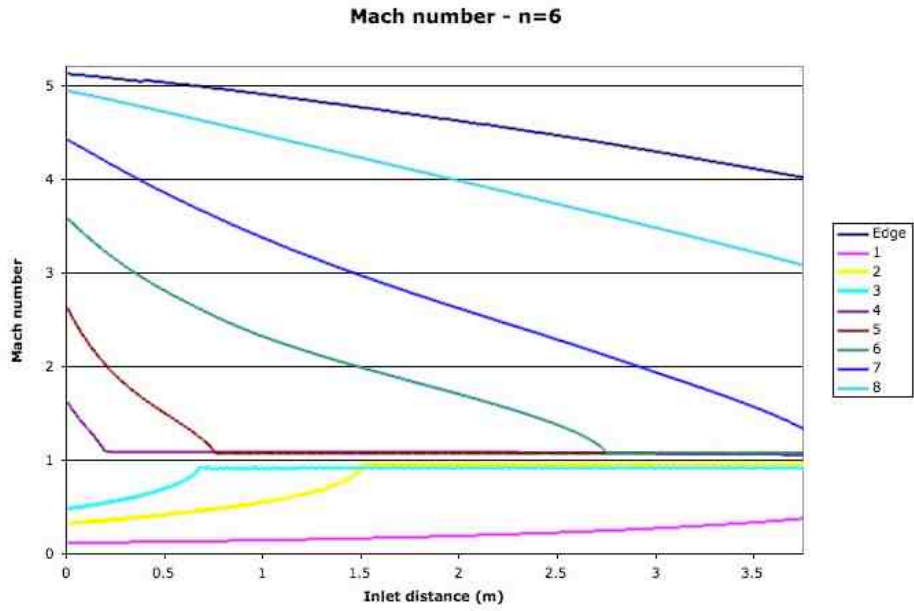
Figure 5.11. Mach number power law inlet – n=6
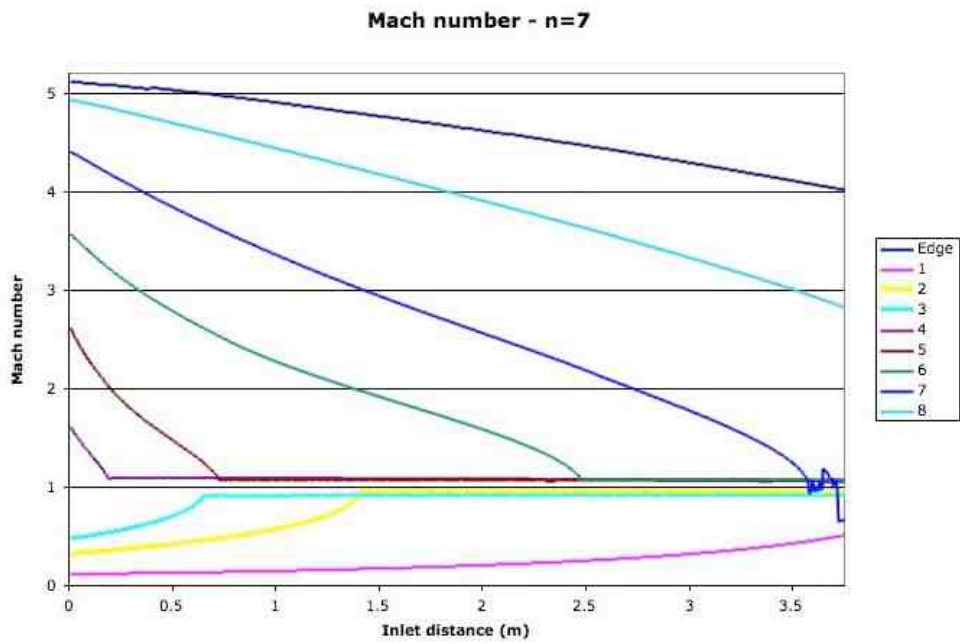
Figure 5.12. Mach number power law inlet – n=7
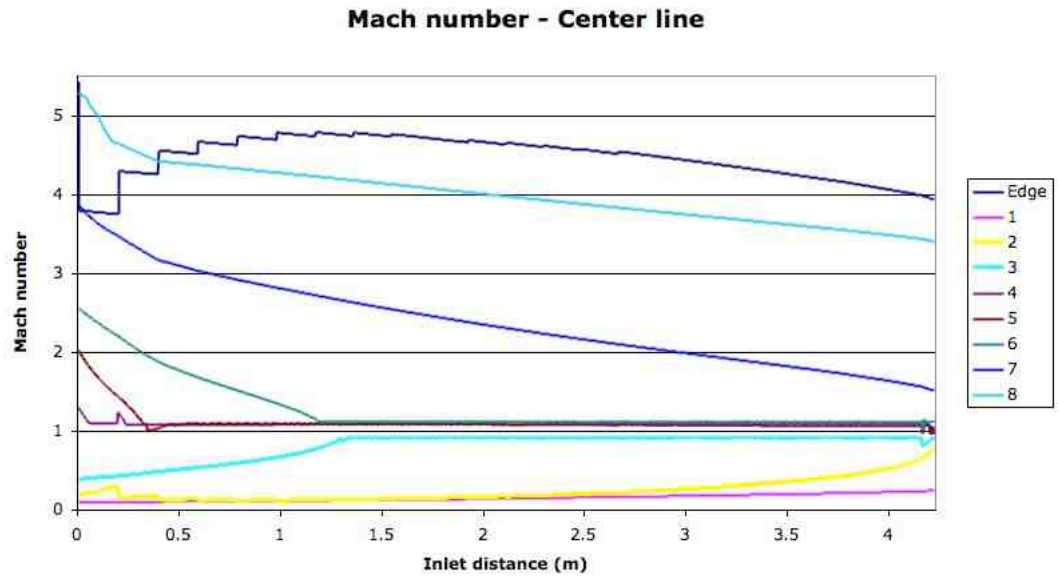
Figure 5.13. Mach number angle-defined inlet – Center line
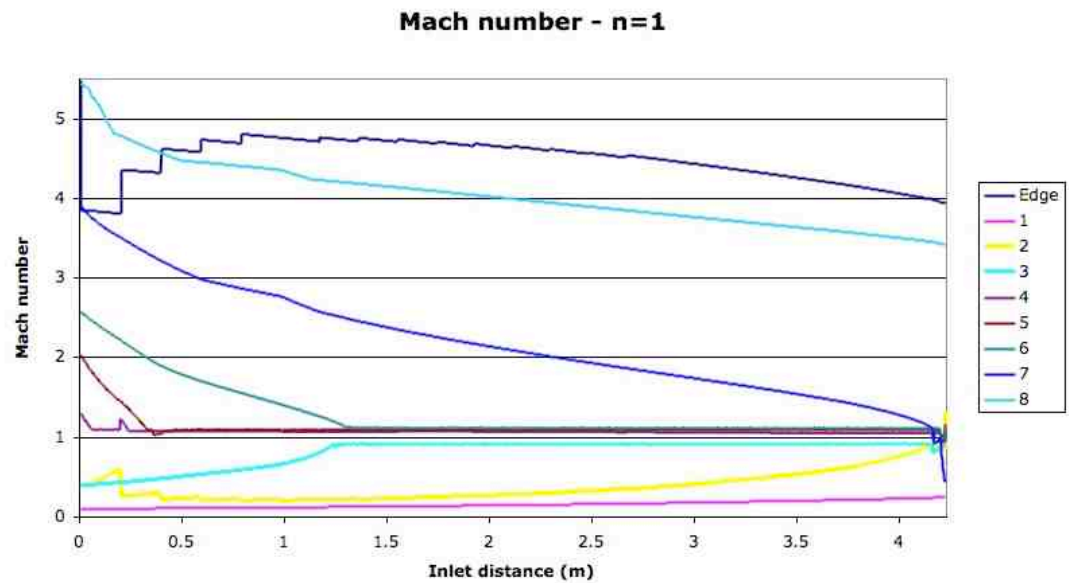
Figure 5.14. Mach number angle-defined inlet – n=1
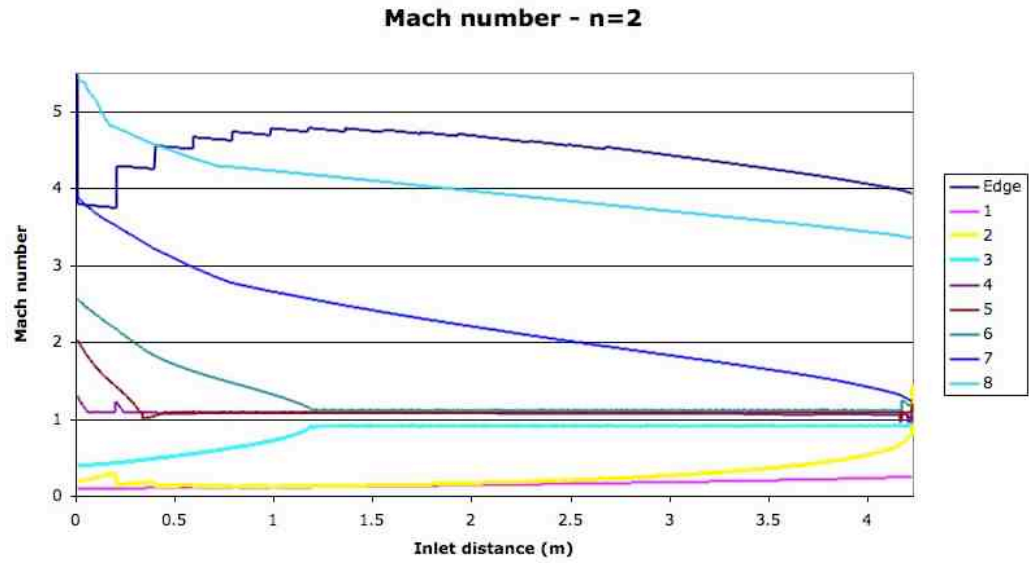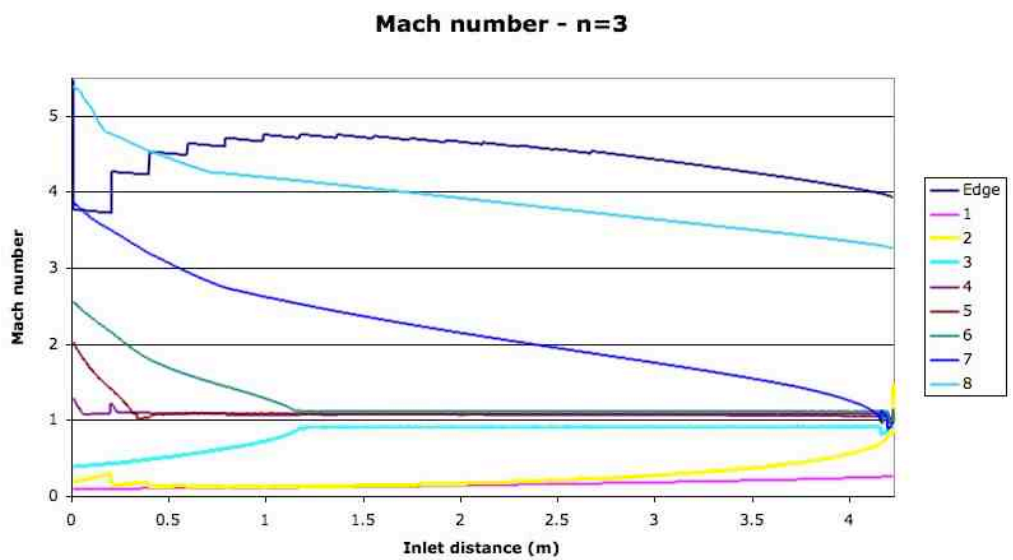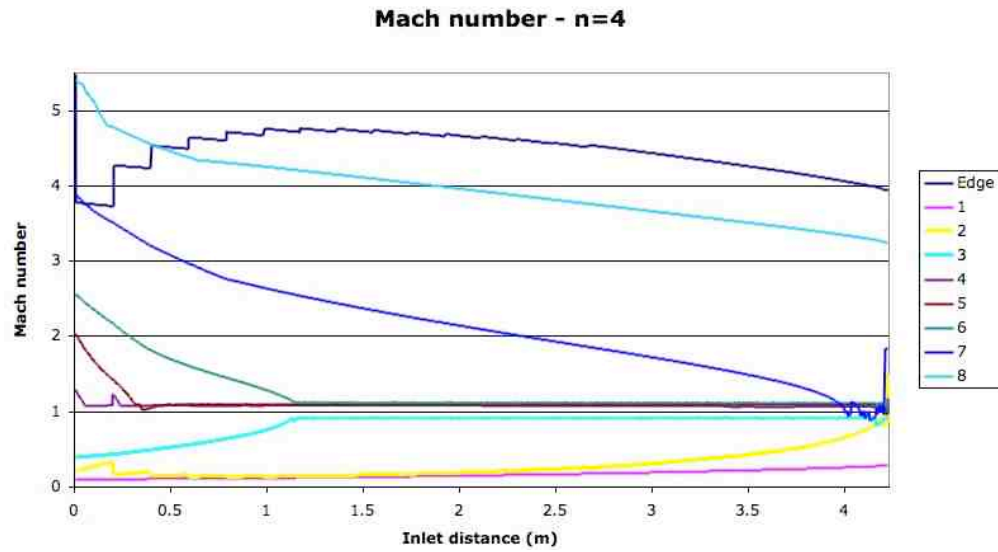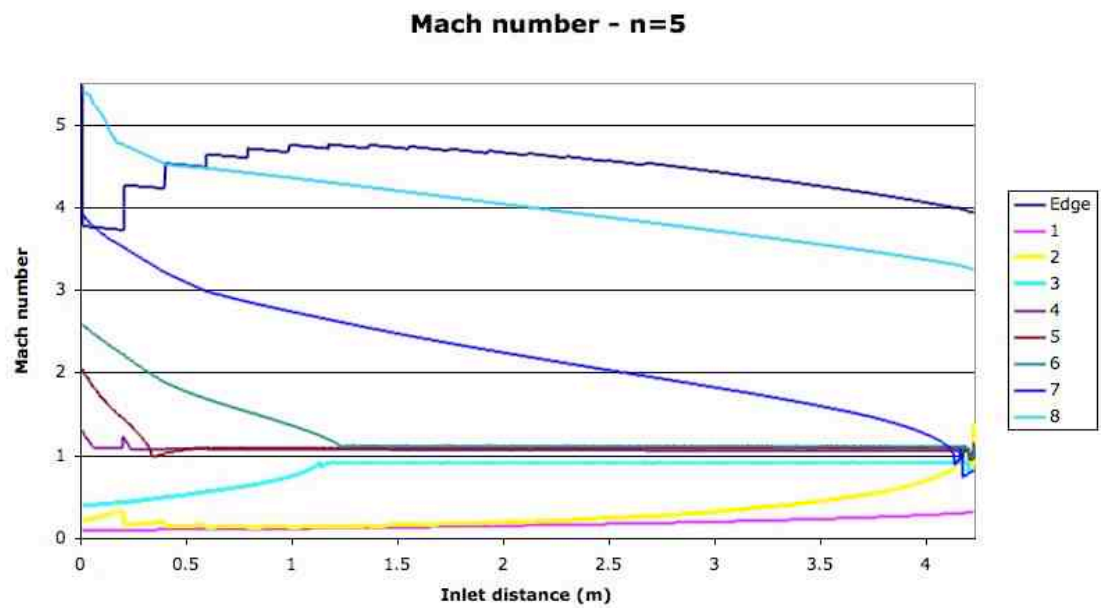
Mach number - n=2

Figure 5.15. Mach number angle-defined inlet – n=2

Mach number - n=3

Figure 5.16. Mach number angle-defined inlet – n=3

Mach number - n=4

Figure 5.17. Mach number angle-defined inlet – n=4

Mach number - n=5

Figure 5.18. Mach number angle-defined – n=5
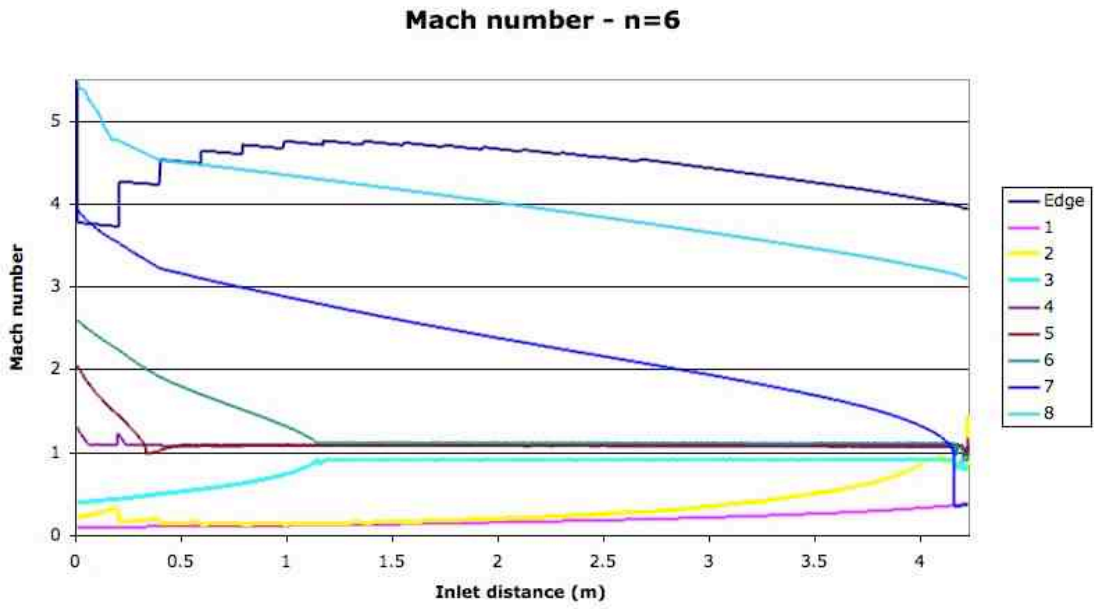
Mach number - n=6

Figure 5.19. Mach number angle-defined – n=6
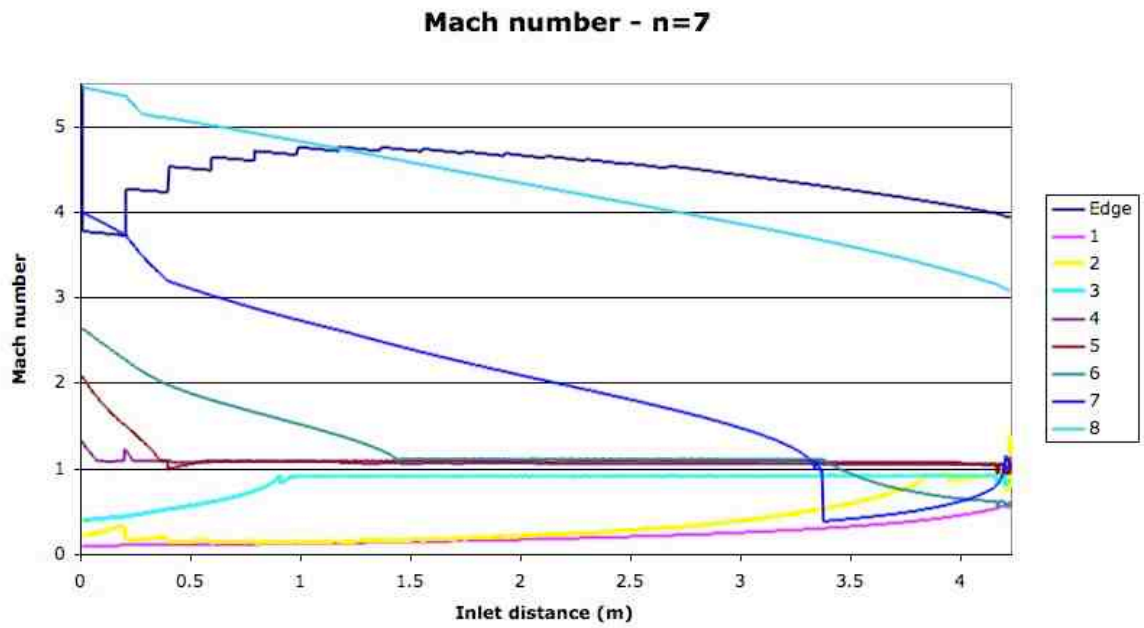
Mach number - n=7

Figure 5.20. Mach number angle-defined – n=7

5.4 Temperature in boundary layer

An alternative method to determining the temperature based on the equations used to construct the original profile needed to be used to produce physical results for temperature. Using Eqn. 2.25 produced a temperature that was lower than the starting temperature, which is inconsistent with compound compressible flow theory. According to the classic influence coefficient method, the temperature in each supersonic streamtube needed to increase and decrease for each subsonic streamtube because the channel area was decreasing and because of the presence of friction. This could suggest that the profile is not being tracked properly; however, the profile looks right until the first streamtube reaches the sonic line. It is more likely because as a streamtube approaches the sonic line from above, it is still increasing in temperature because of the area change and friction but moves a location in the boundary layer profile with a η corresponding to a different temperature. Best results were obtained by setting the temperature constant to the previous value each time a streamtube crossed the trigger Mach number value. Figures 5.21 to 5.36 show the temperature for each streamtube for both inlets.
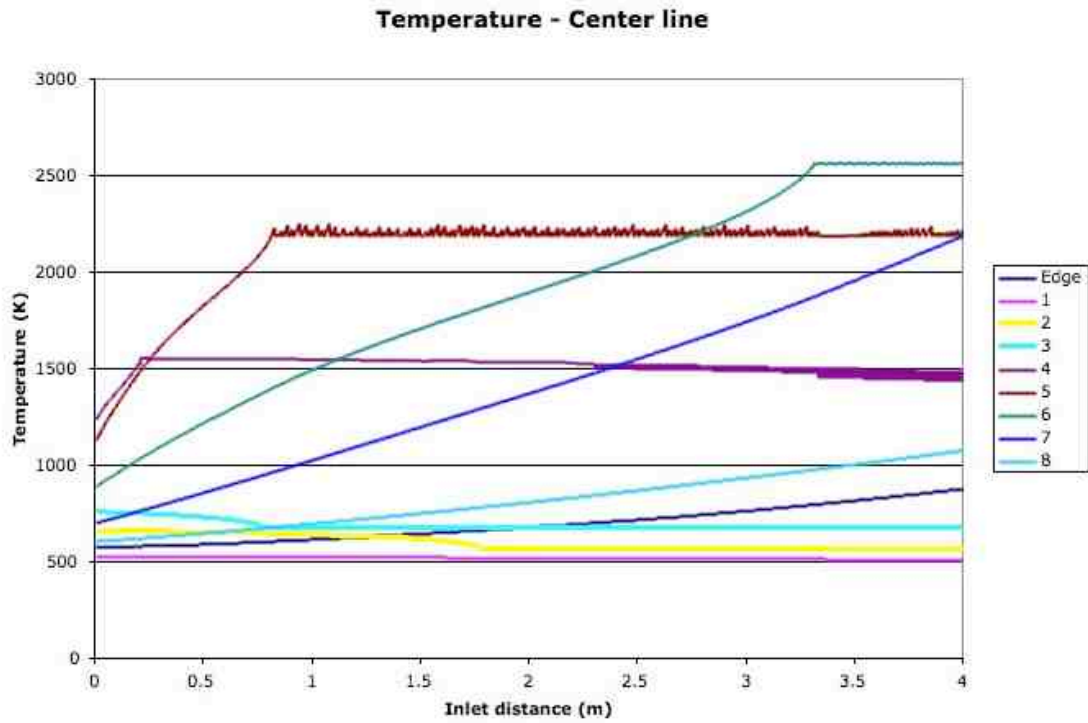
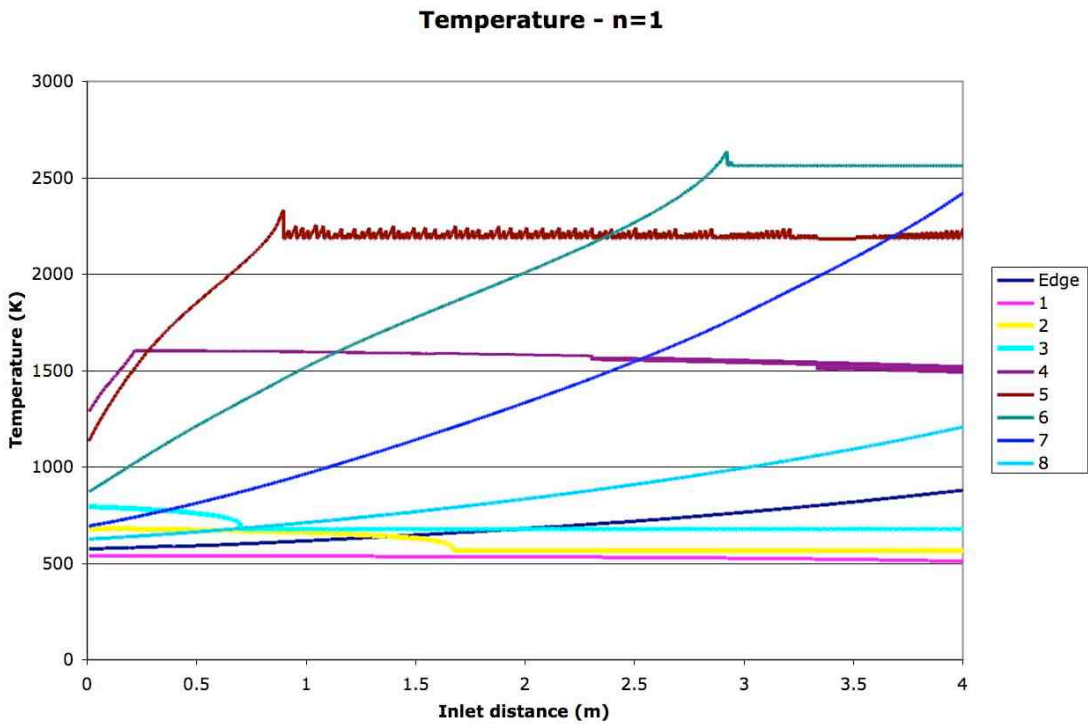Figure 5.21. Temperature in boundary layer for power law inlet – Centerline

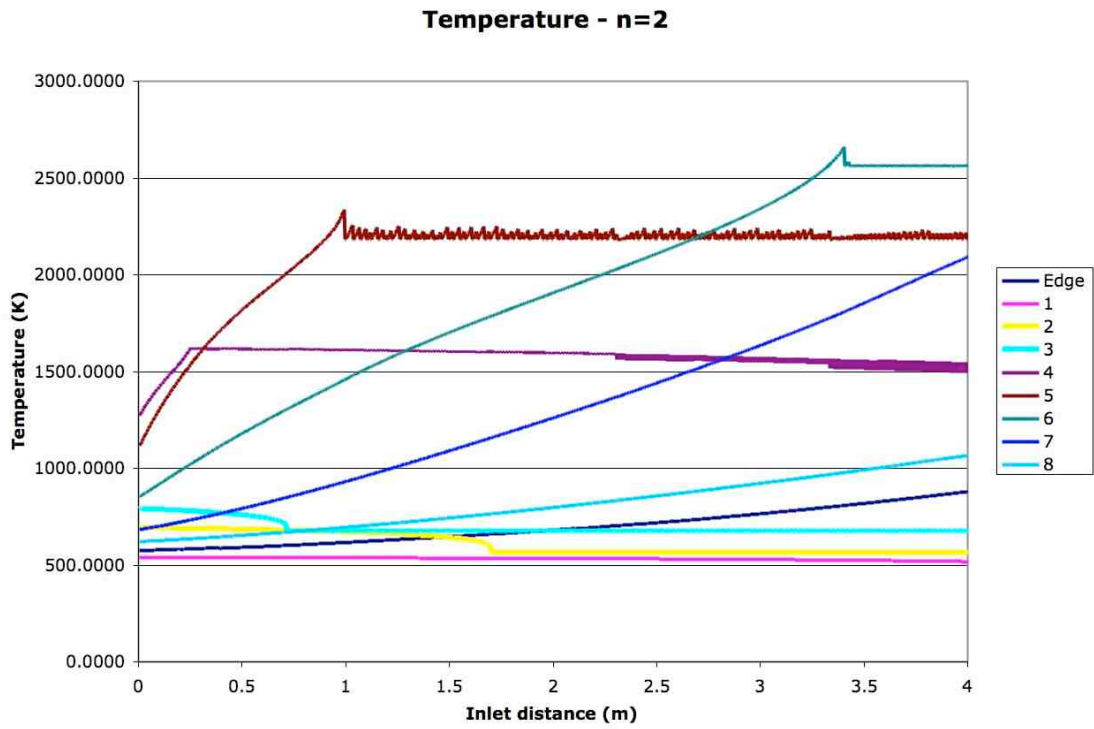Figure 5.22. Temperature in boundary layer for power law inlet – n=1

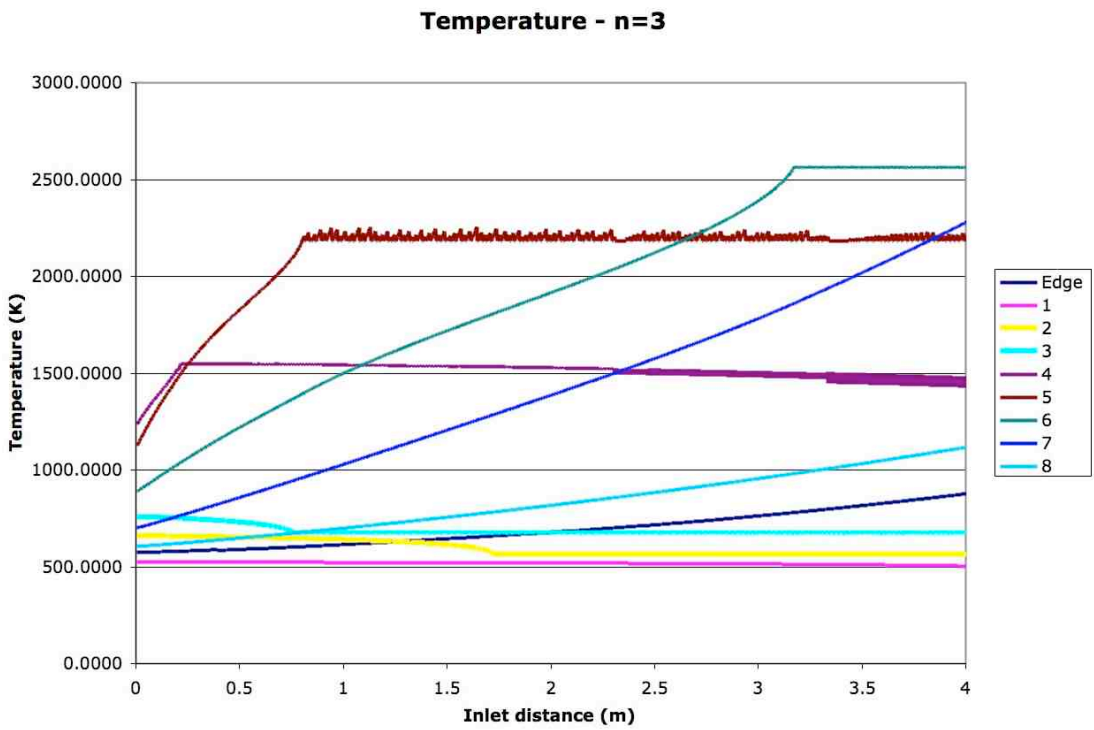Figure 5.23. Temperature in boundary layer for power law inlet – n=2

Figure 5.24. Temperature in boundary layer for power law inlet – n=3
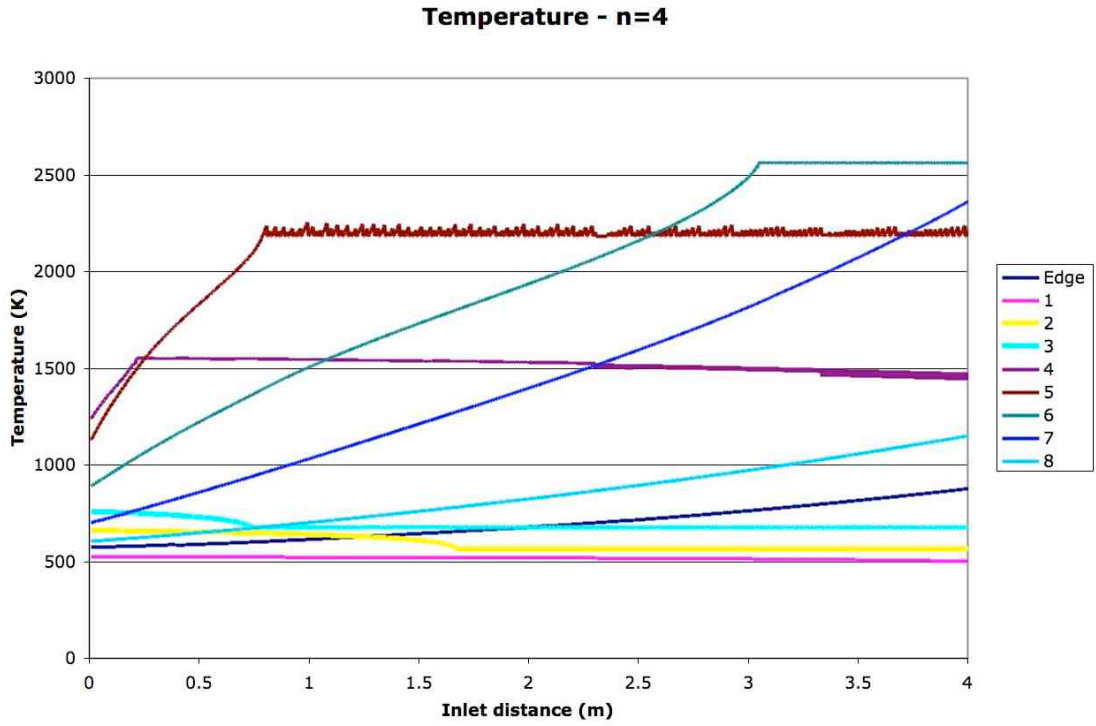
105

Figure 5.25. Temperature in boundary layer for power law inlet – n=4
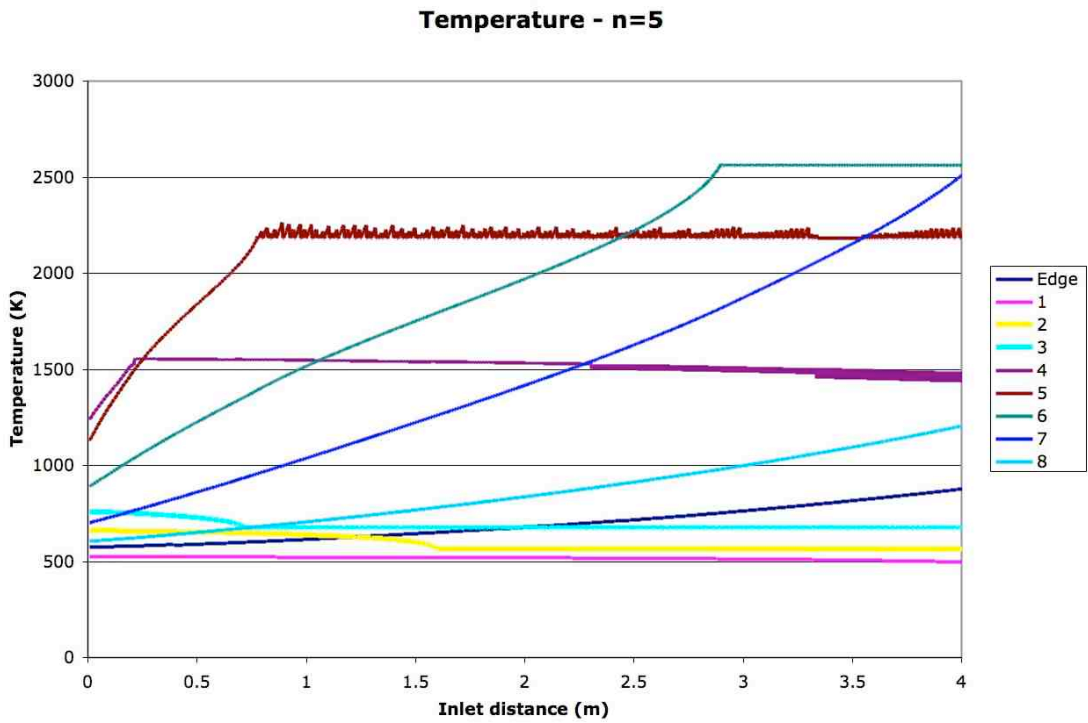

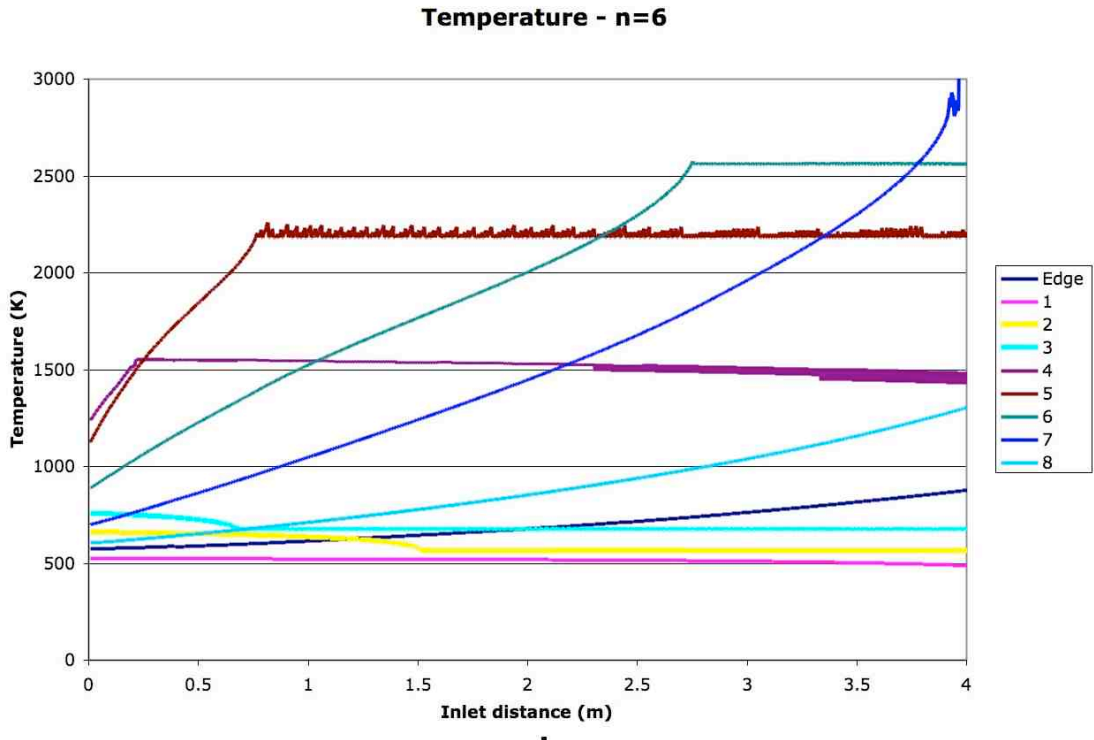Figure 5.26. Temperature in boundary layer for power law inlet – n=5

106

Figure 5.27. Temperature in boundary layer for power law inlet – n=6
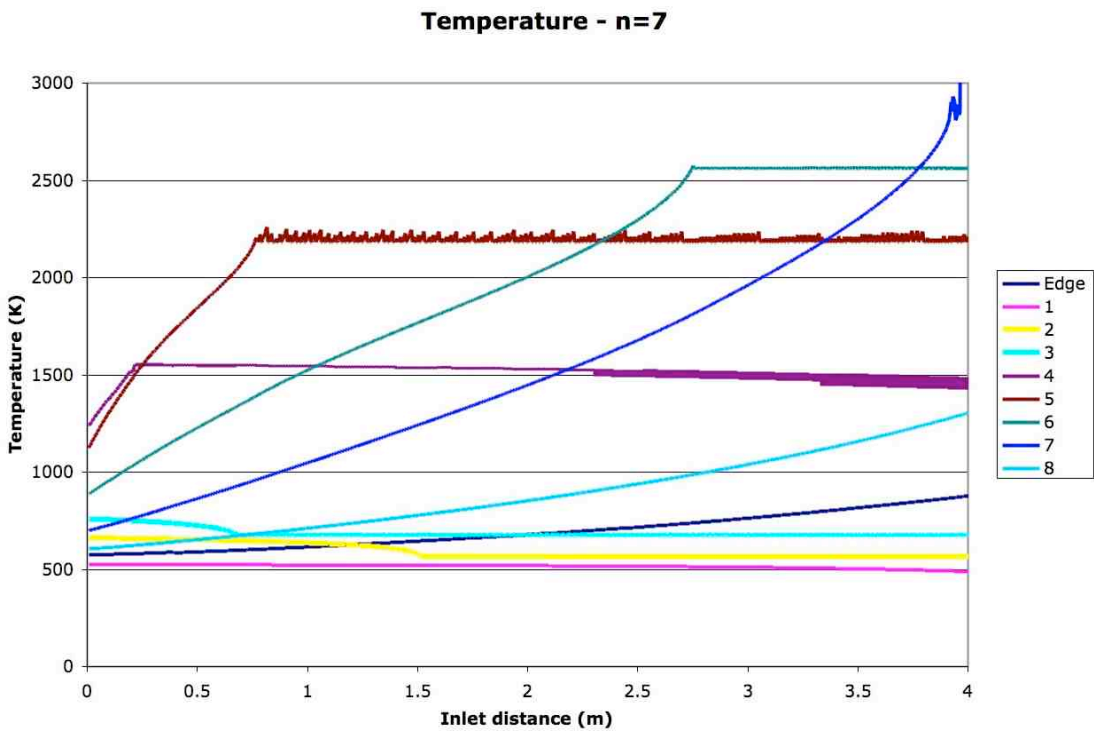
Figure 5.28. Temperature in boundary layer for power law inlet – n=7

Temperature - Center

Figure 5.29. Temperature in boundary layer for angle-defined inlet – Center

Temperature - n=1

Figure 5.30. Temperature in boundary layer for angle-defined inlet –n=1

Temperature - n=2

Figure 5.31. Temperature in boundary layer for angle-defined inlet –n=2

Temperature - n=3

Figure 5.32. Temperature in boundary layer for angle-defined inlet –n=3
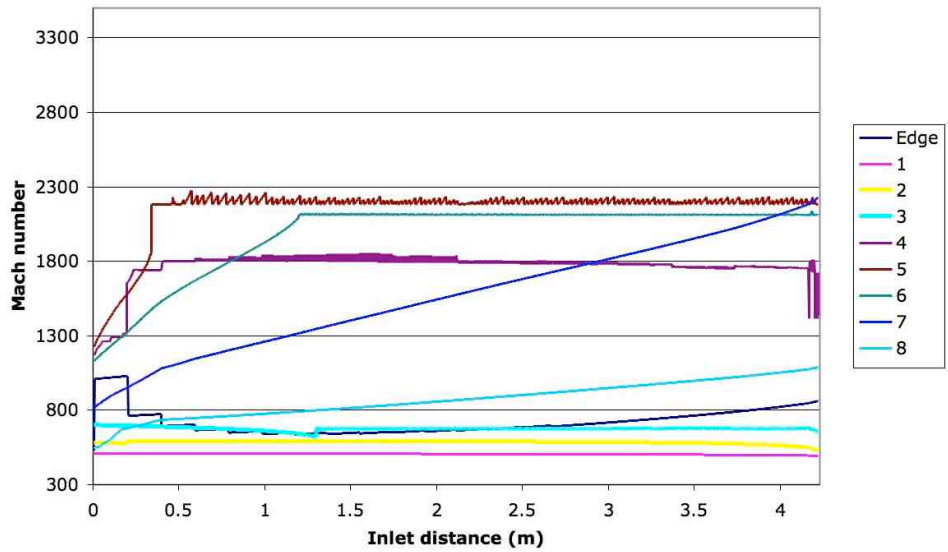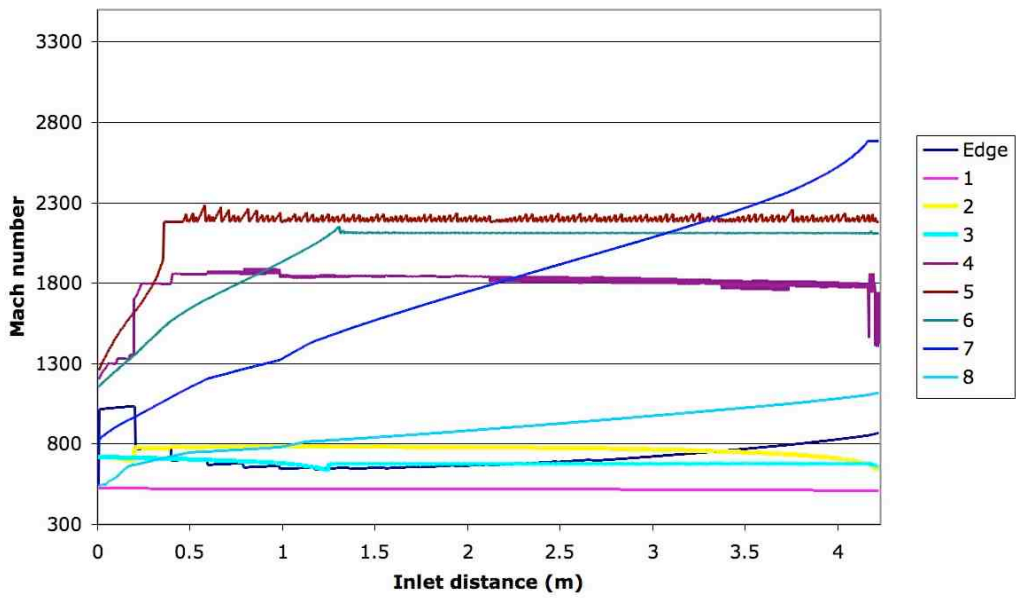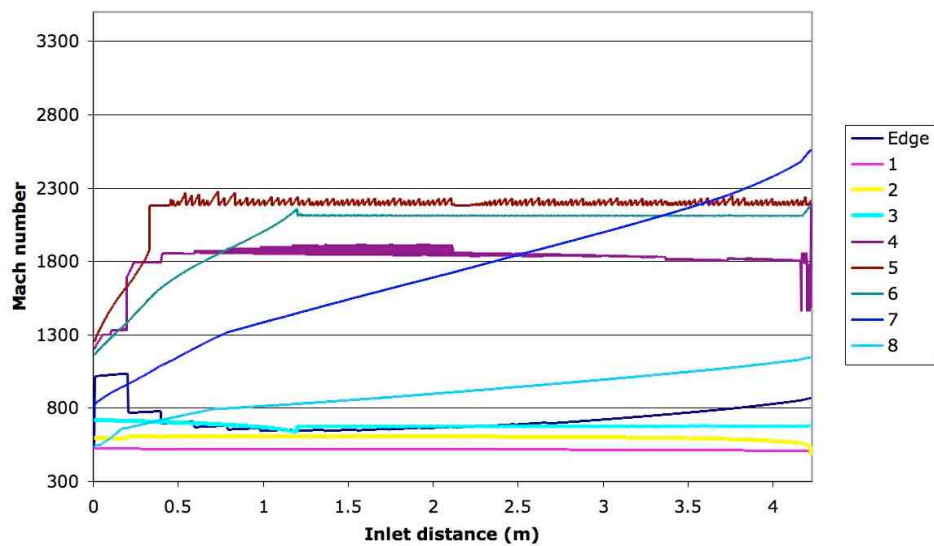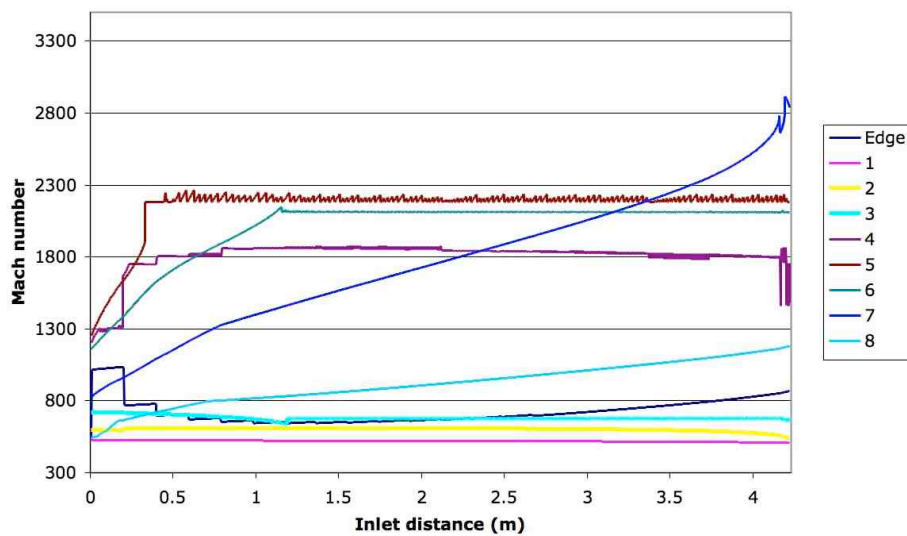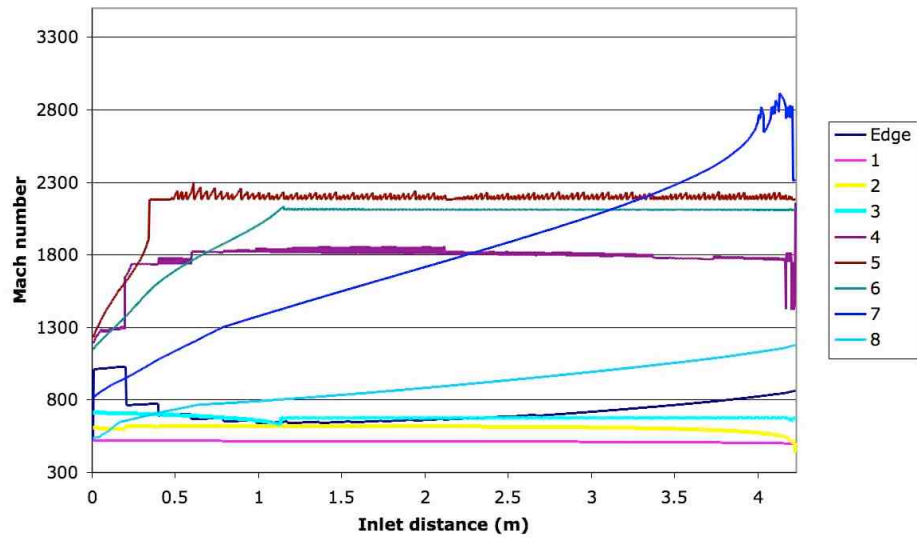
Temperature - n=4

Figure 5.33. Temperature in boundary layer for angle-defined inlet –n=4

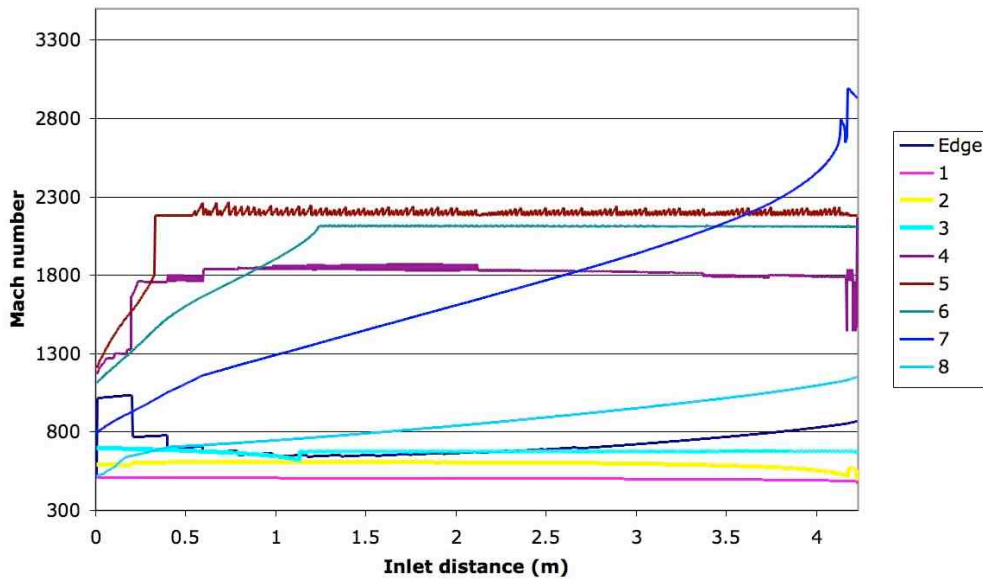**Temperature - n=5**

Figure 5.34. Temperature in boundary layer for angle-defined inlet –n=5
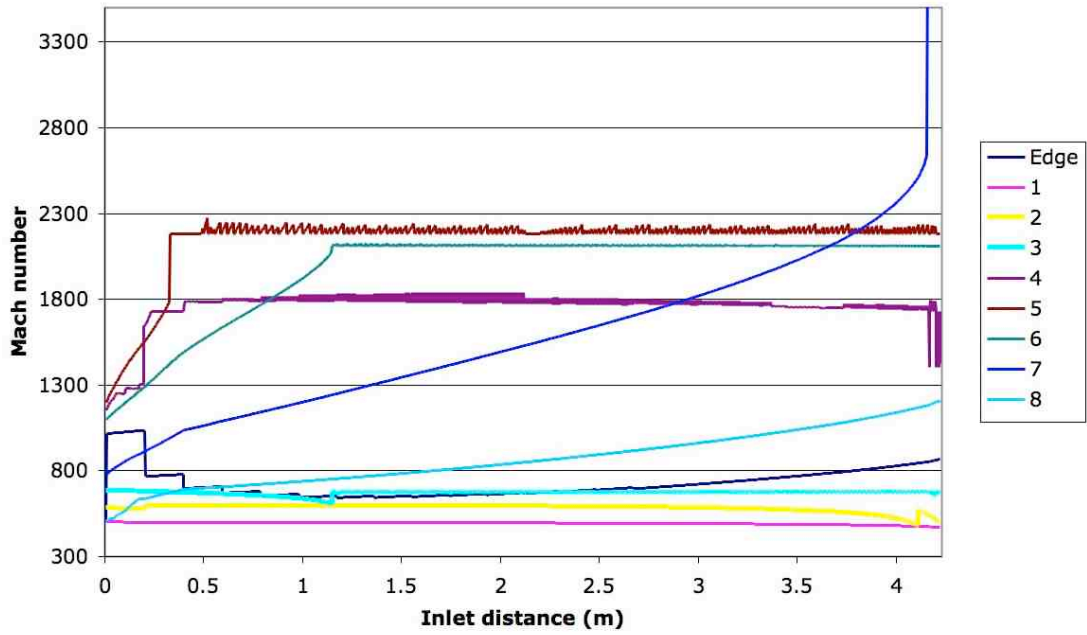
Figure 5.35. Temperature in boundary layer for angle-defined inlet –n=6
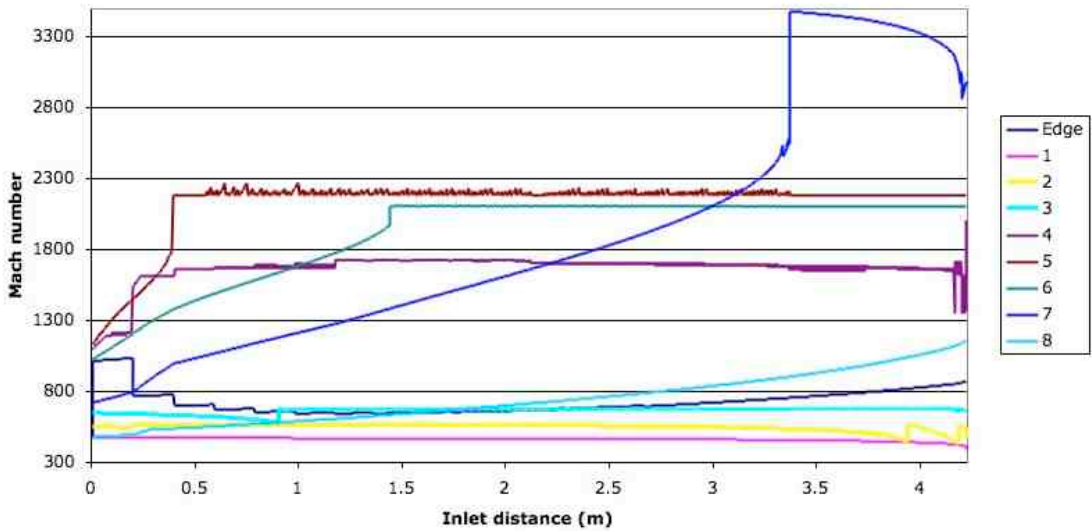
Figure 5.36. Temperature in boundary layer for angle-defined inlet –n=7

111

5.5 Shear profile

The growth of the boundary layer is highly dependent on the method for
calculating the shear gradient. There are several ways of calculating the shear
gradient for each streamtube. Calculating it based on the reference temperature
according to Eqn. 5.2 produces a boundary layer that grows too slowly and in some
cases decreases. For each streamtube, μ_n was calculated based on the temperature
according to Eqn. 2.9. The shear gradient term can also be calculated based on
finding the shear stress τ and the difference between adjacent streamtubes divided by
the difference in their heights. For the profile resolution used, this produced a shear
gradient that was too large, resulting in the top streamtube Mach number decreasing
too rapidly with respect to top streamtube in the inviscid flow and the third and fourth
streamtube in the profile very quickly going to $M=1$. The change in the similarity
coordinate with respect to the change in streamtube height can be similarly
determined or can be determined based on

$$\frac{d\eta}{dy} = \frac{\int_0^{\eta_\delta} \frac{T}{T_0} d\eta}{\delta \frac{T}{T_0}} \tag{5.4}$$

Using Eqn. 5.4 propagated errors from propagating temperature and produced a
smaller boundary layer; whereas, using a finite difference produced errors from
having a discrete streamtube profile and a larger boundary layer. A mix of methods of
calculating $\frac{d\eta}{dy}$ was used with Eqn. 5.4, producing better behaved streamtubes for the

higher streamtubes ($n = 6$ and $n = 7$). The shear gradient for the first and second streamtubes in the profile was calculated based on the shear gradient necessary for the curve-fit for finding the area change for subsonic streamtubes. Using more streamtubes in the profile at each channel might produce a more accurate shear gradient profile and resulting in some of these different ways of calculating the shear gradient producing the same results.

When a streamtube reaches the sonic line, modifications are made to the shear gradient. The new similarity coordinate for sonic streamtubes is calculated as follows:

$$\eta_i = \eta_{i-1} + \frac{d\eta}{dy}\Delta y \qquad (5.5)$$

where Δy is the amount the streamtube is bumped up or down. Recalculating the shear gradient for the sonic streamtubes results in the shear gradient for all the sonic and supersonic streamtubes rapidly decreasing in magnitude to nearly zero. This results in the boundary layer becoming constant after 2.0 meters or slightly decreasing. Setting the shear gradient constant for a sonic streamtube led to the shear gradient for the supersonic streamtubes remaining significant. Setting the shear gradient constant makes physical sense because the shear gradient should be roughly the same for adjacent streamtubes near M=1 even though they are at different heights.

Figures 5.37 and 5.38 show that once the streamtubes reach the sonic line they have roughly the same shear gradient. The instantaneous jumps in the shear gradient for the subsonic streamtubes near the wall comes from calculating the shear gradient
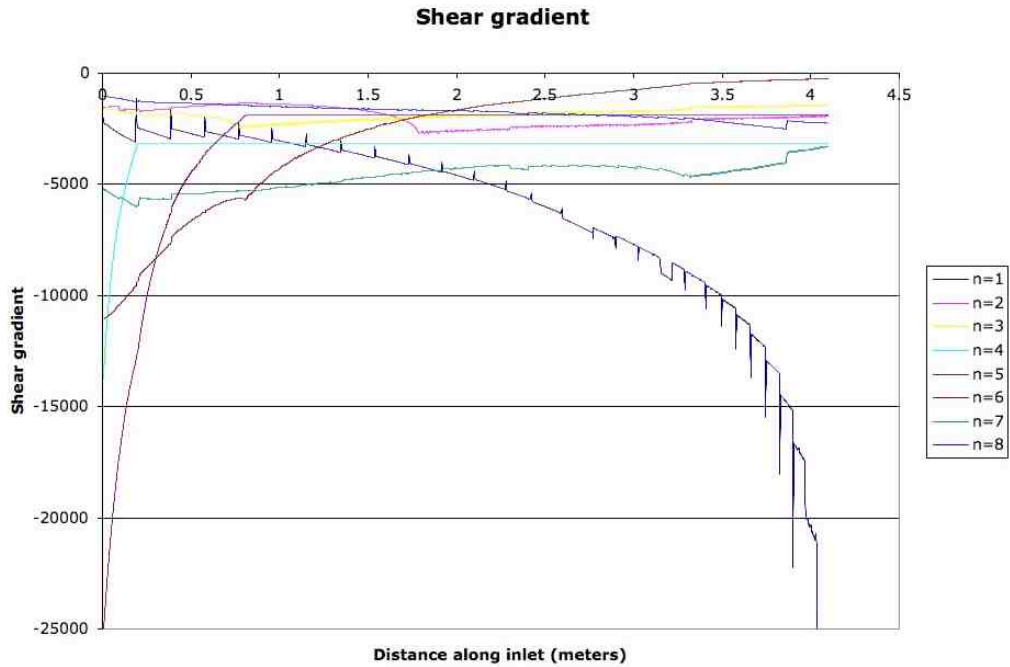
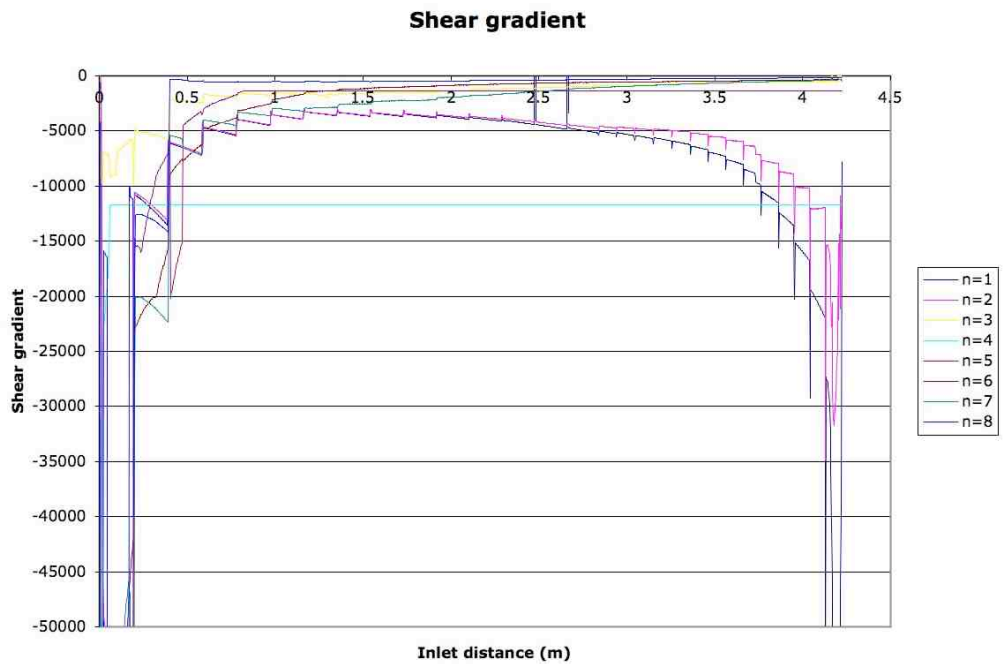Figure 5.37. Shear gradient for each streamtube along the centerline for power law inlet

Figure 5.38. Shear gradient for each streamtube along the centerline for angle-defined

inlet

114

based on curve-fitting the shear gradient to cancel the $\frac{1}{M^2} \to \infty$ near the wall. The

jumps occur at locations where the shock wave is calculated, and thus there is an

adverse pressure gradient behind the shock.

After the first streamtube hits the sonic line, the profile starts to degrade.

Figures 5.39 and 5.40 show the boundary layer profile with the velocity ratio f'

versus the height of each streamtube for the first 1.5 meters and for the whole inlet in

Figures 5.41. The similarity coordinate versus f' for each inlet is shown in Figures

5.42 and 5.43. The profile retains its shape until between 0.4 and 0.5 meters when the

$n = 4$ streamtube hits the sonic line. The sonic streamtubes may need to be bumped

up or down more than they currently are to maintain the profile. The objective is not

to model a profile per-se, the objective is to determine a shear gradient $\frac{d\tau}{dy}$ to

calculate the change in area – the growth of the boundary layer – of the profile.

However, if the shear gradient is determined based on propagating the profile and the

profile is degrading, the shear gradient will likely not be correct. Setting the shear

gradient constant for the sonic streamtubes gets around this problem, but

improvements to the model can be made such that this fix is not necessary. For the

top streamtube with $f' = 0.99$, at the exit of the inlet, f' had decreased to 0.92 for the

power law inlet and 0.96 for the angle-defined inlet.
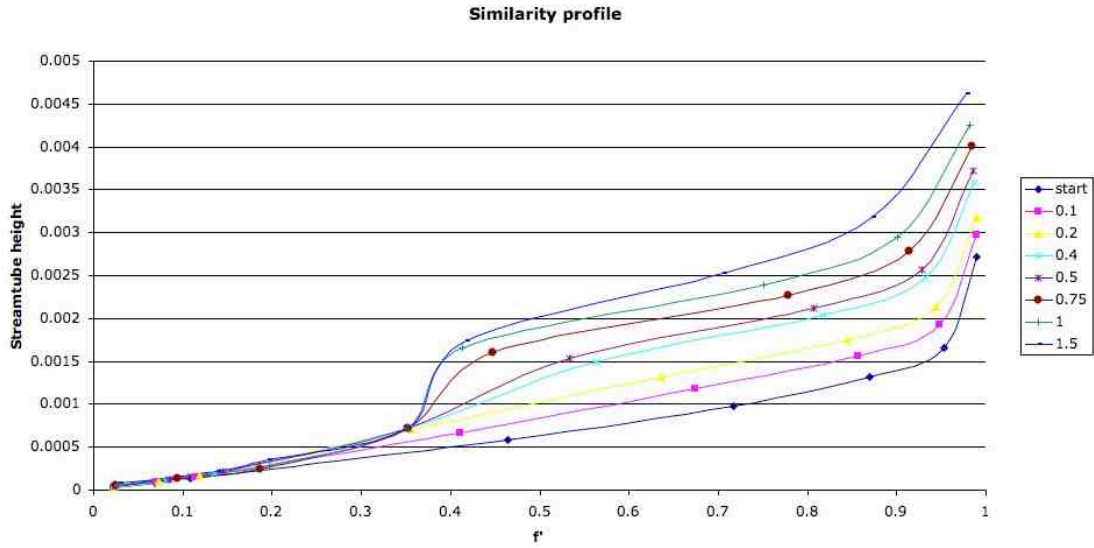
Figure 5.39. Streamtube height versus velocity ratio at the beginning of the inlet –

Power law inlet
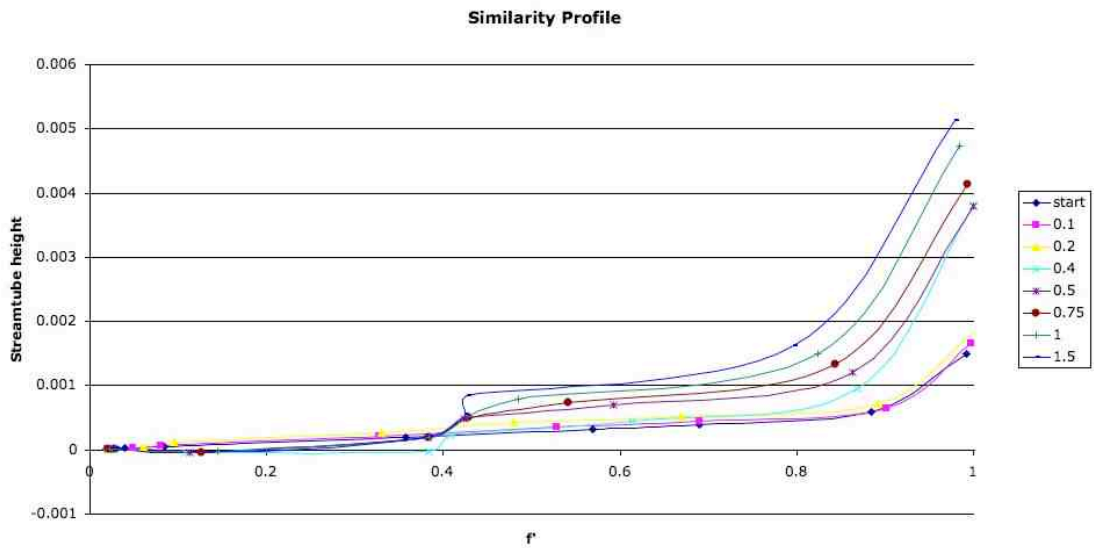
Figure 5.40. Streamtube height versus velocity ratio at the beginning of the inlet –

Angle-defined inlet
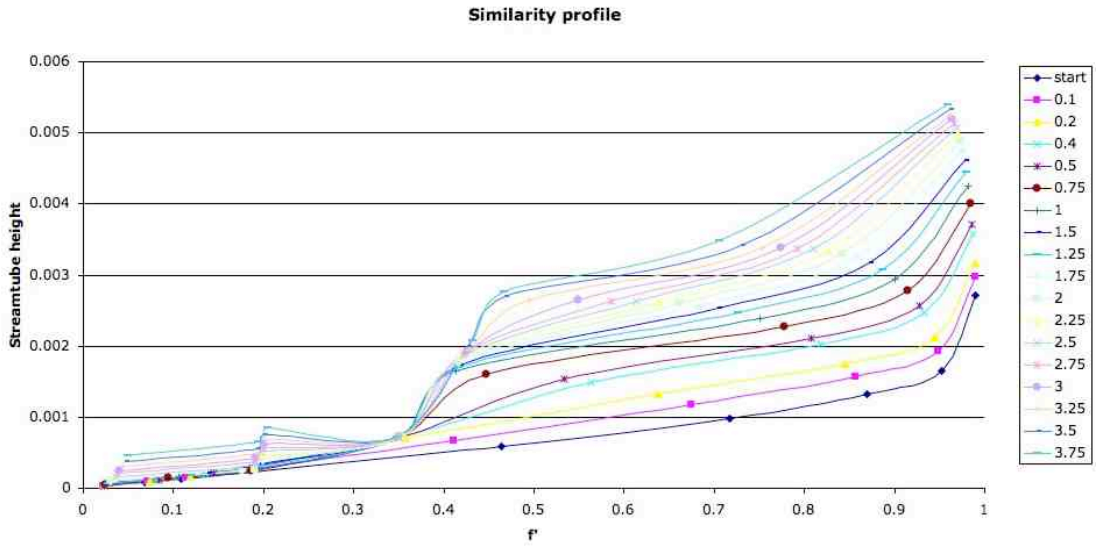
Figure 5.41. Streamtube height versus velocity ratio along inlet – Power law inlet
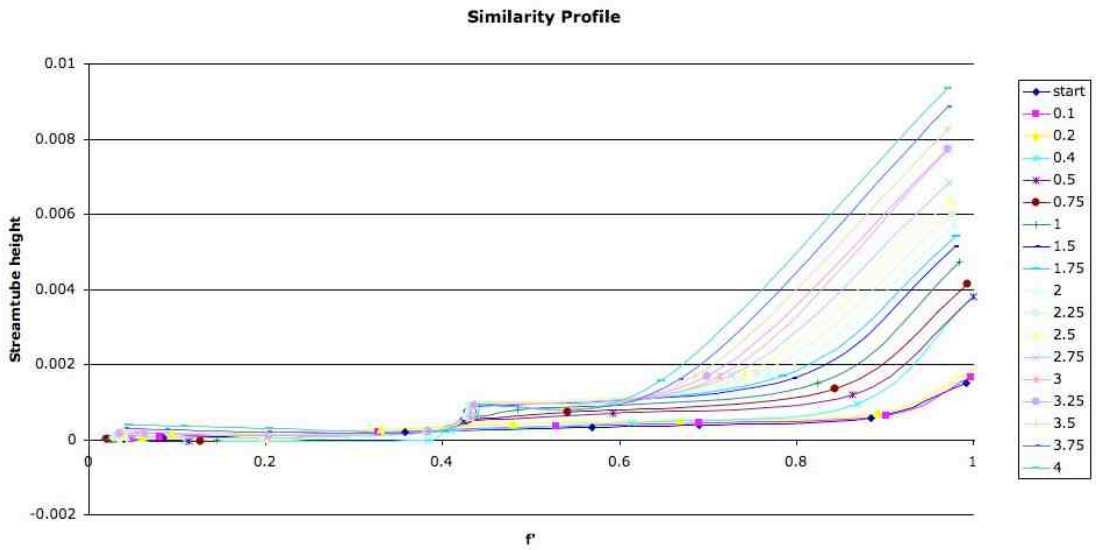
Figure 5.42. Streamtube height versus velocity ratio along inlet – Angle-defined inlet

117
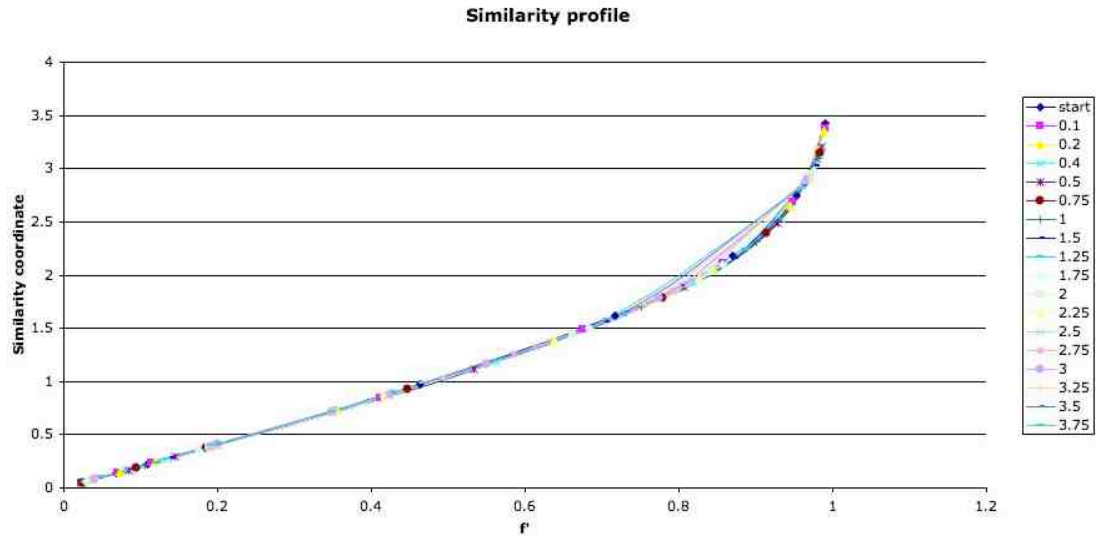
Figure 5.43. Similarity coordinate versus velocity ratio along inlet – Power law inlet

5.6 Shock wave/Boundary layer interactions

While the viscous method developed does not capture the effect of shock/boundary layer interactions or separation physics, Korkegi presents an analytic method to avoid shock/boundary layer interactions in the inviscid design method presented[37]. Shock-induced boundary layer losses can cause significant losses and large separation regions that could cause inlet unstart. Large areas of separated flow also invalidate the use of the boundary layer model. Prior to propagating the inviscid flow, insipient separation criteria developed by Korkegi should be used to determine the maximum shock strength in the inlet. Shock-induced boundary layer interactions are typically classified in two different categories:

118

1) Incipient separation due to a two-dimensional shock wave intersecting a boundary layer – such as those that occur at an un-swept compression ramp or when a planar wave reflects off a surface.

2) Swept interactions intersecting a turbulent boundary layer.

As discussed by Smart[12], neither of these two cases applies for a rectangular-to-circular or elliptical inlet. These inlets involve curved shocks reflecting off of smooth curved surfaces. The shock wave also reflects at the cowl, sweeps across the bottom and side of the inlet where the boundary layer is much less significant than the ingested boundary layer along the top, and strikes the shoulder. For mixed interactions such as this, Korkegi presents an insipient separation criteria:

$$\frac{P_i}{P} = 1 + 0.3M_N^2 \qquad M_N \le 4.5 \qquad\qquad (63a)$$

$$\frac{P_i}{P} = 0.17M_N^2 \qquad M \ge 4.5 \qquad\qquad (63b)$$

where M_N is the Mach number normal to the shock. Incipient separation occurs when the pressure ratio reaches $\frac{P_i}{P} \approx 1.5$. In the two inlets designed, this pressure ratio remains under 1.5 after the cowl. However, in the power law inlet this pressure ratio varies between 1.50 and 1.66 and in the angle-defined inlet, it varies between 1.49 and 1.77 from the inlet entrance to the cowl. This suggests that both inlets designed could have additional losses caused by incipient separation from shock/boundary layer interaction at the beginning of the inlet. A possible fix is to extend the length of the beginning of the inlet so the shock is not as strong.

Chapter 6: Conclusions and Summary

A method was presented to correct or create flow non-uniformities and incorporate multiple oblique shocks into compound compressible flow theory. This method can correct flow non-uniformities by starting with a known downstream flow profile and propagating the solution forward by solving for the necessary oblique shocks and inflow to produce downstream uniform flow with a given area change. Similarly, the method developed also adds upon previous work by providing a method for correctly incorporating multiple oblique shock waves into compound compressible flow theory by starting with a known downstream flow and solving for the freestream conditions. A pressure gradient behind the shock wave can be chosen to design a shock wave under the assumptions of compound compressible flow theory and the conservation equations.

The feasibility of this method was demonstrated by evaluating the inviscid and viscous performance of an inlet with a rectangular capture area and a circular combustor. An efficient inlet is a crucial part of scramjet operation, and a three-dimensional inlet with a rectangular capture area and circular or elliptical combustor has the potential for high performance. These inlets performed similarly under inviscid flow assumptions to other inlets with a transition from a rectangular capture area to a circular or elliptical combustor and better than rectangular inlets. Under inviscid flow assumptions, both inlets had a total pressure recovery of 0.93, kinetic energy efficiency of 0.997, and adiabatic compression efficiency of 0.98. This

method can produce an inflow for a three-dimensional inlet with acceptable performance characteristics.

In addition, uniform flow or a specific flow profile entering a scramjet combustor is often desired. An incoming non-uniform flow profile was created for two arbitrary inlets with uniform flow at the throat. Inlet placement is no longer confined to ensuring uniform flow into the inlet. In addition, non-uniformities can be created by altering the transition duct by matching the location of streamtubes at the throat with where in the inlet that streamtube crosses the shockwave.

Although this method was shown with a rectangular capture area and a circular combustor, it could be used for a variety of three-dimensional inlet shapes or hypersonic duct flow problems with multiple shock waves. Future work could focus on analyzing the performance of and flow in different types of three-dimensional inlet shapes. This method developed based on compound compressible flow theory provides an analytical way of developing these types of inlets using an aerodynamic-based and streamline tracing method rather than a geometric or mathematical based method. As a flow profile designed with the inviscid method presented is streamline traced, it potentially could result in better viscous performance for these inlets.

One of the main contributions of this research is the development of a simple and rapid inlet design tool. As the equations are algebraic, it is not computationally extensive and can be run relatively quickly for rapid initial design analysis with a

121

variety of software including a simple spreadsheet application. Design iterations can be done relatively quickly. A viscous boundary layer correction and initial viscous analysis can also be quickly produced to shrink the design space without resorting to a full-blown Navier-Stokes computational solution.

A method was developed for incorporating a boundary layer correction to an inlet and for handling singularities in boundary layers for streamtubes near the sonic line. The boundary layer correction calculated comprised about 3% and 6% of the exit plane in the power law and angle-defined inlet, respectively. These results are similar to other theoretical calculations for boundary layer growth. However, this model with the number of streamtubes used is highly dependent on the starting conditions for the streamtube profile and method for calculating the shear gradient. Using more than eight streamtubes in a vertical profile and increasing the numeric precision of the model should remove the dependency on the starting profile and the effect of inaccuracies in the shear gradient and produce a more representative boundary layer.

However, there are some limitations and potential pitfalls with this methodology. It is only accurate for inlets or area changes with relatively small wedge angles – between four and eight degrees – and with moderate surface curvature such that centrifugal effects can be neglected; however, an efficient inlet will not have large wedge angles or significant centrifugal effects. In addition, not all area change profiles will produce physical solutions. Using too small a streamtube resolution in the vertical direction – as attempted with 7 instead of 15 for the first

inlet – not only can reduce accuracy and produce different answers, but can result in unphysical solutions as a consequence of the pressure being too small behind a shock that does not occur when more streamtubes are used. Lengthening the surface could also mitigate some of the issues – too high pressure gradients near the cowl and capture plane or unphysical shock solutions – that resulted from having too high wedge angles. This method also will not account for the effects of shock/boundary layer interaction nor predict and model separation physics.

Chapter 7: Future Work

This research presents several opportunities for future study. For example, future work could focus on analyzing the performance of and flow in different types of three-dimensional inlet shapes. This method can be used for a variety of hypersonic flow applications with multiple oblique shock waves – not just three-dimensional inlets. It would be worthwhile to find other specific applications for which the method presented can be adopted and develop modifications for use in those applications. Several more transition duct profiles could be modeled to find design guidelines for three-dimensional shape-changing inlets.

Future work might include examining creating different profiles at the throat – either a pressure or Mach number profile as the methodology discussed can correct flow non-uniformities to create a desired profile. For example, well-placed non-uniformities in pressure, Mach number, or temperature could improve engine performance. A free-stream flow could be designed to create a pressure profile at the throat.

In addition, it would be useful to compare inlets designed with this method at off-design condition; however, a compound compressible flow method is ill suited to analyze off-design effects, resulting mostly from viscous shock losses and separation.

Bibliography

[1] Heiser, W.H. and Pratt, D. T. *"Hypersonic Airbreathing Propulsion."* American Institute of Aeronautics and Astronautics, 1994.

[2] Siebenhaar, A. and Bogar, T.J. "The Impact of Round Combustors on TBCC Propulsion and Hypersonic Cruise Vehicles, " AIAA Paper 2006-7986, Nov. 2006.

[3] Busemann, A. "Die achsensymmetrische kegeligeUebershallstromung," Luftfahrforschung 19, 137-144 (1942).

[4] Molder, Sannu and Szpiro, Edward J. "Busemann Inlet for Hypersonic Speeds." *Journal of Spacecraft and Rockets.* Vol. 3, mo.8 Aug 1966. pp 1303-1304.

[5] Van Wie, David and Molder, Sannu. "Applications of Busemann Inlet Designs for Flight at Hypersonic Speeds," AIAA Paper 22-1210. Feb 1992.

[6] Kantrowitz, A. and Donaldson, C., "Preliminary Investigation of Supersonic Diffusers," NACA ACR L5D20, May 1945.

[7] Billig, Frederick and Kothari, Ajay P. "Streamline Tracing: Technique for Designing Hypersonic Vehicles." *Journal of Propulsion and Power,* Vol 16, No.3, May – June 2000.

[8] Drayna, Travis W., Nompelis, Ioannis, and Candler, Graham V. "Hypersonic Inward Turning Inlets: Design and Optimization"

[9] Ramasubramanian, Vijay, Starkey, Ryan, and Lewis, Mark J. "An Euler Numerical Study of Busemann and Quasi-Busemann Hypersonic Inlets at On- and Off-Design Speeds."

[10] Ramasubramanian, Vijay, Starkey, Ryan, and Lewis, Mark J."Numerical Simulations of Busemann Hypersonic Inlets at Finite Flight Angles." AIAA 2008-7497, 17-21 August 2008.

[11] Billig, Frederick S. "SCRAM-A Supersonic Combustion Ramjet Missile," AIAA 93-2329. June 28-30.

[12] M.K. Smart, "Design of Three-Dimensional Hypersonic Inlets with Rectangular-to-Elliptical Shape Transition." *Journal of Propulsion and Power.* Vol. 15, No.3 May-June 1999.

[13] M.K. Smart, "Design of Three-Dimensional Hypersonic Inlets with Rectangular-to-Elliptical Shape Transition, " AIAA-1998-960-848, 1997.

[14] Barger, R.L. "A Procedure for Designing Forebodies with Constraints on Cross-Section Shape and Axial Area Distribution," NASA TP 1881, July 1981.

[15] Smart, M.K. "Experimental Testing of a Hypersonic Inlet with a Rectangular-to-Elliptical Shape Transition." AIAA Aerospace Sciences Meeting and Exhibit, January 1999.

[16] Sabean, John W. and Mark J. Lewis. "Computational Optimization of a Hypersonic Rectangular-to-Circular Inlet." *Journal of Propulsion and Power.* Vol. 17, No. 3. May-June 2001.

[17] Sabean, John W. *Optimization of a Hypersonic Inlet with a Rectangular-to-Circular Transition Duct*. Ph.d. dissertation, Department of Aerospace Engineering, University of Maryland – College Park 1999.

[18] Taylor, Trent M. and David Van Wie. "Performance Analysis of Hypersonic Shape-changing Inlets Derived From Morphing Streamline Traced Flowpath" AIAA 2008-2635, April 2008.

[19] Bernstein, A., Heiser, W., and Hevenor, C., 'Compound Compressible Nozzle Flow," *Journal of Applied Mechanics,* 34:548-554, 1967.

[20] Shapiro, Ascher. *The Dynamics and Thermodynamics of Compressible Fluid Flow.* Ronald Press, New York. 1953. Ch.. 8.

[21] Lewis, Mark J. and Daniel E. Hastings. "Application of Compound Compressible Flow to Non-uniformities in Hypersonic Propulsion Systems." Journal of Spacecraft and Propulsion. Vol. 5, No. 5. Sept. 1988.

[22] Lewis, Mark J. and Daniel E. Hastings. "Some consequences of flow non-uniformities on the fore-body of a trans-atmospheric vehicle." AIAA-1988-3057

[23] Barkmeyer, Daniel E.F. and Mark J. Lewis. "Velocity Profile Modification in High-Speed Flows." AIAA 2003-0909. Dec. 2003.

[24] Lewis, M. *Prediction of Inlet Flow Stratification and its Influence on the Performance of Air-Breathing Hypersonic Propulsion Systems*, Sc.D. thesis, Department of Aeronautics and Astronautics, MIT June 1988.

[25] Walsh, P.C., Tahir, R.B., and Molder, C. "Boundary-Layer Correction for the Busemann Hypersonic Air Inlet." *Canadian Aeronautics and Space Journal.* Vol. 49, No. 1, March 2003.

[26] Sheetz, "Ballistic Range Boundary-Layer Transition Measurements on Cones at Hypersonic Speeds," In C.S. Wells, editor, *Viscous Drag Reduction*, Plenum Press, New York, 1980, pp 53-84.

[27] Malik, M.R., Zang, T., Bushnell, D. "Boundary layer transition in hypersonic. Flows", AIAA 90-5232, 1990.

[28] Mack, L. M., "Boundary Layer Linear Stability Theory", in *Special Course on Stability and Transition of Laminar Flow,* AGARD Report 709, (1984).

[29] Perry, J.H. and East, R.A. "Experimental Measurements of Cold Wall Turbulent Hypersonic Boundary Layer." *AGARD Hypersonic Boundary Layers and Flow Fields,* May 1968.

[30] Bertram, M. H. and Cary Jr., A.M. "Experiments with Hypersonic Turbulent Boundary Layers on Flat Plates and Delta Wings." *AGARD Hypersonic Boundary Layers and Flow Fields.* May 1968.

[31] Cohen, Clarence B. and Reshotko, Eli. "Similar Solutions for the Compressible Laminar Boundary Layer with Heat Transfer and Pressure Gradient." Lewis Flight Propulsion Laboratory. TR 1293, 1957.

[32] White, Frank. *Viscous Fluid Flow.* 1st ed., McGraw-Hill, New York. 1974. pp 591.

[33] CD of inlet lines provided by Brink, Charles F. and Richard C. Mutzman at ARFL.

[34] Hank, Joseph M., Murphy, James S. and Richard C. Mutzman. "The X-51A Scramjet Engine Flight Demonstration Program." 19th AIAA International Space Planes and Hypersonics Systems and Technologies Conference. 28 April – 1 May 2008, Dayton, Ohio.

[35] Bertram, M.H. and Blackstock, T.A. "Some Simple Solutions to the Problem of Predicting Boundary-Layer Self-Induced Pressures," NASA TN D-798, 1961.

[36] Van Wie, David. "Scramjet Inlets " in *Scramjet Propulsion*, E.T. Curran, S.N.B. Murthy. Pg 463. Vol. 189. AIAA. 2000.

[37] Korkegi, R.H. "A Comparison of Shock Induced Two- and Three- Dimensional Incipient Turbulent Seperation," *AIAA Journal*, Vol. 13, No. 4, 1975, pp 534, 535.